# Chapter 4: A standardised look at the Complete Freund's Adjuvant (CFA) model in male and female mice regarding nociception and anxiety-like behaviours

**A standardised look at the Complete Freund's Adjuvant (CFA) model in male and female mice regarding nociception and anxiety-like behaviours**

Caitlin Fenech[1,2,3], Neda Assareh[2,4] and Karin R Aubrey[1,2]

[1]Pain Management Research Laboratories, Kolling Institute, Royal North Shore Hospital NSLHD and Faculty of Medicine and Health, University of Sydney, Sydney NSW Australia

[2]Sydney Pain Consortium, Faculty of Medicine and Health, University of Sydney, Sydney NSW Australia

[3]School of Medical Sciences, Faculty of Medicine and Health, University of Sydney, Sydney NSW Australia

[4]Brain and Mind Centre, Faculty of Science, University of Sydney, Sydney NSW Australia

Prepared for submission to **PAIN Reports**

Contributions- Caitlin Fenech: conceptualisation, formal analysis, investigation, methodology, visualisation, writing-original draft, writing- review and editing. Neda Assareh: conceptualisation, methodology, supervision, writing- review and editing. Karin Aubrey: conceptualisation, funding acquisition, supervision, writing- review and editing

Acknowledgements: The authors thank Amanda Purcell and Bryton Forster for feedback.

**Summary:** The extensively used CFA-induced persistent inflammatory pain model reliably induces mechanical and thermal hypersensitivity but fails to robustly translate anxiety-like behaviours seen in chronic pain.

## 4.1 Abstract

**Introduction:** Chronic pain in humans is characterised by a combination of heightened nociceptive sensitivity along with emotional comorbidities, with more women impacted than men. A limitation of preclinical models is that they often fail to encapsulate this complexity, and few studies directly compared behavioural outcomes between male and female mice. The Complete Freund's Adjuvant (CFA) inflammatory pain model is a widely used preclinical model that reliably induces persistent mechanical and thermal hypersensitivity and involves sex-dependent signalling differences. However, the literature regarding the duration of pain hypersensitivity and the presence or absence of associated locomotor and anxiety-like changes in the CFA model is inconsistent.

**Objective:** To systematically evaluate the CFA model's reliability to model common chronic pain comorbidities in animals of both sexes and better define its strengths and limitations for use in future studies.

**Methods:** Following intraplantar injections of either CFA or saline, male and female mice were assessed over three weeks for mechanical and cold nociceptive sensitivity (von Frey and acetone test), locomotion (open field test), and anxiety-like behaviours (light-dark and elevated plus maze tests).

**Results:** Mechanical hypersensitivity and cold allodynia were measured in both males and females, with notable variations in duration of these effects post-CFA injection. Locomotion deficits and anxiety-like behaviours were observed only transiently in male mice, but after one week, no differences were detected compared to controls.

**Conclusion:** The CFA model is a valid preclinical model for pronociceptive states in male and female mice but not for interrogating comorbid pain effects.

## 4.2 Introduction

Chronic pain is a debilitating health condition that is highly prevalent throughout the world, affecting 1 in 5 people (Treede et al., 2015). The problem of chronic pain is exacerbated by the fact that current pharmacotherapies are only partially effective in around half of patients (Dworkin et al., 2010). Most patients also develop comorbidities, including depression, anxiety, and sleep disorders (Treede et al., 2019). Thus, the need for increased understanding of pain circuitry and how nociception interacts with affective (emotional) behaviours is critical. Preclinical pain research using animal models of chronic pain strives to provide this fundamental knowledge and develop novel analgesics. However, the evidence generated across different laboratories is often inconsistent, especially with respect to the development of chronic pain comorbidities, and thus impacting data interpretation, clinical relevance, and translatability (Soliman & Denk, 2024).

Complete Freund's Adjuvant (CFA) injection into the hind paw is a commonly used preclinical persistent pain model to induce inflammatory pain (Knight et al., 1992; Stein et al., 1988). It is most reliably characterised by persistent mechanical and heat hypersensitivity in the injected paw, typically lasting between 3-4 weeks (Burek et al., 2022; Wei et al., 2025). However, it is sometimes reported to endure for up to six weeks (Burek et al., 2021; Knight et al., 1992; Urban et al., 2011), or resolve within two weeks (Baumbach et al., 2024; Liu et al., 2015; Pitzer et al., 2016, 2019; Sheahan et al., 2017). In addition to mechanical and heat hypersensitivity, studies have reported that the CFA model produces deficits in general locomotion and anxiety-like behaviours (Burek et al., 2021; Cardenas et al., 2021; Chen et al., 2013; Hofmann et al., 2017; Liu et al., 2015; Narita et al., 2006; Parent et al., 2012; Pitzer et al., 2016, 2019; Refsgaard et al., 2016; Sheahan et al., 2017; Zhou et al., 2019), suggesting the model replicates both sensory deficits and affective comorbidities observed in individuals with chronic pain. Conversely, some studies using the same combination of nociceptive and affective tests fail to measure significant changes (Flores-García et al., 2025; Gaspar et al., 2021; Urban et al., 2011).

Further, the bulk of studies have been completed in male mice, with female mice only recently being systematically included in preclinical studies (Burek et al., 2022; Kilkenny et al., 2010; Wei et al., 2025), resulting in a relative scarcity of CFA model data in female animals for any of the behaviours described (Cardenas et al., 2021; Flores-García et al., 2025; Papadogiannis

& Dimitrov, 2022; Pitzer et al., 2019; Refsgaard et al., 2016; Zhang et al., 2024). To date, only one study has reported both nociception and anxiety-like behaviours in female C57Bl/6 mice, the most used mouse strain for pain studies (Pitzer et al., 2019). Thus, despite clear evidence of different immune profiles in males and female mice following CFA (Sorge et al., 2015), it remains unclear if the behavioural sex differences are measurable in the CFA model. This highlights a critical gap that needs to be addressed, especially considering that 50% of chronic pain conditions, including chronic inflammatory pain conditions like rheumatoid arthritis, are more prevalent in women (Greenspan et al., 2007; Mogil, 2012).

Some of the variability and conflicting results observed are likely related to many confounding variables. A recent systematic review and meta-analysis revealed significant variability in behavioural outcomes across animal species, strain and sourcing (Burek et al., 2022), with another study revealing the substantial influence of housing conditions, both between and within cages (Pitzer et al., 2016; Zhang et al., 2024). In addition, the injury model (i.e. volume injected into the hind paw), experimental design, handling, and apparatus habituation schedules are not consistently carried out or reported across the studies, which is likely to contribute to some of the variability and conflicting results observed (Burek et al., 2021; Sensini et al., 2020; Sorge et al., 2014).

This study aims to concurrently assess the nociceptive, locomotion, and anxiety-like behavioural outcomes of hind paw CFA injection in male and female mice, keeping strain, source, species, housing conditions, researcher, and handling consistent. Building a systematic repository of replicable data on multiple relevant behavioural outcomes for chronic pain models is necessary to highlight the strengths and limitations of each model. This will enable improved interpretation of the data generated using this model, and increase the model's relevance and translatability, ultimately leading to better preclinical to clinical translation.

## 4.3 Methods

### Animals

All experiments were conducted in accordance with the Australian Code for the Care and Use of Animals for Scientific Purposes and approved by the University of Sydney Animal Ethics Committee (Protocol: 2022/2085). Adult male and female mice (8-9 weeks, C57Bl/6), obtained from the institutional wildtype colony (Kearns Animal Facility), were housed in ventilated cage (up to four/cage), maintained on a 12/12h light/dark cycle (23°C, 70% humidity) with food and water provided *ad libitum*. Cages were enriched with a house igloo, tissues for nesting, and paddle pop sticks. Mice were regularly monitored for general health and well-being and weighed twice a week.

### CFA-induced paw edema

The Complete Freund's Adjuvant (CFA) preclinical model of persistent inflammatory pain was used in this study (Knight et al., 1992; Stein et al., 1988). Mice were anaesthetised with 2-3% isoflurane (1L/min $O_2$) and sedation was confirmed by the absence of a toe pinch reflex. Mice then received a single unilateral intraplantar left hind paw injection of 20µL undiluted CFA (Sigma-Aldrich). Similarly, control mice were injected unilaterally in the left hind paw with 20µL of 0.9% sterile saline.

### Experimental Timeline

To see the effect of CFA injection over time, an extensive three-week behavioural assay was used (Figure 1). Throughout this protocol, nociception testing refers to the two nociceptive tests used in this experiment: von Frey (mechanical hypersensitivity) and acetone (cold allodynia), with a 5-minute interval between tests to ensure results are independent (Anderson et al., 2014; François et al., 2017; Mitchell et al., 2021). After the five-day handling protocol, the mice underwent baseline nociception testing. 30 minutes after the conclusion of the nociceptive testing, the mice were injected with either CFA or saline (see *CFA-induced paw edema*). 4 hours after injection, the mice underwent nociception testing. Following this, nociception testing was repeated at PID 1, 3, 6, 10, 15, 21 (PID: post injection day). On PID 2, 8, and 12 light-dark testing occurred in the late afternoon (3-5pm) where it was paired with open field (9-11am) on

PID 2 and 12 (this order of testing has been used previously, from least to most stressful (Pitzer et al., 2019). Testing on the elevated plus maze (EPM) occurred on PID 4. As CFA has been shown to induce persistent inflammation for up to 6 weeks, these time points were chosen so that different stages from injection could be tested (e.g., immediately after injection versus more than one week from injection).

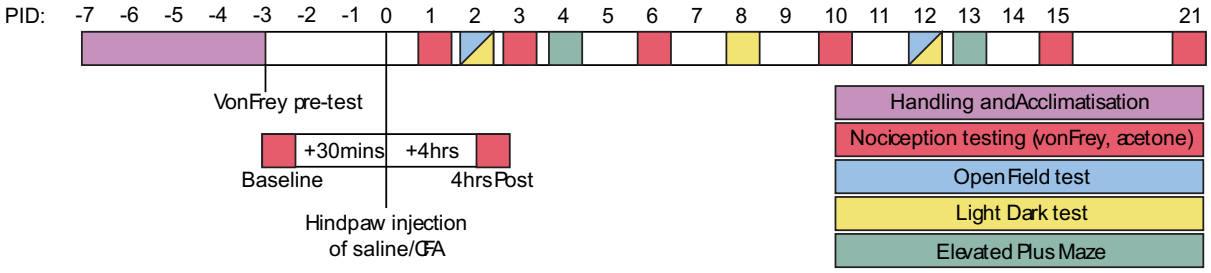


**Figure 1: Experimental timeline.** PID: Post injection day, CFA: Complete Freund's Adjuvant.

## Handling and habituation

Behavioural experiments began at 10 weeks of age and mice were split into separate cohorts by sex. Mice were handled by the one experimenter for a period of five days preceding any behavioural testing. The handling consisted of gently lifting the mouse by the base of the tail onto the experimenter's wrist and transferring the mouse between their hands for one minute. The last three days of the handling protocol were paired with 10 minutes of acclimatisation to the experimental room and one minute habituation to the von Frey/acetone stand with dim red light. On the fifth day, the mice underwent a von Frey pre-test to reduce test-related stress. By the conclusion of the five-day handling protocol, all the mice were confirmed to exhibit no obvious stress response (no presentation of shaking, vocalisation, or jumping) to handling by the experimenter, the room, or the apparatus.

For each experimental cohort, animal groups were randomly allocated between cages (all cage mates were of the same treatment group). In addition, for all anxiolytic behavioural tests (open field, light-dark box, elevated plus maze), the mice were tested in an alternative saline-CFA order to avoid the confound of time of day or circadian rhythm effects across the duration of a testing session. It should be noted that all nociception behavioural testing occurred around midday (except for baseline and 4 hours post testing). CFA administration results in visually obvious paw edema, which prevents a fully blinded experimental design.

**von Frey (mechanical hypersensitivity)**

To assess mechanical hypersensitivity induced by CFA, we used the simplified up-down method (SUDO) using von Frey filaments (Bonin et al., 2014). Animals were placed in elevated Perspex enclosures with wire mesh bases and given 30 minutes to acclimatise to the testing environment under dim red light (<3 lux). Testing began with a 0.95 g von Frey hair which was pressed perpendicularly against the injected (left) hind paw and held for approximately two seconds. If the animal sharply withdrew their paw, licked their paw, or flinched upon removal of the von Frey filament, a withdrawal response was noted. The von Frey test was repeated four times on the injected paw with at least a two-minute interval between tests. If a positive withdrawal response was observed, the subsequent test used a lighter filament, whereas if no withdrawal response was seen, the subsequent test used the next heavier filament. The final paw withdrawal threshold was calculated as the lightest force required to produce a withdrawal response.

**Acetone (cold allodynia)**

To assess cold allodynia induced by CFA, we used the acetone test (Yoon et al., 1994). Five minutes after the conclusion of the von Frey test, the animals remained in the elevated Perspex enclosures with wire mesh bases, and 20 µL of acetone was sprayed on the centre of the injected (left) hind paw through the wire grid. The number of licks was recorded over a 30 second period and if the mouse was seen to lick their paw for more than two seconds, one lick per two seconds was noted (i.e. a four second lick would count as two licks). The test was repeated once on the same paw with at least five minutes between tests. The final value used for statistical analysis was the average of the number of licks between the two tests.

**Open Field (locomotor activity and anxiety-like behaviours)**

Locomotor activity was measured using the open field test. After a 10-minute acclimatisation period to the testing room under a dim white light (30 ± 10 lux), the mice were individually placed in an enclosed open-top arena (50 cm x 50 cm x 50 cm). An overhead camera recorded their behaviour for a 15-minute period. This period allowed for the monitoring of locomotion and anxiety-like behaviours (Bailey & Crawley, 2009). Between animals, 20% ethanol was used to clean the apparatus to remove odour cues. The number of faecal boli, supported rearing

responses, and jumping responses was scored manually while the total distance travelled (m), average speed (m/s), time in the centre zone (s), number of entries into the centre zone, and time mobile was obtained through ANY-Maze video tracking software (version 7; Stoelting Co.). The centre zone was classified as the middle 25 cm x 25 cm zone.

**Light-Dark (anxiety-like behaviours)**

The light-dark box test was used to test anxiety-like behaviours (Bourin & Hascoët, 2003). After a 10-minute acclimatisation period to the testing room under a dim white light, the mice were individually placed in the light-dark box (dark chamber: 20 cm wide x 18 cm x 30 cm high; light chamber (60 ± 10 lux): 28 cm wide x 27 cm long x 30 cm high). The mice were placed in the light chamber facing the entry to the dark chamber (~ 18 cm from entrance) and allowed to explore freely for five minutes. Between animals, 20% ethanol was used to clean the apparatus to remove odour cues. An overhead camera recorded their behaviour, and the following measures were obtained following ANY-Maze video tracking software analysis (version 7; Stoelting Co.): number of entries into the light zone, time in the light zone (s), and total distance travelled in the light zone (m).

**Elevated Plus Maze (anxiety-like behaviours)**

The elevated plus maze (EPM) test was also used to test anxiety-like behaviours. After a 10-minute acclimatisation period to the testing room under dim white light (40 ± 10 lux), the animals were individually placed in the centre of the elevated plus maze facing a closed arm (two 60cm arms, 5cm wide with 15cm high walls). An overhead camera recorded their behaviour for a five-minute period. Between animals, 20% ethanol was used to clean the apparatus to remove odour cues. The time spent (s) in the open and closed arms was obtained using ANY-Maze video tracking software (version 7; Stoelting Co.).

**Statistical analysis**

All data was analysed using GraphPad Prism (version 10, GraphPad Software, Inc., La Jolla, CA) and presented as mean ± SEM. Significance, as indicated by an asterisk, was defined as $p < 0.05$ *a priori*. For all datasets, a Shapiro-Wilk test was performed to test normality. For the

nociception tests, significance was analysed via a mixed-effects analysis with the Geisser-Greenhouse correction, followed by Bonferroni's multiple comparison test. For the open field, light-dark, and elevated plus maze results, unpaired t-tests were used (Supplementary Table 1). All behavioural test schematics were created with BioRender.

## 4.4 Results

### CFA-induced persistent inflammatory pain causes nociceptive hypersensitivity

To test the effect of persistent inflammatory pain induced by hind paw injection of CFA, nociceptive tests were conducted (von Frey, acetone) on male and female mice, compared to saline injection. The tests were conducted four hours post injection and repeated at post injection day (PID) 1, 3, 6, 10, 15, 21 to see the progression of the persistent pain state across a three-week period.

Mechanical sensitivity was measured using the von Frey test. In male mice, CFA hind paw injection significantly reduced the paw withdrawal threshold at four hours post ($p<0.05$), PID 1 ($p<0.001$), 3 ($p<0.001$), 6 ($p<0.01$), 10 ($p<0.001$), and 15 ($p<0.05$) but not 21 when compared to saline injection (Figure 2A). Similarly, CFA injection into the hind paw of female mice significantly reduced mechanical paw withdrawal thresholds, four hours post injection ($p<0.01$), PID 1 ($p<0.001$), 3 ($p<0.01$), 6 ($p<0.001$), 10 ($p<0.01$), 15 ($p<0.05$) and this effect persisted at 21 ($p<0.01$) compared to saline injected controls (Figure 2B). In addition, in the acetone test, male CFA-injected animals had a significantly increased number of responses (licking, shaking etc.) four hours post injection, and on PID 1($p<0.01$), 3, 6, 10 ($p<0.05$), and 15 ($p<0.01$) but not 21 compared to saline injection (Figure 2C). Female CFA-injected animals had delayed and milder acetone effects, with significant increases in responses measured only on PID 1,3 ($p<0.05$), 6 ($p<0.001$), and 15 ($p<0.05$) compared to saline injected controls (Figure 2D).

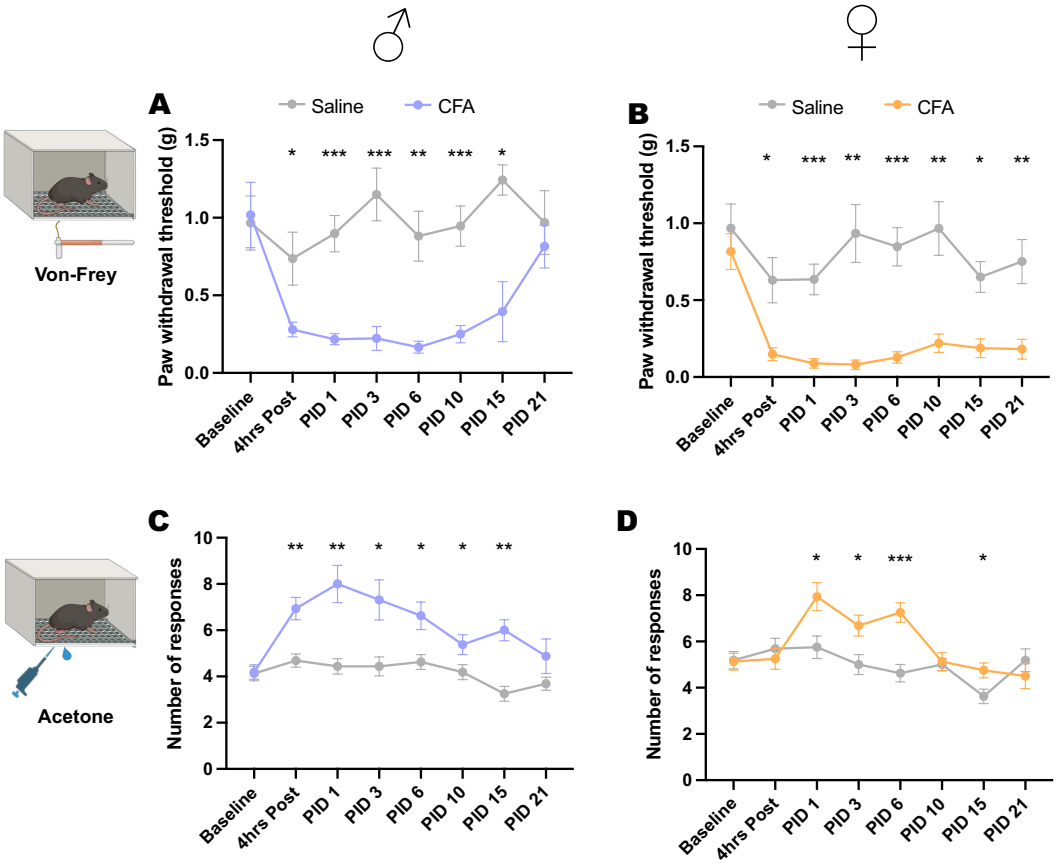


**Figure 2: Persistent inflammatory pain induced by CFA reduced mechanical sensitivity and increases cold allodynia in both male and female mice.** CFA injection significantly reduced mechanical hind paw withdrawal thresholds for more than two weeks in male mice (A) and up to three weeks in female mice (B) when compared to saline. Application of acetone to the hind paw significantly increased the number of responses in male mice for more than two weeks (C) and increased responses after six days post injection for female mice (D) when compared to saline mice. CFA: Complete Freund's Adjuvant, PID: Post injection day. Values are presented as mean ± SEM (n=8 for all groups/timepoints except PID 15 (n=4/group)). Significance was analysed via a mixed-effect analysis with post hoc Bonferroni correction; *p<0.05, **p<0.01, ***p<0.001, ****p<0.0001.

## Open field behaviours in male mice

As CFA injection has been reported to have inconsistent effects on locomotor behaviours and anxiety-like behaviours across a wide range of studies (Burek et al., 2021, 2022; Cardenas et al., 2021; Chen et al., 2013; Flores-García et al., 2025; Gaspar et al., 2021; Hofmann et al., 2017; Liu et al., 2015; Narita et al., 2006; Parent et al., 2012; Pitzer et al., 2016, 2019; Refsgaard et al., 2016; Sheahan et al., 2017; Urban et al., 2011; Wei et al., 2025; Zhou et al., 2019), we used the open field test, light-dark test, and the elevated plus maze to compare

behaviour of saline- and CFA-injected animals in our experimental conditions (Riebe & Wotjak, 2012).

First, locomotor and centre zone activity, as well as rearing and jumping behaviour, was assessed during a 20-minute open field test carried out at PID 2 and PID 12. Across the two time points, CFA injection significantly reduced the total distance travelled ($p<0.05$), average speed ($p<0.05$), and time mobile ($p<0.01$) in male mice at PID 2 compared to saline injection (Figure 3B-D). There were no significant differences in centre zone activity, rearing, or jumping behaviours at the same time point (Figure 3E-I). By PID 12, the reduction of the locomotor activity induced by CFA was lost (Figure 3K-P), although a small increase in rearing responses was detected in CFA compared to saline-injected animals (Figure 3Q).

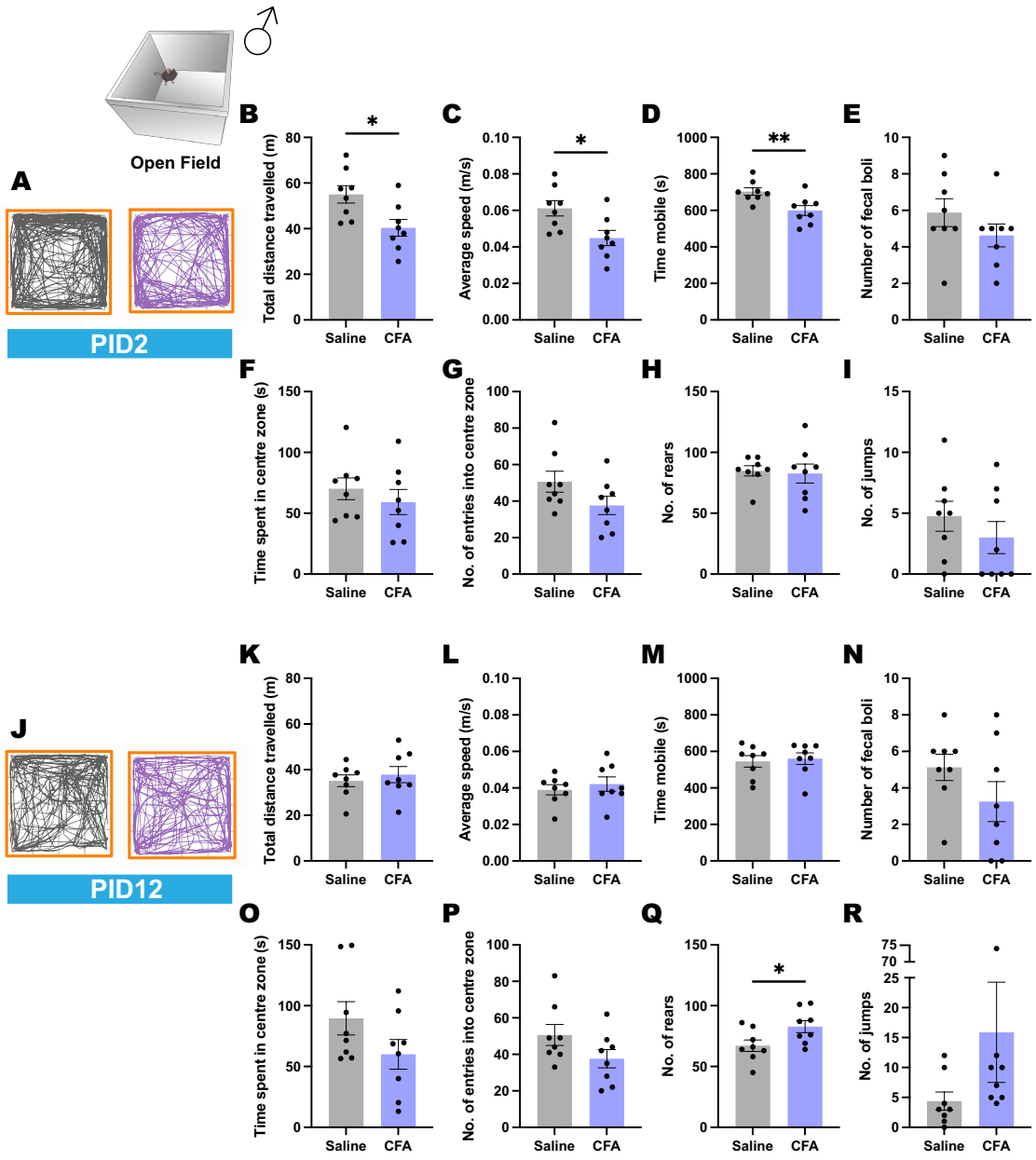

**Figure 3: Persistent inflammatory pain induced by CFA reduced locomotor activity in male mice (two days post injection).** Track plots of centre point in the open field of saline (left) and CFA (right) males at PID 2 in the open field (A). In males at PID 2, CFA mice had a significantly lower total distance travelled (B), average speed (C), and time mobile (D), but no changes in number of faecal boli (E), time spent in the centre zone (F), number of entries into centre zone (G), number of rears (H), or number of jumps (I) when compared to saline. Track plots of centre point in the open field of saline (left) and CFA (right) males at PID 12 in the open field (J). In males at PID 12, CFA mice had no changes in total distance travelled (K), average speed (L), time mobile (M), number of faecal boli (N), time spent in the centre zone (O), number of entries into centre zone (P) or number of jumps (R) when compared to saline. Number of rears (Q) in CFA male mice at PID 12 was significantly increased when compared to saline. CFA: Complete Freund's Adjuvant, PID: Post injection day. Individual animals are indicated on the graphs (n=8/group) and values are presented as mean ± SEM. Significance was analysed via unpaired t-tests; *$p<0.05$, **$p<0.01$, ***$p<0.001$, ****$p<0.0001$.

## Open field behaviours in female mice

In females, at PID 2 and PID 12, there were no changes in horizontal locomotor activity as well as centre zone activity when compared to saline-injected mice (Figure 4). However, at PID 12, the number of faecal boli ($p<0.05$; Figure 4N) and the number of jumps ($p<0.01$; Figure 4R) was increased in CFA-injected mice. These differences in open field behaviours provide light evidence that persistent inflammatory pain induced by CFA might be associated with increased anxiety or escape behaviours in female mice, but this evidence requires robust validation.

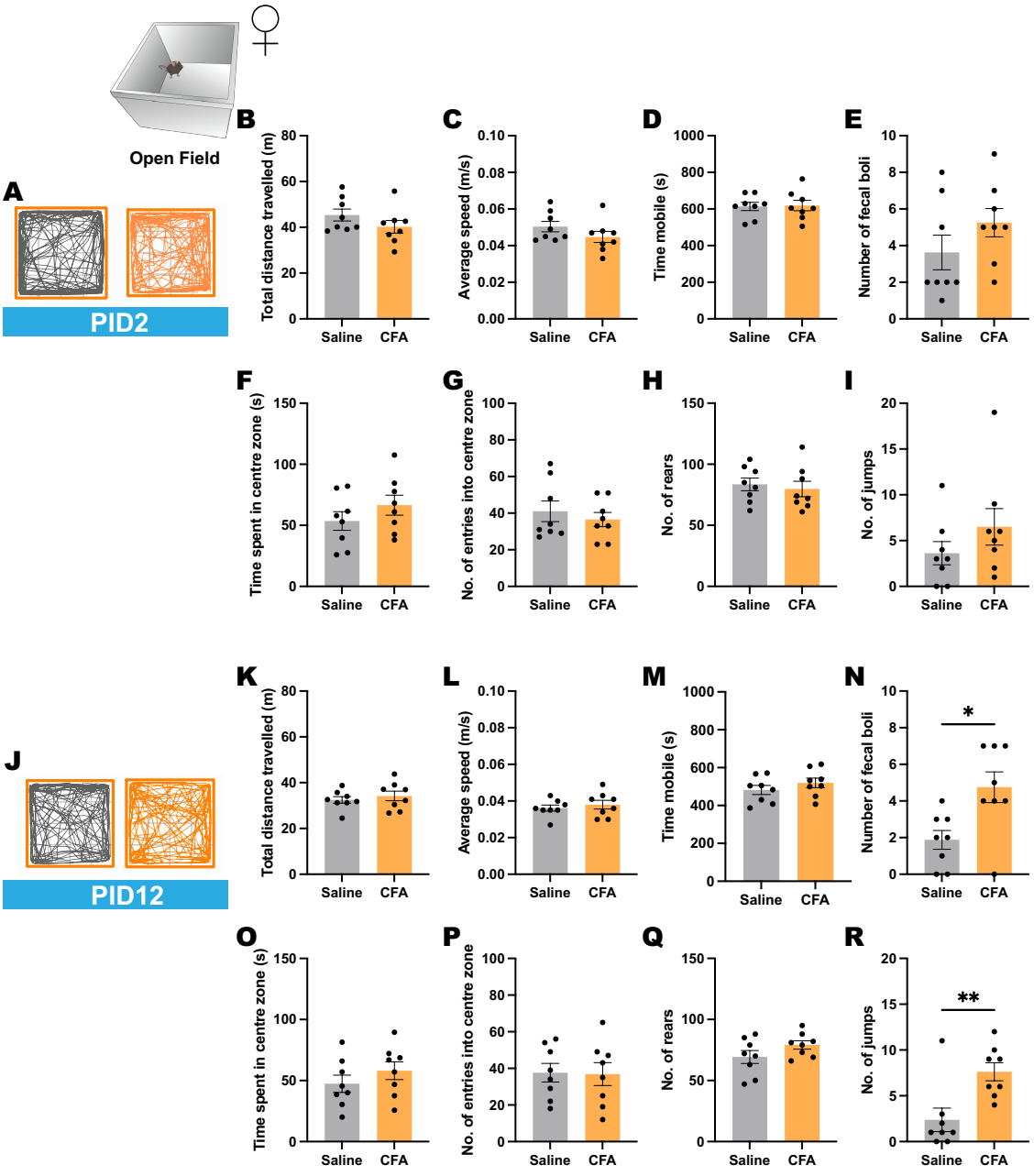


**Figure 4: Persistent inflammatory pain induced by CFA affected female animals differentially in the open field test.** Track plots of centre point in the open field of saline (left) and CFA (right) females at PID 2 in the open field (A). at PID 2, CFA mice had no changes in total distance travelled (B), average speed (C), time mobile (D), number of faecal boli (E), time spent in the centre zone (F), number of entries into centre zone (G), number of rears (H) or number of jumps (I) when compared to saline. Track plots of centre point in the open field of saline (left) and CFA (right) females at PID 12 in the open field (J). at PID 12, CFA mice had no changes in total distance travelled (K), average speed (L), time mobile (M), time spent in the centre zone (O), number of entries into centre zone (P) or number of rears (Q) when compared to saline. Number of faecal boli (N) and number of jumps (R) in CFA female mice at PID 12 was significantly increased when compared to saline. CFA: Complete Freund's Adjuvant, PID: Post injection day. Individual

animals are indicated on the graphs (n=8/group) and values are presented as mean ± SEM. Significance was analysed via unpaired t-tests; *p<0.05, **p<0.01, ***p<0.001, ****p<0.0001.

## Anxiety-like behaviours are seen in male mice with persistent inflammatory pain induced by CFA

To best assess anxiety-like behaviours, multiple behavioural assays to assess anxiety-like responses is recommended to enhance the reliability of findings and minimise the influence of confounding factors associated with individual tests (Riebe & Wotjak, 2012). Therefore, we carried out both the light-dark and the elevated plus maze test in male and female CFA- and saline-injected mice. In the light-dark test, there were no significant differences in time spent in the light zone or number of entries into the light zone between the CFA- and saline-injected mice of either sex at any of the time points measured (Figure 5). Total distance travelled in the light zone was also analysed to ensure locomotor activity changes due to CFA did not interfere with the light zone measurements.

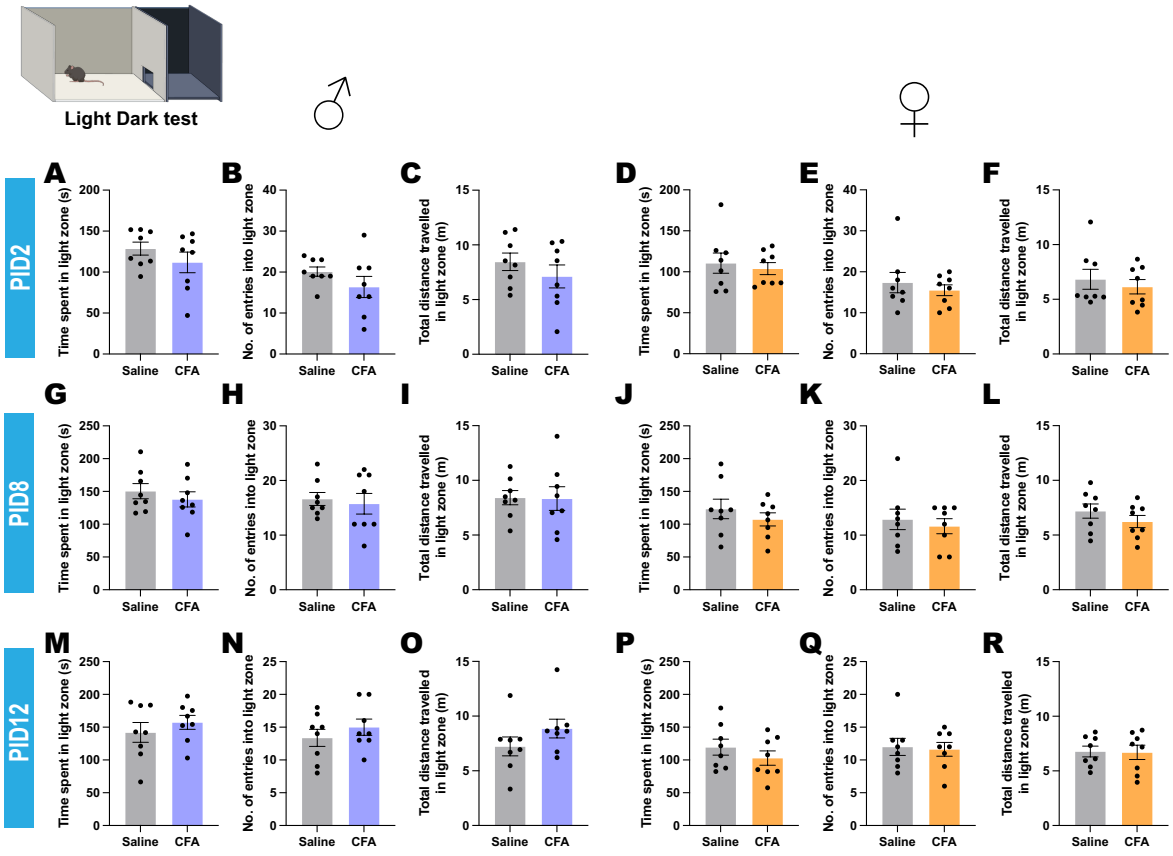


**Figure 5: Persistent inflammatory pain induced by CFA does not change anxiety-like behaviours in a light dark test in male and female mice (up to twelve days post injection).** In

males at PID 2 (A-C), PID 8 (G-I) and PID 12 (M-O), there was no significant difference in time spent in the light zone (A, G, M), number of entries into the light zone (B, H, N) and total distance travelled in the light zone (C, I, O) in CFA mice when compared to saline mice. In females at PID 2 (D-F), PID 8 (J-L) and PID 12 (P-R), there was no significant difference in time spent in the light zone (D, J, P), number of entries into the light zone (E, K, Q) and total distance travelled in the light zone (F, L, R), in CFA mice when compared to saline mice. CFA: Complete Freund's Adjuvant, PID: Post injection day. Individual animals are indicated on the graphs (n=8/group) and values are presented as mean ± SEM. Significance was analysed unpaired t-tests; *p<0.05, **p<0.01, ***p<0.001, ****p<0.0001.

For the elevated plus maze, the time spent in the open and closed arms was measured (Figure 6). On PID 4, time spent in the open arms was reduced following CFA in only males (p<0.05; Figure 6C) and not females (Figure 6E). However, at PID 13, time spent in the open and closed arms was unchanged in both males and females (Figure 6I-L).

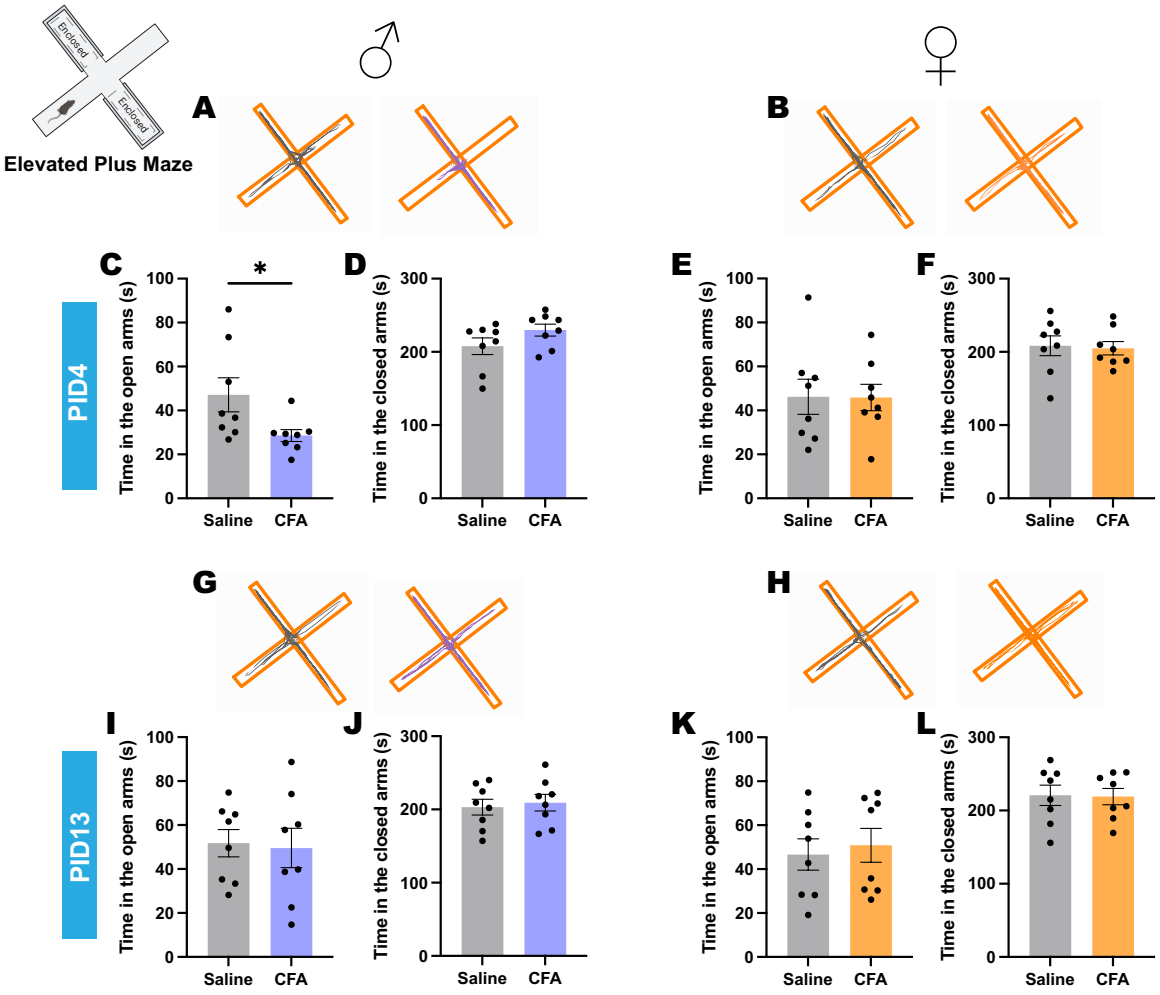

**Figure 6: Persistent inflammatory pain induced by CFA increases anxiety-like behaviours in the elevated plus maze in males but not in female mice (four days post injection).** Representative plot of the animals' centre point during the elevated plus maze for males (A: PID 4; G: PID 13) and females (B: PID 4; H: PID 13); saline: left, CFA: right. On PID 4, time spent in the open arms was reduced following CFA in only males (C) and not females (E), while time spent in the closed arms was unchanged (D, F). However, at PID 13, time spent in the open and closed arms was unchanged in both males and females (I-L). CFA: Complete Freund's Adjuvant, PID: Post injection day. Individual animals are indicated on the graphs (n=8/group) and values are presented as mean ± SEM. Significance was analysed via unpaired t-tests; *p<0.05, **p<0.01, ***p<0.001, ****p<0.0001.

## 4.5 Discussion

### Results Summary

Using a systematic approach to compare nociceptive and affective behaviours in the CFA model of persistent inflammation in male and female mice, we found that nociceptive responses to mechanical and acetone application are reliably altered in both male and female mice following CFA hind paw injection compared to saline injection for a period of two to three weeks. After this period, nociceptive behavioural responses resolved in male mice, but were maintained in female mice. In tests to assess changes in locomotor and anxiety-like behaviours, no consistent behavioural changes were detected. In males, some changes were seen early at PID 2 in locomotor activity and PID 4 in anxiety-like behaviours. There was a modest indication of increased anxiety-like behaviour in the female CFA-injected mice on PID 12 with increased faecal boli and increased jumps in the open field, although this was an isolated result as it was not supported by any changes in anxiety-like behaviours in the other relevant measures (Table 1).

**Table 1: Summary of behavioural responses altered following CFA.** *PID: Post Injection Day, X: No change between saline- and CFA-injected mice.

| BEHAVIOURAL RESPONSE | MALE | FEMALE |
|---|---|---|
| **MECHANICAL WITHDRAWAL THRESHOLD** | ↓ (4 hours – PID 15) | ↓ (4 hours – PID 21) |
| **COLD ALLODYNIA** | ↓ (4 hours – PID 15) | ↓ (PID 1-6, 15) |
| **OPEN FIELD-LOCOMOTION** | ↓ (PID 2), X (PID 12) | X |
| **OPEN FIELD-ANXIETY-LIKE BEHAVIOURS** | X | X (PID 2), ↑ (PID 12) |
| **LIGHT DARK-ANXIETY-LIKE BEHAVIOURS** | X | X |
| **ELEVATED PLUS MAZE- ANXIETY-LIKE BEHAVIOURS** | ↑ (PID 4), X (PID 13) | X |

### Strengths of CFA model

Firstly, a major strength of the CFA model is that it is accessible and causes robust nociceptive mechanical and thermal hypersensitivity (Burek et al., 2021; Cardenas et al., 2021; Chen et al.,

2013; Cobos et al., 2012; Flores-García et al., 2025; Gaspar et al., 2021; Kandasamy et al., 2016; Liu et al., 2015; Narita et al., 2006; Papadogiannis & Dimitrov, 2022; Parent et al., 2012; Pitzer et al., 2016, 2019; Refsgaard et al., 2016; Rivera-García et al., 2024; Sheahan et al., 2017; Urban et al., 2011; Zhang et al., 2024; Zhou et al., 2019). In our findings, mechanical hypersensitivity was the strongest effect and would be most useful when investigating interventions or treatments to alleviate the hypersensitivity. In addition, the CFA-induced persistent inflammatory pain model requires limited technical experience (i.e. no surgery) and has a rapid onset of nociceptive hypersensitivity, unlike other preclinical models of chronic pain, like neuropathic chronic pain (Bennett & Xie, 1988). This is a major advantage in preclinical research, ensuring that experiments are not heavily time-consuming.

Another advantage of the CFA model is its ability to model nociceptive hypersensivity in both males and females as seen in human chronic inflammatory pain pathologies (Greenspan et al., 2007; Mogil, 2012). Prior to the publication of the ARRIVE guidelines to standardise preclinical research in 2010, most behavioural studies exclusively used male rodents (Kilkenny et al., 2010). The current study aligns with most previous studies that show mechanical and thermal hypersensitivity in female mice, following CFA injection, is consistently demonstrated for a period of up to two weeks post injection (Cardenas et al., 2021; Flores-García et al., 2025; Papadogiannis & Dimitrov, 2022; Pitzer et al., 2019; Zhang et al., 2024). Our results also show subtle differences in anxiety-like behaviours between males and females, reflecting possible changes in ethological behaviours between sex (Meseguer Henarejos et al., 2020; Sensini et al., 2020). The one other study that used C57Bl/6 male and female mice did also observe sex differences in anxiety behaviours (Pitzer et al., 2019). Indeed, there is clear evidence that different immune profiles are seen between males and females following CFA injection (Sorge et al., 2015) and changes to signalling within central pain circuitry (Tonsfeldt et al., 2016; Yu et al., 2021), which would contribute to our findings. Future experiments could explore the biological mechanisms underlying the CFA model at key time points post injection in both males and females to determine their effect. Thus, the CFA model is useful for observing nociception and anxiety-like behaviours in both males and females.

### Limitations of the CFA model

A major limitation of the CFA model is its inability to robustly model common chronic pain comorbidities in animals such as anxiety-like and depression-like behaviours. A recent report

from Chronic Pain Australia, found that 1 in 5 respondents with chronic pain had sought mental health help, highlighting the need for preclinical models to translate to the human condition (Chronic Pain Australia, 2024). The current standard methodologies for assessing pain-induced anxiety and depression behaviours in preclinical models have been criticised for their lack of translatability (Mogil, 2009). However, ethological behaviours such as nesting (Negus et al., 2015), facial expressions (Mogil et al., 2020), and pain-related behaviours in the place escape/avoidance paradigm (PEAP) (Refsgaard et al., 2016) have been shown to be affected by the CFA model and their implementation could improve researchers' ability to translate affective pain behaviours in preclinical models.

Another limitation of the CFA model is that it is not chronic. This study demonstrates the transient nociceptive hypersensitivity caused by this model. For studies investigating long-term treatment interventions, the CFA-induced persistent inflammatory model is not ideal because it is not long-lasting like other preclinical models of chronic pain such as diabetic neuropathic pain or osteoarthritis which can last for months in rodents (Drevet et al., 2022; O'Brien et al., 2014). Two studies have reported reduced mechanical thresholds for five to six weeks, although no anxiety-like behaviours were seen in this period (Burek et al., 2021; Urban et al., 2011). Overall, the CFA model is transient.

**Recommendations for using this model**

This study aimed to systematically define the CFA-induced persistent inflammatory pain model in nociceptive, locomotor, and anxiety-like behaviours in both males and females. We have developed a list of recommendations when considering the use of this model in future experiments:

1. Experiments should be conducted within a two-week period from hind paw injection to ensure mechanical and thermal hypersensitivity
2. Both male and female mice should be used, as nociceptive hypersensitivity is present in both
3. Nociceptive and other behaviours are time-sensitive, so ensure that the post injection day is kept consistent between treatment groups
4. Do not expect this model to robustly replicate chronic pain-induced anxiety-like behaviours using standard anxiety preclinical tests

5. Limit confounding variables such as handling, habituation schedules, and animal source

Therefore, this study concurrently assessed the behavioural outcomes of hind paw CFA injection in male and female mice with respect to its nociceptive mechanical and thermal effects as well as locomotion and anxiety-like behaviours over the time period that corresponds to maximal nociceptive effect. We demonstrated that the CFA model captures nociception deficits of persistent inflammatory pain, modelling the chronic pain pathologies in humans. However, it does a poor job at reliably modelling other aspects associated with the pain state, such as anxiety. These findings highlight the need for proper refinement of models and underscore the importance of developing better preclinical models of pain.

## 4.6 References (Chapter 4)


Anderson, W. B., Gould, M. J., Torres, R. D., Mitchell, V. A., & Vaughan, C. W. (2014). Actions of the dual FAAH/MAGL inhibitor JZL195 in a murine inflammatory pain model. *Neuropharmacology*, *81*, 224–230. https://doi.org/10.1016/j.neuropharm.2013.12.018

Bailey, K. R., & Crawley, J. N. (2009). Anxiety-Related Behaviors in Mice. In J. J. Buccafusco (Ed.), *Methods of Behavior Analysis in Neuroscience* (2nd ed.). CRC Press/Taylor & Francis. http://www.ncbi.nlm.nih.gov/books/NBK5221/

Baumbach, J. L., Leonetti, A. M., & Martin, L. J. (2024). Inflammatory injury induces pain sensitization that is expressed beyond the site of injury in male (and not in female) mice. *Behavioural Brain Research*, *475*, 115215. https://doi.org/10.1016/j.bbr.2024.115215

Bennett, G. J., & Xie, Y.-K. (1988). A peripheral mononeuropathy in rat that produces disorders of pain sensation like those seen in man. *Pain*, *33*(1), 87–107. https://doi.org/10.1016/0304-3959(88)90209-6

Bonin, R. P., Bories, C., & De Koninck, Y. (2014). A Simplified Up-Down Method (SUDO) for Measuring Mechanical Nociception in Rodents Using von Frey Filaments. *Molecular Pain*, *10*, 1744-8069-10–26. https://doi.org/10.1186/1744-8069-10-26

Bourin, M., & Hascoët, M. (2003). The mouse light/dark box test. *European Journal of Pharmacology*, *463*(1–3), 55–65. https://doi.org/10.1016/s0014-2999(03)01274-3

Burek, D. J., Massaly, N., Doering, M., Zec, A., Gaelen, J., & Morón, J. A. (2021). Long-term inflammatory pain does not impact exploratory behavior and stress coping strategies in mice. *Pain*, *162*(6), 1705–1721. https://doi.org/10.1097/j.pain.0000000000002179

Burek, D. J., Massaly, N., Yoon, H. J., Doering, M., & Morón, J. A. (2022). Behavioral outcomes of complete Freund adjuvant–induced inflammatory pain in the rodent hind paw: A systematic review and meta-analysis. *PAIN*, *163*(5), 809. https://doi.org/10.1097/j.pain.0000000000002467

Cardenas, A., Papadogiannis, A., & Dimitrov, E. (2021). The role of medial prefrontal cortex projections to locus ceruleus in mediating the sex differences in behavior in mice with inflammatory pain. *The FASEB Journal*, *35*(7), e21747. https://doi.org/10.1096/fj.202100319RR

Chen, J., Song, Y., Yang, J., Zhang, Y., Zhao, P., Zhu, X.-J., & Su, H. (2013). The contribution of TNF-α in the amygdala to anxiety in mice with persistent inflammatory pain. *Neuroscience Letters*, *541*, 275–280. https://doi.org/10.1016/j.neulet.2013.02.005

Chronic Pain Australia. (2024). *2024 National Pain Report: The social and economic cost of chronic pain*.

Cobos, E. J., Ghasemlou, N., Araldi, D., Segal, D., Duong, K., & Woolf, C. J. (2012). Inflammation-induced decrease in voluntary wheel running in mice: A nonreflexive test for evaluating inflammatory pain and analgesia. *PAIN®*, *153*(4), 876–884. https://doi.org/10.1016/j.pain.2012.01.016

Drevet, S., Favier, B., Brun, E., Gavazzi, G., & Lardy, B. (2022). Mouse Models of Osteoarthritis: A Summary of Models and Outcomes Assessment. *Comparative Medicine*, *72*(1), 3–13. https://doi.org/10.30802/AALAS-CM-21-000043

Dworkin, R. H., O'Connor, A. B., Audette, J., Baron, R., Gourlay, G. K., Haanpää, M. L., Kent, J. L., Krane, E. J., LeBel, A. A., Levy, R. M., Mackey, S. C., Mayer, J., Miaskowski, C., Raja, S. N., Rice, A. S. C., Schmader, K. E., Stacey, B., Stanos, S., Treede, R.-D., … Wells, C. D. (2010). Recommendations for the Pharmacological Management of Neuropathic Pain: An Overview and Literature Update. *Mayo Clinic Proceedings*, *85*(3 Suppl), S3–S14. https://doi.org/10.4065/mcp.2009.0649

Flores-García, M., Flores, Á., Aso, E., Otero-López, P., Ciruela, F., Videla, S., Grau-Sánchez, J., Rodríguez-Fornells, A., Bonaventura, J., & Fernández-Dueñas, V. (2025). Dopamine dynamics in chronic pain: Music-induced, sex-dependent, behavioral effects in mice. *PAIN Reports*, *10*(1), e1205. https://doi.org/10.1097/PR9.0000000000001205

François, A., Low, S. A., Sypek, E. I., Christensen, A. J., Sotoudeh, C., Beier, K. T., Ramakrishnan, C., Ritola, K. D., Sharif-Naeini, R., Deisseroth, K., Delp, S. L., Malenka, R. C., Luo, L., Hantman, A. W., & Scherrer, G. (2017). A Brainstem-Spinal Cord Inhibitory Circuit for Mechanical Pain Modulation by GABA and Enkephalins. *Neuron*, *93*(4), 822-839.e6. https://doi.org/10.1016/j.neuron.2017.01.008

Gaspar, J. C., Healy, C., Ferdousi, M. I., Roche, M., & Finn, D. P. (2021). Pharmacological Blockade of PPARα Exacerbates Inflammatory Pain-Related Impairment of Spatial Memory in Rats. *Biomedicines*, *9*(6), Article 6. https://doi.org/10.3390/biomedicines9060610

Greenspan, J. D., Craft, R. M., LeResche, L., Arendt-Nielsen, L., Berkley, K. J., Fillingim, R. B., Gold, M. S., Holdcroft, A., Lautenbacher, S., Mayer, E. A., Mogil, J. S., Murphy, A. Z., Traub, R. J., & the Consensus Working Group of the Sex, G. (2007). Studying sex and gender differences in pain and analgesia: A consensus report. *PAIN*, *132*, S26. https://doi.org/10.1016/j.pain.2007.10.014

Hofmann, L., Karl, F., Sommer, C., & Üçeyler, N. (2017). Affective and cognitive behavior in the alpha-galactosidase A deficient mouse model of Fabry disease. *PLOS ONE*, *12*(6), e0180601. https://doi.org/10.1371/journal.pone.0180601

Kandasamy, R., Calsbeek, J. J., & Morgan, M. M. (2016). Home cage wheel running is an objective and clinically relevant method to assess inflammatory pain in male and female rats. *Journal of Neuroscience Methods*, *263*, 115–122. https://doi.org/10.1016/j.jneumeth.2016.02.013

Kilkenny, C., Browne, W. J., Cuthill, I. C., Emerson, M., & Altman, D. G. (2010). Improving bioscience research reporting: The ARRIVE guidelines for reporting animal research. *Journal of Pharmacology & Pharmacotherapeutics*, *1*(2), 94–99. https://doi.org/10.4103/0976-500X.72351

Knight, B., Katz, D. R., Isenberg, D. A., Ibrahim, M. A., Le Page, S., Hutchings, P., Schwartz, R. S., & Cooke, A. (1992). Induction of adjuvant arthritis in mice. *Clinical and Experimental Immunology*, *90*(3), 459–465. https://doi.org/10.1111/j.1365-2249.1992.tb05868.x

Liu, Y., Yang, L., Yu, J., & Zhang, Y.-Q. (2015). Persistent, comorbid pain and anxiety can be uncoupled in a mouse model. *Physiology & Behavior*, *151*, 55–63. https://doi.org/10.1016/j.physbeh.2015.07.004

Meseguer Henarejos, A. B., Popović, N., Bokonjić, D., Morales-Delgado, N., Alonso, A., Caballero Bleda, M., & Popović, M. (2020). Sex and Time-of-Day Impact on Anxiety and Passive Avoidance Memory Strategies in Mice. *Frontiers in Behavioral Neuroscience*, *14*. https://doi.org/10.3389/fnbeh.2020.00068

Mitchell, V. A., Harley, J., Casey, S. L., Vaughan, A. C., Winters, B. L., & Vaughan, C. W. (2021). Oral efficacy of Δ(9)-tetrahydrocannabinol and cannabidiol in a mouse neuropathic pain model. *Neuropharmacology*, *189*, 108529. https://doi.org/10.1016/j.neuropharm.2021.108529

Mogil, J. S. (2009). Animal models of pain: Progress and challenges. *Nature Reviews Neuroscience*, *10*(4), 283–294. https://doi.org/10.1038/nrn2606

Mogil, J. S. (2012). Sex differences in pain and pain inhibition: Multiple explanations of a controversial phenomenon. *Nature Reviews Neuroscience*, *13*(12), 859–866. https://doi.org/10.1038/nrn3360

Mogil, J. S., Pang, D. S. J., Silva Dutra, G. G., & Chambers, C. T. (2020). The development and use of facial grimace scales for pain measurement in animals. *Neuroscience & Biobehavioral Reviews*, *116*, 480–493. https://doi.org/10.1016/j.neubiorev.2020.07.013

Narita, M., Kaneko, C., Miyoshi, K., Nagumo, Y., Kuzumaki, N., Nakajima, M., Nanjo, K., Matsuzawa, K., Yamazaki, M., & Suzuki, T. (2006). Chronic Pain Induces Anxiety with Concomitant Changes in Opioidergic Function in the Amygdala. *Neuropsychopharmacology*, *31*(4), 739–750. https://doi.org/10.1038/sj.npp.1300858

Negus, S. S., Neddenriep, B., Altarifi, A. A., Carroll, F. I., Leitl, M. D., & Miller, L. L. (2015). Effects of ketoprofen, morphine, and kappa opioids on pain-related depression of nesting in mice. *PAIN*, *156*(6), 1153. https://doi.org/10.1097/j.pain.0000000000000171

O'Brien, P. D., Sakowski, S. A., & Feldman, E. L. (2014). Mouse Models of Diabetic Neuropathy. *ILAR Journal*, *54*(3), 259–272. https://doi.org/10.1093/ilar/ilt052

Papadogiannis, A., & Dimitrov, E. (2022). A Possible Mechanism for Development of Working Memory Impairment in Male Mice Subjected to Inflammatory Pain. *Neuroscience*, *503*, 17–27. https://doi.org/10.1016/j.neuroscience.2022.09.007

Parent, A. J., Beaudet, N., Beaudry, H., Bergeron, J., Bérubé, P., Drolet, G., Sarret, P., & Gendron, L. (2012). Increased anxiety-like behaviors in rats experiencing chronic inflammatory pain. *Behavioural Brain Research*, *229*(1), 160–167. https://doi.org/10.1016/j.bbr.2012.01.001

Pitzer, C., Kuner, R., & Tappe-Theodor, A. (2016). Voluntary and evoked behavioral correlates in inflammatory pain conditions under different social housing conditions. *Pain Reports*, *1*(1), e564. https://doi.org/10.1097/PR9.0000000000000564

Pitzer, C., La Porta, C., Treede, R.-D., & Tappe-Theodor, A. (2019). Inflammatory and neuropathic pain conditions do not primarily evoke anxiety-like behaviours in C57BL/6 mice. *European Journal of Pain*, *23*(2), 285–306. https://doi.org/10.1002/ejp.1303

Refsgaard, L. K., Hoffmann-Petersen, J., Sahlholt, M., Pickering, D. S., & Andreasen, J. T. (2016). Modelling affective pain in mice: Effects of inflammatory hypersensitivity on place escape/avoidance behaviour, anxiety and hedonic state. *Journal of Neuroscience Methods*, *262*, 85–92. https://doi.org/10.1016/j.jneumeth.2016.01.019

Riebe, C. J., & Wotjak, C. T. (2012). A Practical Guide to Evaluating Anxiety-Related Behavior in Rodents. In A. Szallasi & T. Bíró (Eds.), *TRP Channels in Drug Discovery: Volume II* (pp. 167–185). Humana Press. https://doi.org/10.1007/978-1-62703-095-3_10

Rivera-García, L. G., Francis-Malavé, A. M., Castillo, Z. W., Uong, C. D., Wilson, T. D., Ferchmin, P. A., Eterovic, V., Burton, M. D., & Carrasquillo, Y. (2024). Anti-hyperalgesic and anti-inflammatory effects of 4R-tobacco cembranoid in a mouse model of inflammatory pain. *Journal of Inflammation (London, England)*, *21*(1), 2. https://doi.org/10.1186/s12950-023-00373-8

Sensini, F., Inta, D., Palme, R., Brandwein, C., Pfeiffer, N., Riva, M. A., Gass, P., & Mallien, A. S. (2020). The impact of handling technique and handling frequency on laboratory mouse welfare is sex-specific. *Scientific Reports*, *10*(1), 17281. https://doi.org/10.1038/s41598-020-74279-3

Sheahan, T. D., Siuda, E. R., Bruchas, M. R., Shepherd, A. J., Mohapatra, D. P., Gereau, R. W., & Golden, J. P. (2017). Inflammation and nerve injury minimally affect mouse voluntary behaviors proposed as indicators of pain. *Neurobiology of Pain*, *2*, 1–12. https://doi.org/10.1016/j.ynpai.2017.09.001

Soliman, N., & Denk, F. (2024). Practical approaches to improving translatability and reproducibility in preclinical pain research. *Brain, Behavior, and Immunity*, *115*, 38–42. https://doi.org/10.1016/j.bbi.2023.09.023

Sorge, R. E., Mapplebeck, J. C. S., Rosen, S., Beggs, S., Taves, S., Alexander, J. K., Martin, L. J., Austin, J.-S., Sotocinal, S. G., Chen, D., Yang, M., Shi, X. Q., Huang, H., Pillon, N. J., Bilan, P. J., Tu, Y., Klip, A., Ji, R.-R., Zhang, J., … Mogil, J. S. (2015). Different immune cells mediate mechanical pain hypersensitivity in male and female mice. *Nature Neuroscience*, *18*(8), 1081–1083. https://doi.org/10.1038/nn.4053

Sorge, R. E., Martin, L. J., Isbester, K. A., Sotocinal, S. G., Rosen, S., Tuttle, A. H., Wieskopf, J. S., Acland, E. L., Dokova, A., Kadoura, B., Leger, P., Mapplebeck, J. C. S., McPhail, M., Delaney, A., Wigerblad, G., Schumann, A. P., Quinn, T., Frasnelli, J., Svensson, C. I., … Mogil, J. S. (2014). Olfactory exposure to males, including men, causes stress and related analgesia in rodents. *Nature Methods*, *11*(6), 629–632. https://doi.org/10.1038/nmeth.2935

Stein, C., Millan, M. J., & Herz, A. (1988). Unilateral inflammation of the hindpaw in rats as a model of prolonged noxious stimulation: Alterations in behavior and nociceptive thresholds. *Pharmacology Biochemistry and Behavior*, *31*(2), 445–451. https://doi.org/10.1016/0091-3057(88)90372-3

Tonsfeldt, K. J., Suchland, K. L., Beeson, K. A., Lowe, J. D., Li, M., & Ingram, S. L. (2016). Sex Differences in GABAA Signaling in the Periaqueductal Gray Induced by Persistent Inflammation. *Journal of Neuroscience*, *36*(5), 1669–1681. https://doi.org/10.1523/JNEUROSCI.1928-15.2016

Treede, R.-D., Rief, W., Barke, A., Aziz, Q., Bennett, M. I., Benoliel, R., Cohen, M., Evers, S., Finnerup, N. B., First, M. B., Giamberardino, M. A., Kaasa, S., Korwisi, B., Kosek, E., Lavand'homme, P., Nicholas, M., Perrot, S., Scholz, J., Schug, S., … Wang, S.-J. (2019). Chronic pain as a symptom or a disease: The IASP Classification of Chronic Pain for the International Classification of Diseases (ICD-11). *PAIN*, *160*(1), 19. https://doi.org/10.1097/j.pain.0000000000001384

Treede, R.-D., Rief, W., Barke, A., Aziz, Q., Bennett, M. I., Benoliel, R., Cohen, M., Evers, S., Finnerup, N. B., First, M. B., Giamberardino, M. A., Kaasa, S., Kosek, E., Lavand'homme, P., Nicholas, M., Perrot, S., Scholz, J., Schug, S., Smith, B. H., … Wang, S.-J. (2015). A classification of chronic pain for ICD-11. *PAIN*, *156*(6), 1003. https://doi.org/10.1097/j.pain.0000000000000160

Urban, R., Scherrer, G., Goulding, E. H., Tecott, L. H., & Basbaum, A. I. (2011). Behavioral indices of ongoing pain are largely unchanged in male mice with tissue or nerve injury-induced mechanical hypersensitivity. *PAIN*, *152*(5), 990–1000. https://doi.org/10.1016/j.pain.2010.12.003

Wei, N., Guo, Z., Ye, R., Guan, L., Ren, J., Liang, Y., Shao, X., Fang, J., Fang, J., & Du, J. (2025). A systematic review of the pain-related emotional and cognitive impairments in chronic inflammatory pain induced by CFA injection and its mechanism. *IBRO Neuroscience Reports*, *18*, 414–431. https://doi.org/10.1016/j.ibneur.2025.02.015

Yoon, C., Wook, Y. Y., Sik, N. H., Ho, K. S., & Mo, C. J. (1994). Behavioral signs of ongoing pain and cold allodynia in a rat model of neuropathic pain. *PAIN*, *59*(3), 369. https://doi.org/10.1016/0304-3959(94)90023-X

Yu, W., Pati, D., Pina, M. M., Schmidt, K. T., Boyt, K. M., Hunker, A. C., Zweifel, L. S., McElligott, Z. A., & Kash, T. L. (2021). Periaqueductal gray/dorsal raphe dopamine neurons contribute to sex differences in pain-related behaviors. *Neuron*, *109*(8), 1365-1380.e5. https://doi.org/10.1016/j.neuron.2021.03.001

Zhang, Y., Luo, W., Heinricher, M. M., & Ryabinin, A. E. (2024). CFA-treated mice induce hyperalgesia in healthy mice via an olfactory mechanism. *European Journal of Pain*, *28*(4), 578–598. https://doi.org/10.1002/ejp.2201

Zhou, W., Jin, Y., Meng, Q., Zhu, X., Bai, T., Tian, Y., Mao, Y., Wang, L., Xie, W., Zhong, H., Zhang, N., Luo, M.-H., Tao, W., Wang, H., Li, J., Li, J., Qiu, B.-S., Zhou, J.-N., Li, X., … Zhang, Z. (2019). A neural circuit for comorbid depressive symptoms in chronic pain. *Nature Neuroscience*, *22*(10), 1649–1658. https://doi.org/10.1038/s41593-019-0468-2

## 4.7 Supplementary Data

### Supplementary Table 1: Statistical analysis details.

| PID | n/group | mean +/- SEM | Test | Main effect | F (DFn, DFd) | *p* value | Post-hoc | Saline-CFA | *p* value |
|---|---|---|---|---|---|---|---|---|---|
| 4hrs post-PID21 | 8 saline, 8 CFA (4 saline and 4 CFA for PID15 only) | - | Mixed-effect analysis | Time | F (3.668, 47.16) = 4.117 | 0.0074 | Bonferroni | Baseline | 0.8545 |
| | | | | Treatment | F (1, 14) = 28.96 | <0.0001 | | 4hrs Post | 0.033 |
| | | | | Time x Treatment | F (3.668, 47.16) = 3.470 | 0.0169 | | PID1 | 0.0005 |
| | | | | | | | | PID3 | 0.0006 |
| | | | | | | | | PID6 | 0.0027 |
| | | | | | | | | PID10 | 0.0007 |
| | | | | | | | | PID15 | 0.0143 |
| | | | | | | | | PID21 | 0.547 |
| 4hrs post-PID21 | 8 saline, 8 CFA (4 saline and 4 CFA for PID15 only) | - | Mixed-effect analysis | Time | F (3.740, 55.57) = 4.406 | 0.0044 | Bonferroni | Baseline | 0.4557 |
| | | | | Treatment | F (1, 104) = 90.23 | <0.0001 | | 4hrs Post | 0.0134 |
| | | | | Time x Treatment | F (3.740, 55.57) = 1.828 | 0.1404 | | PID1 | 0.0007 |
| | | | | | | | | PID3 | 0.0026 |
| | | | | | | | | PID6 | 0.0005 |
| | | | | | | | | PID10 | 0.0032 |
| | | | | | | | | PID15 | 0.011 |
| | | | | | | | | PID21 | 0.0048 |

| | | | | | | | | | |
|---|---|---|---|---|---|---|---|---|---|
| 4hrs post-PID21 | 8 saline, 8 CFA (4 saline and 4 CFA for PID15 only) | - | Mixed-effect analysis | Time | F (4.320, 55.54) = 7.050 | <0.0001 | Bonferroni | Baseline | 0.8891 |
| | | | | Treatment | F (1, 14) = 21.84 | 0.0004 | | 4hrs Post | 0.002 |
| | | | | Time x Treatment | F (4.320, 55.54) = 3.243 | 0.0161 | | PID1 | 0.0025 |
| | | | | | | | | PID3 | 0.0133 |
| | | | | | | | | PID6 | 0.0135 |
| | | | | | | | | PID10 | 0.0466 |
| | | | | | | | | PID15 | 0.0036 |
| | | | | | | | | PID21 | 0.1692 |
| 4hrs post-PID21 | 8 saline, 8 CFA (4 saline and 4 CFA for PID15 only) | - | Mixed-effect analysis | Time | F (5.469, 70.32) = 6.944 | <0.0001 | Bonferroni | Baseline | 0.9067 |
| | | | | Treatment | F (1, 14) = 6.317 | 0.0248 | | 4hrs Post | 0.5057 |
| | | | | Time x Treatment | F (5.469, 70.32) = 5.084 | 0.0003 | | PID1 | 0.0147 |
| | | | | | | | | PID3 | 0.0175 |
| | | | | | | | | PID6 | 0.0004 |
| | | | | | | | | PID10 | 0.7947 |
| | | | | | | | | PID15 | 0.0468 |
| | | | | | | | | PID21 | 0.3595 |
| PID2 | 8 saline, 8 CFA | Saline (55.04 ± 3.807), CFA (40.37 ± 3.683) | two-tailed, unpaired t-test | | t=2.768, df=14 | 0.0151 | | | |
| PID2 | 8 saline, 8 CFA | Saline (0.06113 ± 0.004185), CFA (0.04488 ± 0.004168) | two-tailed, unpaired t-test | | t=2.751, df=14 | 0.0156 | | | |
| PID2 | 8 saline, 8 CFA | Saline (703.2 ± 20.47), CFA (599.4 ± 27.03) | two-tailed, unpaired t-test | | t=3.060, df=14 | 0.0085 | | | |

| | | | | | |
|---|---|---|---|---|---|
| PID2 | 8 saline, 8 CFA | Saline (5.875 ± 0.7662), CFA (4.625 ± 0.6250) | two-tailed, unpaired t-test | t=1.264, df=14 | 0.2268 |
| PID2 | 8 saline, 8 CFA | Saline (70.13 ± 8.962), CFA (59.23 ± 10.32) | two-tailed, unpaired t-test | t=0.7975, df=14 | 0.4385 |
| PID2 | 8 saline, 8 CFA | Saline (50.63 ± 5.747), CFA (37.63 ± 5.028) | two-tailed, unpaired t-test | t=1.702, df=14 | 0.1108 |
| PID2 | 8 saline, 8 CFA | Saline (84.88 ± 4.129), CFA (82.63 ± 7.853) | two-tailed, unpaired t-test | t=0.2536, df=14 | 0.8035 |
| PID2 | 8 saline, 8 CFA | Saline (4.75 ± 1.236), CFA (3 ± 1.323) | two-tailed, unpaired t-test | t=0.9667, df=14 | 0.3501 |
| PID12 | 8 saline, 8 CFA | Saline (35.11 ± 2.56), CFA (37.86 ± 3.528) | two-tailed, unpaired t-test | t=0.6306, df=14 | 0.5384 |
| PID12 | 8 saline, 8 CFA | Saline (0.039 ± 0.00279), CFA (0.04213 ± 0.003889) | two-tailed, unpaired t-test | t=0.6529, df=14 | 0.5244 |
| PID12 | 8 saline, 8 CFA | Saline (545.2 ± 31.57), CFA (560.3 ± 31.85) | two-tailed, unpaired t-test | t=0.3370, df=14 | 0.7411 |
| PID12 | 8 saline, 8 CFA | Saline (5.125 ± 0.7181), CFA (3.25 ± 1.098) | two-tailed, unpaired t-test | t=1.429, df=14 | 0.1749 |
| PID12 | 8 saline, 8 CFA | Saline (89.59 ± 13.69), CFA (60.01 ± 12.19) | two-tailed, unpaired t-test | t=1.614, df=14 | 0.1289 |

| | | | | | |
|---|---|---|---|---|---|
| PID12 | 8 saline, 8 CFA | Saline (50.63 ± 5.747), CFA (37.63 ± 5.028) | two-tailed, unpaired t-test | t=1.702, df=14 | 0.1108 |
| PID12 | 8 saline, 8 CFA | Saline (67.13 ± 4.692), CFA (82.75 ± 4.992) | two-tailed, unpaired t-test | t=2.281, df=14 | 0.0387 |
| PID12 | 8 saline, 8 CFA | Saline (4.375 ± 1.523), CFA (15.88 ± 8.365) | two-tailed, unpaired t-test | t=1.352, df=14 | 0.1977 |
| PID2 | 8 saline, 8 CFA | Saline (45.39 ± 2.603), CFA (40.22 ± 2.769) | two-tailed, unpaired t-test | t=1.362, df=14 | 0.1949 |
| PID2 | 8 saline, 8 CFA | Saline (0.05038 ± 0.002834), CFA (0.04475 ± 0.003057) | two-tailed, unpaired t-test | t=1.349, df=14 | 0.1987 |
| PID2 | 8 saline, 8 CFA | Saline (613.9 ± 22.66), CFA (618.6 ± 28.25) | two-tailed, unpaired t-test | t=0.1308, df=14 | 0.8978 |
| PID2 | 8 saline, 8 CFA | Saline (3.625 ± 0.9437), CFA (5.25 ± 0.7734) | two-tailed, unpaired t-test | t=1.332, df=14 | 0.2042 |
| PID2 | 8 saline, 8 CFA | Saline (53.53 ± 7.637), CFA (66.51 ± 8.191) | two-tailed, unpaired t-test | t=1.160, df=14 | 0.2655 |
| PID2 | 8 saline, 8 CFA | Saline (41 ± 5.632), CFA (36.5 ± 3.85) | two-tailed, unpaired t-test | t=0.6597, df=14 | 0.5202 |
| PID2 | 8 saline, 8 CFA | Saline (83.5 ± 5.165), CFA (79.75 ± 6.259) | two-tailed, unpaired t-test | t=0.4621, df=14 | 0.6511 |
| PID2 | 8 saline, 8 CFA | Saline (3.625 ± 1.267), CFA (6.5 ± 1.991) | two-tailed, unpaired t-test | t=1.218, df=14 | 0.2433 |

| | | | | | |
|---|---|---|---|---|---|
| PID12 | 8 saline, 8 CFA | Saline (32.47 ± 1.462), CFA (34.19 ± 2.127) | two-tailed, unpaired t-test | t=0.6675, df=14 | 0.5153 |
| PID12 | 8 saline, 8 CFA | Saline (0.03613 ± 0.001652), CFA (0.038 ± 0.00236) | two-tailed, unpaired t-test | t=0.6508, df=14 | 0.5257 |
| PID12 | 8 saline, 8 CFA | Saline (482.2 ± 24.39), CFA (519.3 ± 25.44) | two-tailed, unpaired t-test | t=1.0533, df=14 | 0.3103 |
| PID12 | 8 saline, 8 CFA | Saline (1.875 ± 0.5154), CFA (4.75 ± 0.8399) | two-tailed, unpaired t-test | t=2.918, df=14 | 0.0112 |
| PID12 | 8 saline, 8 CFA | Saline (47.39 ± 7.022), CFA (58.06 ± 7.295) | two-tailed, unpaired t-test | t=1.054, df=14 | 0.3096 |
| PID12 | 8 saline, 8 CFA | Saline (37.63 ± 5.095), CFA (36.88 ± 6.212) | two-tailed, unpaired t-test | t=0.09335, df=14 | 0.9269 |
| PID12 | 8 saline, 8 CFA | Saline (69.25 ± 5.358), CFA (79.13 ± 3.42) | two-tailed, unpaired t-test | t=1.554, df=14 | 0.1426 |
| PID12 | 8 saline, 8 CFA | Saline (2.375 ± 1.281), CFA (7.625 ± 0.9808) | two-tailed, unpaired t-test | t=3.254, df=14 | 0.0058 |
| PID2 | 8 saline, 8 CFA | Saline (128.6 ± 7.950), CFA (111.9 ± 12.64) | two-tailed, unpaired t-test | t=1.125, df=14 | 0.2797 |
| PID2 | 8 saline, 8 CFA | Saline (20.13 ± 1.141), CFA (16.38 ± 2.591) | two-tailed, unpaired t-test | t=1.325, df=14 | 0.2065 |

| | | | | | |
|---|---|---|---|---|---|
| PID2 | 8 saline, 8 CFA | Saline (8.455 ± 0.7961), CFA (7.121 ± 1.054) | two-tailed, unpaired t-test | t=1.010, df=14 | 0.3295 |
| PID2 | 8 saline, 8 CFA | Saline (110.6 ± 12.36), CFA (103.9 ± 7.326) | two-tailed, unpaired t-test | t=0.4688, df=14 | 0.6464 |
| PID2 | 8 saline, 8 CFA | Saline (17.38 ± 2.478), CFA (15.5 ± 1.323) | two-tailed, unpaired t-test | t=0.6675, df=14 | 0.5153 |
| PID2 | 8 saline, 8 CFA | Saline (6.827 ± 0.9115), CFA (6.147 ± 0.6581) | two-tailed, unpaired t-test | t=0.6047, df=14 | 0.555 |
| PID8 | 8 saline, 8 CFA | Saline (150.4 ± 11.48), CFA (138 ± 11.6) | two-tailed, unpaired t-test | t=0.7630, df=14 | 0.4581 |
| PID8 | 8 saline, 8 CFA | Saline (16.63 ± 1.179), CFA (15.75 ± 1.897) | two-tailed, unpaired t-test | t=0.3917, df=14 | 0.7011 |
| PID8 | 8 saline, 8 CFA | Saline (8.42 ± 0.6481), CFA (8.334 ± 1.079) | two-tailed, unpaired t-test | t=0.06812, df=14 | 0.9467 |
| PID8 | 8 saline, 8 CFA | Saline (123.4 ± 14.85), CFA (107.4 ± 10.03) | two-tailed, unpaired t-test | t=8923, df=14 | 0.3873 |
| PID8 | 8 saline, 8 CFA | Saline (12.88 ± 1.875), CFA (11.63 ± 1.375) | two-tailed, unpaired t-test | t=0.5376, df=14 | 0.5993 |
| PID8 | 8 saline, 8 CFA | Saline (7.196 ± 0.6534), CFA (6.236 ± 0.5589) | two-tailed, unpaired t-test | t=1.116, df=14 | 0.2832 |

| | | | | | |
|---|---|---|---|---|---|
| PID12 | 8 saline, 8 CFA | Saline (142 ± 15.1), CFA (157.4 ± 10.59) | two-tailed, unpaired t-test | t=0.8350, df=14 | 0.4177 |
| PID12 | 8 saline, 8 CFA | Saline (13.38 ± 1.295), CFA (15 ± 1.239) | two-tailed, unpaired t-test | t=0.9067, df=14 | 0.3799 |
| PID12 | 8 saline, 8 CFA | Saline (7.235 ± 0.8608), CFA (8.866 ± 0.856) | two-tailed, unpaired t-test | t=1.344, df=14 | 0.2005 |
| PID12 | 8 saline, 8 CFA | Saline (119.5 ± 12.18), CFA (103 ± 10.94) | two-tailed, unpaired t-test | t=1.01, df=14 | 0.3295 |
| PID12 | 8 saline, 8 CFA | Saline (12 ± 1.309), CFA (11.63 ± 1.051) | two-tailed, unpaired t-test | t=0.2233, df=14 | 0.8265 |
| PID12 | 8 saline, 8 CFA | Saline (6.778 ± 0.4923), CFA (6.699 ± 0.656) | two-tailed, unpaired t-test | t=0.09617, df=14 | 0.9248 |
| PID4 | 8 saline, 8 CFA | Saline (47.11 ± 7.723), CFA (28.6 ± 2.731) | two-tailed, unpaired t-test | t=2.260, df=14 | 0.0403 |
| PID4 | 8 saline, 8 CFA | Saline (207.8 ± 11.41), CFA (229.8 ± 8.194) | two-tailed, unpaired t-test | t=1.564, df=14 | 0.1402 |
| PID4 | 8 saline, 8 CFA | Saline (46.2 ± 7.989), CFA (45.89 ± 5.979) | two-tailed, unpaired t-test | t=0.03132, df=14 | 0.9755 |
| PID4 | 8 saline, 8 CFA | Saline (208.4 ± 13.48), CFA (205 ± 9.221) | two-tailed, unpaired t-test | t=0.2081, df=14 | 0.8381 |
| PID13 | 8 saline, 8 CFA | Saline (51.75 ± 6.234), CFA (49.58 ± 8.942) | two-tailed, unpaired t-test | t=0.1995, df=14 | 0.8447 |

| | | | | | |
|---|---|---|---|---|---|
| PID13 | 8 saline, 8 CFA | Saline (203.2 ± 10.71), CFA (209.2 ± 11.3) | two-tailed, unpaired t-test | t=0.3902, df=14 | 0.7023 |
| PID13 | 8 saline, 8 CFA | Saline (46.66 ± 7.133), CFA (50.85 ± 7.701) | two-tailed, unpaired t-test | t=0.3989, df=14 | 0.696 |
| PID13 | 8 saline, 8 CFA | Saline (220.8 ± 13.8), CFA (219.1 ± 11.08) | two-tailed, unpaired t-test | t=0.09607, df=14 | 0.9248 |

# Chapter 5: The role of glycinergic neurons in the periaqueductal grey is altered in a chronic inflammatory pain state

**The role of glycinergic neurons in the periaqueductal grey is altered in a chronic inflammatory pain state**

Caitlin Fenech[1,2,3], Rebecca Power[1,2,3], Jonathan Tan[1,2,3], Neda Assareh[2,4], Yo Otsu[1,2] and Karin R Aubrey[1,2]

[1]Pain Management Research Laboratories, Kolling Institute, Royal North Shore Hospital NSLHD and Faculty of Medicine and Health, University of Sydney, Sydney NSW Australia

[2]Sydney Pain Consortium, Faculty of Medicine and Health, University of Sydney, Sydney NSW Australia

[3]School of Medical Sciences, Faculty of Medicine and Health, University of Sydney, Sydney NSW Australia

[4]Brain and Mind Centre, Faculty of Science, University of Sydney, Sydney NSW Australia

Contributions- Caitlin Fenech: conceptualisation, formal analysis, investigation (Figures 1-8), methodology, visualisation, writing -original draft, writing- review and editing. Rebecca Power: investigation (Figure 7), visualisation. Jonathan Tan: investigation (Figure 7). Neda Assareh: conceptualisation, investigation (Figure 7). Yo Otsu: conceptualisation, investigation (Figure 5), visualisation, writing-review and editing. Karin Aubrey: conceptualisation, funding acquisition, methodology, supervision, writing-review and editing.

## 5.1 Abstract

Chronic pain is a debilitating health condition, and the PAG is a key brain region involved with the dysfunctions associated with chronic pain states, including neuropathic pain and inflammatory pain. In a mouse model of persistent inflammatory pain (via hind paw injection of Complete Freund's Adjuvant, CFA), alterations in PAG function and modulation have been reported, although there is still much to learn about which cell types and pathways are affected and how they contribute. Glycinergic neurons in the ventrolateral column of the PAG ($PAG^{GlyT2}$ neurons) are a subpopulation of inhibitory projection neurons that modulate not only nociceptive responses but also locomotor, anxiety-like and aversion behaviours in a naïve state and thus, this study aimed to investigate the role of $PAG^{GlyT2}$ neurons in a mouse model of CFA-induced persistent inflammatory pain. We unexpectedly found that unlike in the naïve state, the ability of $PAG^{GlyT2}$ neurons to modulate nociceptive responses is lost in a CFA model. However, the ability of $PAG^{GlyT2}$ neurons to modulate locomotor and anxiety-like behaviours remained, but only in females. Interestingly, fibre photometry data suggests that these neurons are still engaged in this CFA state, but neuronal activity marking suggests that differential engagement of projection targets contribute to this shift in behavioural output. cFos and pPDH expression following chemogenetic activation via CNO suggests that one or more $PAG^{GlyT2}$ projections to the RVM, LH and PVT are responsible for nociceptive modulation. Overall, this study reveals that $PAG^{GlyT2}$ neurons are not a functionally homogenous group of cells and gives insight into the shift in midbrain circuitry between naïve and chronic pain states.

## 5.2 Introduction

Chronic pain is a highly debilitating condition that affects approximately 20% of the world's population (Goldberg & McGee 2011). Pharmacotherapies are reported to only be partially effective in less than half of patients (Dworkin et al. 2010) and many people suffering from chronic pain also have comorbidities including depression, anxiety and sleep disorders (Treede et al. 2019). Currently, the knowledge surrounding brain circuitry underlying chronic pain conditions and its complexity is incomplete and this study addresses this need through preclinical research.

The periaqueductal grey (PAG), in particular the ventrolateral column (vlPAG), is an important region in modulating acute and chronic pain. It is a major part of the ascending pain pathways, receiving noxious information directly from the spinal cord and connecting to a range of thalamic and cortical areas involved in processing nociceptive information and coordinating responses. It also is a major region in the descending analgesic pathway, directly modulating incoming noxious signal at the level of the spinal cord, via the rostral ventromedial medulla (RVM) (Basbaum et al. 2009, Denk et al. 2014, Lau & Vaughan 2014). The vlPAG is known to be involved with the dysfunctions associated with chronic pain states, including neuropathic pain and inflammatory pain (Samineni et al. 2019, Xie et al. 2023, McPherson et al. 2023, Kimmey et al. 2025, Yang et al. 2022, Zhu et al. 2024).

Several studies have reported key signalling changes in endogenous opioid and cannabinoid signalling in the vlPAG in response to CFA induced persistent inflammatory pain (Bouchet et al. 2023, Tonsfeldt et al. 2016, Wilson-Poe et al. 2021, Coutens et al. 2025, Kimmey et al. 2025, McPherson et al. 2023, Hurley & Hammond 2000). The Complete Freund's Adjuvant (CFA) persistent inflammatory pain model is widely used and involves a hind paw injection of the inflammatory agent, CFA, which causes inflammation that persists for weeks and reliably induces mechanical and thermal hypersensitivity in both rats and mice (Knight et al. 1992, Stein et al. 1988, Burek et al. 2022, Wei et al. 2025; see Chapter 4), modelling human chronic inflammatory pain pathologies. The vlPAG consists of ~104 different neuronal subtypes (Vaughn et al. 2022), although the understanding on the specific role and contribution of different neurons in persistent inflammatory pain is still being built upon. Glycinergic neurons, marked by the glycine transporter GlyT2, in the vlPAG ($PAG^{GlyT2}$) have been shown to respond to and modulate nociceptive and affective responses in a naïve state, potentially through their

projections to ascending and descending regions (*Chapter 3*), but their role in a persistent inflammatory pain state is unknown.

Therefore, this study aims to investigate if $PAG^{GlyT2}$ neuronal activity can modulate nociception, locomotion and anxiety-like behaviours in a CFA induced persistent inflammatory pain model. In addition, we will investigate if $PAG^{GlyT2}$ neurons are engaged during CFA and if chemogenetic modulation of $PAG^{GlyT2}$ neurons engages projection regions in a naïve and CFA state. As chemogenetic inhibition of $PAG^{GlyT2}$ neurons is analgesic, we hypothesise that in a CFA state it will alleviate nociceptive hypersensitivity.

## 5.3 Methods

### Animals

All experiments were conducted in accordance with the Australian Code for the care and use of animals for scientific purposes and approved by the University of Sydney Animal Ethics Committee (Protocol: 2023/2295). Adult male and female GlyT2::Cre (a gift from H.U. Zeilhofer; Foster et al., 2015) or GlyT2::cre x Ai14 mice (Jackson Laboratory; B6.Cg-Gt(ROSA)26Sortm14(CAG-tdTomato)Hze/J, Strain #: 007914) were bred and housed in the Kearns Animal Facility in ventilated cages with a maximum of four mice per cage. 12/12h light/dark cycle (23°C, 70% humidity) were maintained and food and water provided ad libitum. Cages were enriched with a house igloo, toilet paper roll, tissues for nesting and wooden blocks. All behavioural experiments were conducted during the light cycle between 9AM and 5PM under dim white light (30 ± 10 Lux).

### Stereotaxic surgery

Brain injections were carried out in a stereotaxic frame (Kopf Instruments) in adult mice (8-12 weeks old) under isoflurane anaesthesia (1.0-3% isoflurane in 1L/min O2). Pain relief was provided at the incision site (0.25% bupivacaine s.c) and viral vectors were injected with a nano-volume needle (200-300 mL; SEG Syringe 1mL, 0.63 mm OD, part #00500) using a motorized injector (50 nL/min, UMP3T-2 with SMARTouch, WPI). The following coordinates were used to target the vlPAG, from Bregma, AP: -4.65-4.7 mm, ML: ±0.35mm, DV: -3.00mm or AP: -4.65mm, ML: ±0.85mm, DV: -2.54mm on an 8 degree angle (which reduced loss of vector in the aqueduct and improved bilateral injection hit rate). Bilateral injections were made for all chemogenetic experiments and unilateral for fibre photometry. Unilateral injections were included in this study as it has been previously demonstrated to not be significantly different to bilateral (*Chapter 3*). After injection, the needle was kept in place for five minutes, retracted 0.1mm and left for a further five minutes before complete withdrawal.

For fibre photometry studies, following viral injection into the left or right vlPAG (counterbalanced across animals), a fibreoptic implant (200 µm diameter, 0.39 NA, RWD Science) was implanted at the vlPAG injection site and secured with the help of two small skull screws and Superbond C & B (Sun Medical) and Vertex self-Curing (Vertex Dental) applied to fix the fibre in place. Monocryl sutures 6-0 were used to close the wound and pain relief was

administered (buprenorphine, 0.05-0.1mg/g mice, s.c.). Following surgery, the mice were individually housed for recovery (two days) before being returned to their home cage. Experiments were commenced two (fibre photometry) or three weeks later (behaviour, electrophysiology or histology). For the chemogenetic study, animals were randomly allocated into a vehicle (10% DMSO and saline) or CNO (3mg/kg hM3D(Gq) or 5mg/kg hM4D(Gi)/mCherry control) i.p. injection group (mCherry controls were just injected with CNO to control for CNO off target effects). Behavioural experiments began 1 hour after i.p. injection.

**CFA-induced paw edema**

The Complete Freund's Adjuvant (CFA) preclinical model of persistent inflammatory pain was used in this study (Knight et al., 1992; Stein et al., 1988). Mice were anaesthetised with 2-3% isoflurane (1L/min $O_2$) and sedation was confirmed by the absence of a toe pinch reflex. Mice then received a single unilateral intraplantar left hind paw injection of 20µL undiluted CFA (Sigma-Aldrich). Similarly, control mice were injected unilaterally in the left hind paw with 20µL of 0.9% sterile saline.

**Nociceptive tests**

Nociceptive tests were all carried out on a single day with a minimum of 5-minute interval between tests except if noted (Assareh et al. 2023, Anderson et al. 2014, François et al. 2017, Mitchell et al. 2021).

**von Frey**

To assess mechanical hypersensitivity, we used the simplified up-down method (SUDO) using Von Frey filaments (Bonin et al. 2014). Animals were placed in elevated Perspex enclosures with wire mesh bases and given 30 minutes to acclimatise to the testing environment. Briefly, testing began with a 0.95 g von Frey hair in which it was pressed perpendicularly against the left hind paw and held for approximately two seconds. If the animal sharply withdrew their paw, licked their paw, or flinched upon removal of the von Frey filament, a withdrawal response was noted. The von Frey test was repeated four times on the injected paw with at least a two-

minute interval between tests. If a positive withdrawal response was observed, the subsequent test used a lighter filament whereas if no withdrawal response was seen the subsequent test used the next heavier filament. The final paw withdrawal threshold was calculated as the lightest force required to produce a withdrawal response.

**Acetone test**

To assess cold allodynia, we used the acetone test (Yoon et al. 1994). Animals remained in the elevated Perspex enclosures with wire mesh bases, and 20µL of acetone was sprayed on the centre of the left hind paw through the wire grid. The number of licks was recorded over a one-minute period. The test was repeated once on the same paw with at least five minutes between tests. The final value used for statistical analysis was the average of the number of licks between the two tests. For the fibre photometry experiments, acetone was applied to the ipsilateral and contralateral paw to the fibre optic cannula in an alternative order for five times each paw.

**Hotplate test**

To assess noxious heat sensitivity, we used the hotplate test. Each animal was placed on a 50℃ hotplate and latency to show either a licking or jumping nocifensive response was recorded. Once observed, the animal was immediately removed from the hotplate and returned to their home cage. Each animal was tested for a minimum of three trials with a fourth and fifth trial added if the results were not within four seconds of each other (Espejo et al. 1994).

**Open Field test**

Locomotor activity was measured using the open field test. One hour after i.p. injection of either vehicle or CNO and acclimatisation to the testing room, the mice were individually placed in an enclosed open-top arena (50 x 50 x 50 cm). An overhead camera recorded their behaviour for a 20-minute period. This period allowed for the monitoring of locomotion and potential anxiety-like behaviours (Bailey & Crawley 2009). Between animals, 20% ethanol was used to clean the apparatus to remove odour cues. The number of supported rearing responses and jumping responses was scored manually using Chronotate (Philipsberg et al. 2023) while the total distance travelled (m), average speed (m/s), total time mobile (s), time in the centre

zone (s) and number of entries into the centre zone was obtained through ANY-Maze video tracking software (Version 7; Stoelting Co.). The centre zone was classified as the middle 25cm x 25cm zone.

**Light-dark test**

The light-dark test was used to test anxiety-like behaviours (Bourin & Hascoët 2003). One hour after i.p. injection of either vehicle or CNO and acclimatisation to the testing room, the mice were individually placed in the light-dark box (dark chamber: 20 cm wide x 18 cm x 30 cm high; light chamber (60 ± 10 lux): 28 cm wide x 27 cm long x 30 cm high). The mice were placed in the light chamber facing the entry to the dark chamber and behaviour monitored with an overhead camera for five minutes. Between animals, 20% ethanol was used to clean the apparatus to remove odour cues. The following measures were obtained following ANY-Maze video tracking software analysis: number of entries into the light zone, time in the light zone (s) and latency to enter the dark zone (s).

**Elevated Plus Maze**

The elevated plus maze test was used in conjunction with the light-dark box to test anxiety-like behaviours (Riebe & Wotjak 2012). One hour after i.p. injection of either vehicle or CNO and acclimatisation to the testing room, the animals were individually placed in the centre of the elevated plus maze facing a closed arm (two 60cm arms, each 5cm wide, one enclosed by 15cm walls, 40cm elevated off the ground). An overhead camera recorded their behaviour for a five-minute period. Between animals, 20% ethanol was used to clean the apparatus to remove odour cues. The number of entries and time spent (s) in the open arms was obtained using ANY-Maze video tracking software.

**Fibre photometry**

Neuronal calcium activity was recorded via with the RWD fibre photometry system (R821 /FR-21Tricolor Multichannel Fiber Photometry System). A 410nm isosbestic signal was recorded to account for motion artefacts and the 470nm signal was used to detect GCaMP activity (30Hz, power = 20-30mW). Z-scores were calculated around events during behavioural

experiments verified with one to two cameras during behavioural recordings using RWD software. The area under the curve (AUC) was calculated before or after events using RWD software.

**Tissue processing**

At the end of the experimental period, mice were deeply anaesthetized (3-5% isoflurane; 1L/min $O_2$) then administered an injection of Lethobarb (200 mg/kg, i.p)) and transcardially perfused first with 0.9% saline containing 72.5 mM NaNO2 and 3 IU/ml heparin (Sigma-Aldrich) and then 4% paraformaldehyde (PFA) in 0.13 M PBS (pH 7.4). Brains were removed and postfixed overnight in the same fixative solution (4% PFA, 4°C). The tissue was then washed in PBS (pH 7.4) and dehydrated in 15% sucrose in PBS for 1-2 days, followed by 30% sucrose in PBS for 1-2 days and stored until cryo-sectioning. Brains were sectioned using a sliding microtome (-20°C, Leica Microsystems, Leica 1080) and four series of 40 $\mu$ m slices were collected and preserved in 0.1 M PBS containing 0.1% sodium azide at 4° C. The PAG slices from one series were mounted onto glass slides with Fluromount-G Mounting Medium (Invitrogen) and a glass coverslip. After drying, coverslip was sealed with nail polish.

**Immunofluorescence and immunohistochemistry**

For the cFos and pPDH immunofluorescence, slices from another series were selected and labelled with immunofluorescence. Separate series (subsequent slices) were used for cFos and pPDH staining as both protein's primary antibodies were from the same host animal (rabbit). Slices were washed in PBS (3 x 10 minutes), then incubated in blocking media (1 hour at RT, 10% donkey serum, 0.3% Triton X detergent in PBS). Then, sections were then incubated in primary antibody over three nights before being washed in PBS (3 x 30 minutes) and incubated with secondary antibody (2 hours at RT;10% donkey serum, 0.1% Triton X Detergent, 1:2000 DAPI antibody). Following a final wash in phosphate buffer (PB, 3 x 30 minutes), slices were mounted as previously described for imaging.

As cFos immunofluorescence expression in the rostral ventromedial medulla (RVM) was very low, colorimetric immunohistochemistry was used for a separate series of these slices (as described in Assareh et al., 2023, Appendix 1).

**Fluorescent and light microscopy**

Slices were imaged across the rostro-caudal axis on a fluorescent microscope (Zeiss Axio M1) and localized to region according to Paxinos and Franklin (2001). As the PAG is very close to the cerebral aqueduct, some DREADDs injections were unilateral, likely due to loss of vector into the aqueduct. The behavioural data obtained from animals with confirmed uni- and bilateral expression of mCherry, hM3D and hM4D was compared previously and no significant differences were detected, so data was pooled. Sparse labelling of neurons in the superior colliculus was occasionally noted near the injection tract.

**Data analysis**

For cFos and pPDH counting, region of interests was determined using the mouse brain atlas (Paxinos & Franklin 2001). For cFos counting, an unbiased automated counting protocol was used using ImageJ Fiji on 10x images. Subtract background was first used to isolate fluorescent signal from the image background, then the ImageJ plug-in Stardist (Schmidt et al. 2018) was used to identify fluorescent cell-like objects based on probability and overlap threshold. The watershed function was then used to isolate overlapping objects and cFos detections >300 pixels in size were excluded to isolate just cell like objects for counting. For the colorimetric RVM cFos images, manual counting was employed by a blinded experimenter (J.T) and the region of interest was set on a 1860131 $\mu m^2$ rectangle placed above the pyramidal tract, as automated counting did not detect cell-like objects authentically. For pPDH analysis, an initial threshold was set per image identifying signal by a blinded experimenter and intensity was calculated per area of region of interest. For each region one slice per animal was used for analysis, except for the LH in which 3/5 animals were averaged over two slices across the rostro-caudal axis and for the RVM colorimetric analyses in which an average of 1-4 slices from -5.6 to -6mm from bregma for each animal was used (identified as key RVM range for descending analgesic pathway activity) (Ganley et al. 2023). Manual counting was used for the Ai14xGlyT2::Cre experiment by a blinded experimenter, due to the inability of automated counting to detect TdTomato+ cells authentically.

All data was analysed using GraphPad Prism (version 10, GraphPad Software, Inc., La Jolla, CA) and presented as mean ± SEM. Significance, as indicated by an asterisk, was defined as $p < 0.05$ a priori. For all datasets, a Shapiro-Wilk test was performed to test normality. Unpaired t-tests were used for all analysis of chemogenetic experiments between CNO and vehicle controls. For comparisons with mCherry-CNO, a one-way ANOVA with Bonferroni correction was used. Fibre photometry experiment was analysed using a two-way ANOVA with Bonferroni correction. Individual unpaired t-tests were used to analyse differences between cFos/pPDH expression between CFA and saline controls or CNO and vehicle controls. A detailed statistical summary can be found in Supplementary Table 1. All behavioural test schematics were created with BioRender.

**Table 1: Vectors and antibodies**

| Name | Company | CAT# | Titre/concentration |
|---|---|---|---|
| **Viral Vectors** | | | |
| AAV5-hSyn-DIO-mCherry | Addgene | 50459 | 8.4*10^12 |
| AAV5-hSyn-DIO-hM3D(Gq)-mCherry | Addgene | 44361 | 2.3*10^13 |
| AAV5-hSyn-DIO-hM4D(Gi)-mCherry | Addgene | 44362 | 2.5*10^13 |
| AAV9-syn-FLEX-jGCamp8s-WPRE | Addgene | 162377 | 2.7*10^13 |
| **Primary antibodies** | | | |
| Rabbit anti-cFos | Cell signalling Tech | 2250T | 1:500 (fluorescence) 1:2000 (colorimetric) |
| Rabbit anti-pPDH | Cell signalling Tech | 37115S | 1:500 |
| Chicken anti-mCherry | Abcam | Ab205402 | 1:1000 |
| **Secondary antibodies** | | | |

| | | | |
|---|---|---|---|
| Donkey anti- rabbit Alexa Fluor 647 | Abcam | Ab150075 | 1:500 |
| Donkey anti-rabbit Alexa Fluor 488 | Abcam | Ab150073 | 1:1000 |

## 5.4 Results

We first aimed to investigate whether PAG$^{GlyT2}$ neurons can modulate nociceptive responses and anxiety-like behaviour in the CFA persistent inflammatory pain model using a similar chemogenetic approach to Chapter 3 (Figure 1, Supplementary Figure 1). On PID 2 and 7, animals underwent an additional von Frey test before vehicle or CNO i.p. injection to assess the progression of mechanical hypersensitivity and we found that females had significantly reduced paw withdrawal threshold at both timepoints, but males only reached significantly reduced paw withdrawal threshold at PID7, when compared to saline-injected animals (Figure 2A). Following vehicle or CNO i.p. injection, on PID7, both males and females had no significant changes in paw withdrawal thresholds (Figure 2B-E). The acetone test revealed that there were also no changes seen in number of responses following activation or inhibition of PAG$^{GlyT2}$ neurons in either males or females (Figure 2F-I). Similarly, in the hotplate test there was no significant differences between paw withdrawal latencies in both males and females (Figure 2J-M). This was also the case at PID 2 for both males and females (Supplementary Figures 2-3). Therefore, unlike in the naïve state (Chapter 3), chemogenetic modulation of PAG$^{GlyT2}$ neurons fail to alter nociceptive responses in the CFA persistent inflammatory pain model.

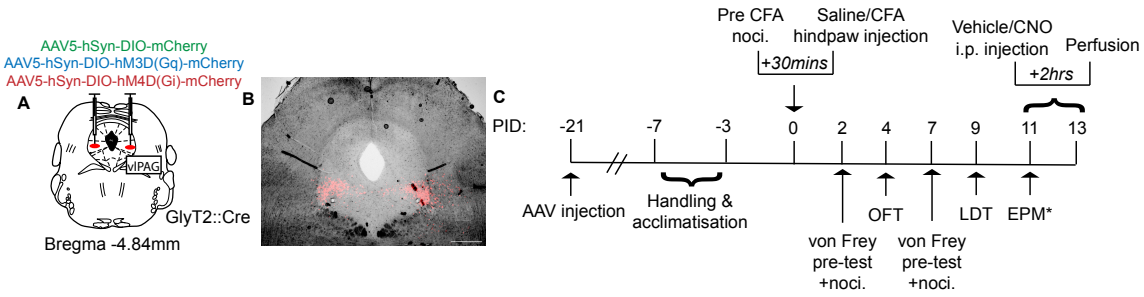


**Figure 1: Experimental groups and timeline for chemogenetic experiments.** (A) Schematic illustrating bilateral injection of viral vectors into the vlPAG of GlyT2::Cre mice (unilaterally injected animals were also included in this study) (B) Representative microscopic image of viral vector expression that was largely restricted within the vlPAG. Scale bar = 500$\mu$m, magnification: 2.5X. (C) Experimental timeline. PID: Post (CFA) injection day, noci: nociception tests (von Frey, acetone, hotplate), OFT: open field test, LDT: light-dark test, EPM: elevated plus maze. All animals were either perfused on PID 11 or PID 13. *The elevated plus maze was only conducted on a subset of animals, for which they were perfused on PID 13.

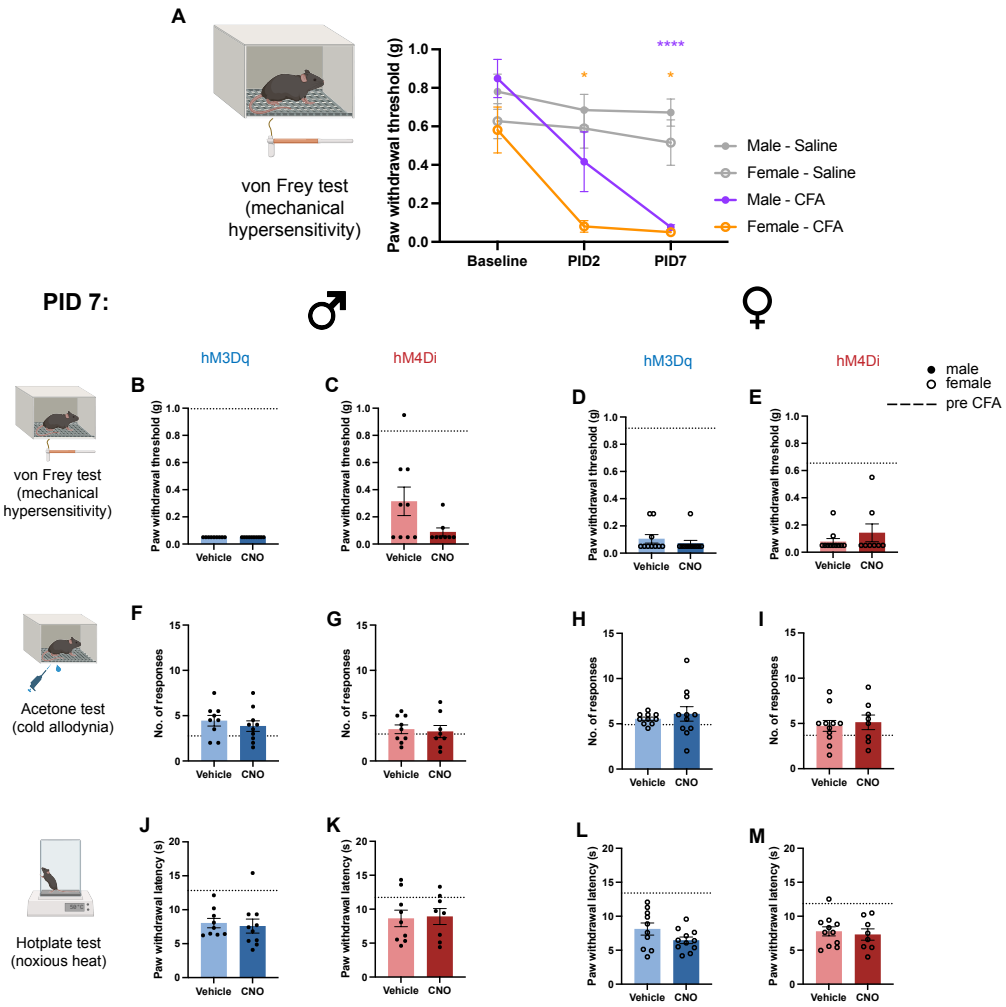


**Figure 2: Chemogenetic modulation of PAG$^{GlyT2}$ neurons does not alter nociceptive responses in the CFA model of persistent inflammatory pain.** (A) von Frey testing at baseline, PID 2 and PID 7 (before vehicle or CNO), confirmed mechanical hypersensitivity in females at PID 2 and PID7, and males at PID 7. At PID 7, there were no significant differences in paw withdrawal threshold, number of responses to acetone or paw withdrawal latency between vehicle and CNO for male (closed circle) and female (open circle) mice (B-M). Individual animals presented with bars representing mean ± SEM. n=7-11/group. Dotted line represents average of baseline values for the groups presented. *p<0.05, **p<0.01, ***p<0.001, ****p<0.0001.

We have previously shown that chemogenetic modulation of these neurons in a naïve state can modulate locomotor behaviours in both male and female mice (Chapter 3). Additionally, 2 days after the development of persistent inflammatory pain, locomotor behaviours in males are altered (Chapter 4). To investigate whether PAG$^{GlyT2}$ neurons continue to modulate locomotor behaviours in the CFA persistent inflammatory pain model we carried out the open field test one hour after i.p. injection of vehicle or CNO (Figure 3A-B). No baseline testing occurred for

the open field test to ensure novelty of the environment (Pitzer et al. 2019). We found that chemogenetic modulation of $PAG^{GlyT2}$ neurons does not change mobility in male mice but significantly increases mobility in female mice compared to vehicle controls (Figure 3C-F). In female mice, chemogenetic activation of $PAG^{GlyT2}$ neurons significantly increases the number of entries into the centre zone (Figure 3G-J) and continues to increase rearing behaviour in female mice compared to vehicle controls, but this function is absent in male animals (Figure 3K-N). Lastly, chemogenetic activation of $PAG^{GlyT2}$ neurons significantly increases jumps in only the female animals when compared to vehicle controls, although this difference may be CNO off-target effect as it is not seen between CNO injected groups (Figure 3O-R, Supplementary Figure 4). Therefore, when mice are in a persistent inflammatory pain state, $PAG^{GlyT2}$ neurons modulate locomotor activity in female but not male mice, this contrasts with the naïve state (Chapter 3) where significant changes in locomotor behaviours are observed in both male and females.

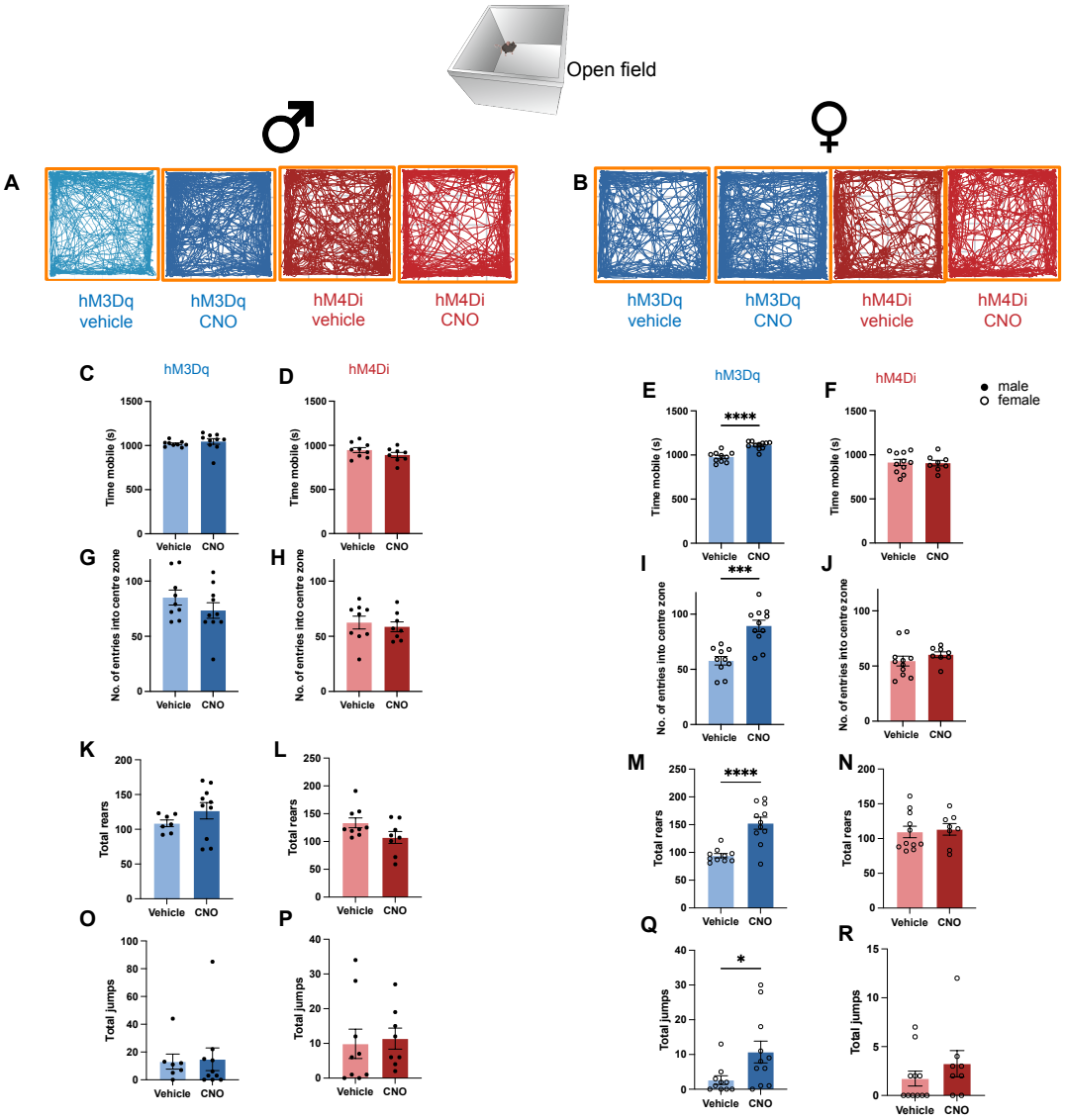


**Figure 3: Chemogenetic modulation of PAG$^{GlyT2}$ neurons does not alter locomotor behaviours in males but does in females.** Track plot of the centre point of male (A) and female (B) mice during the 20-minute open field test. Chemogenetic modulation resulted in no significant difference in mobility time, number of entries into the centre zone, rearing and jumping in the open field for males (closed circles; C, D, G, H, K, L, O, P). In females, chemogenetic activation resulted in significantly increased mobility, number of centre zone entries, rearing and jumping compared to vehicle controls (open circles; E, F, I, J, M, N, Q, R). Individual animals presented with bars representing mean ± SEM. n=7-11/group. Dotted line represents average of baseline values for the groups presented. *p<0.05, **p<0.01, ***p<0.001, ****p<0.0001.

We have previously shown that chemogenetic activation and inhibition of PAG$^{GlyT2}$ neurons reduces and increases anxiety-like behaviours respectively. Thus, we also investigated whether

chemogenetic modulation of PAG$^{GlyT2}$ neurons changes anxiety-like behaviours in mice with persistent inflammatory pain. Note, neither light-dark nor elevated plus maze behaviours are altered by CFA treatment at the time point tested. To test anxiety-like behaviours we did the light-dark test, in combination with the elevated plus maze on a subset of animals (Riebe & Wotjak 2012). Our data showed that chemogenetic activation of PAG$^{GlyT2}$ neurons reliably increased time spent in the light zone of the light dark test as well as time and entries in the open arms of the elevated plus maze in CFA-injected female mice compared to vehicle control groups. No significant changes were detected in light zone time as well as time and entries in the open arms in CFA-injected male mice compared to vehicle control groups (Figure 4, Supplementary Figure 5). Therefore, our data suggests that chemogenetic modulation of PAG$^{GlyT2}$ neurons continues to modulate anxiety-like behaviours in a persistent inflammatory pain state in female but not male mice.

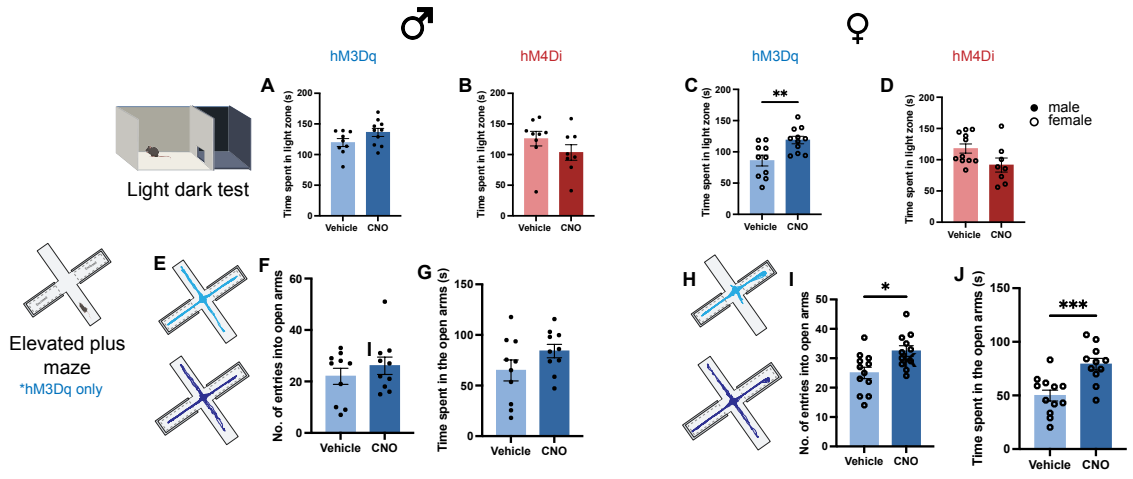


**Figure 4: Chemogenetic modulation of PAG$^{GlyT2}$ neurons alters anxiety-like behaviours in only female mice.** Chemogenetic modulation of PAG$^{GlyT2}$ neurons resulted in no significant differences in time spent in the light zone in the light dark test as well as number of entries or time spent in the open arms in the elevated plus maze in male mice compared to vehicle controls (closed circles; A, B, E, F, G). In females, chemogenetic activation significantly increased time spent in the light zone in the light dark test as well as significantly increased entries and time spent in the open arms in the elevated plus maze compared to vehicle controls (open circles; C, D, H, I, J). Track plot of the centre point of male (E) and female (H) mice during the 5-minute elevated plus maze test. Individual animals presented with bars representing mean ± SEM. n=7-11/group. Dotted line represents average of baseline values for the groups presented. *p<0.05, **p<0.01, ***p<0.001, ****p<0.0001.

To determine if PAG$^{GlyT2}$ neurons continue to be engaged during cold stimuli in a CFA state, as observed in a naïve state, we measured PAG$^{GlyT2}$ activity using calcium-dependent fibre photometry in male mice (Figure 5A, Supplementary Figure 6). The animals underwent an initial acetone test on both paws before hind paw injection of CFA in the contralateral paw to the fibre optic implant and an additional acetone test was carried out two days later (Figure 5B). Consistent with our previous findings, PAG$^{GlyT2}$ neuron calcium activity significantly increased in response to acetone application to the hind paw and no significant differences in signal amplitude was detected between the two paws (Figure 5C-E). Two days after CFA injection, this result was unchanged, with significant increases in PAG$^{GlyT2}$ neurons calcium activity in response to acetone on either the non-injected (ipsilateral) or the injected (contralateral) paw, with no significant difference between the two paws (Figure 5F-H). Although chemogenetic modulation of PAG$^{GlyT2}$ neurons in the CFA state loses the ability to modify nociceptive responses, these photometry experiments suggests that they are still engaged in response to cold stimuli.

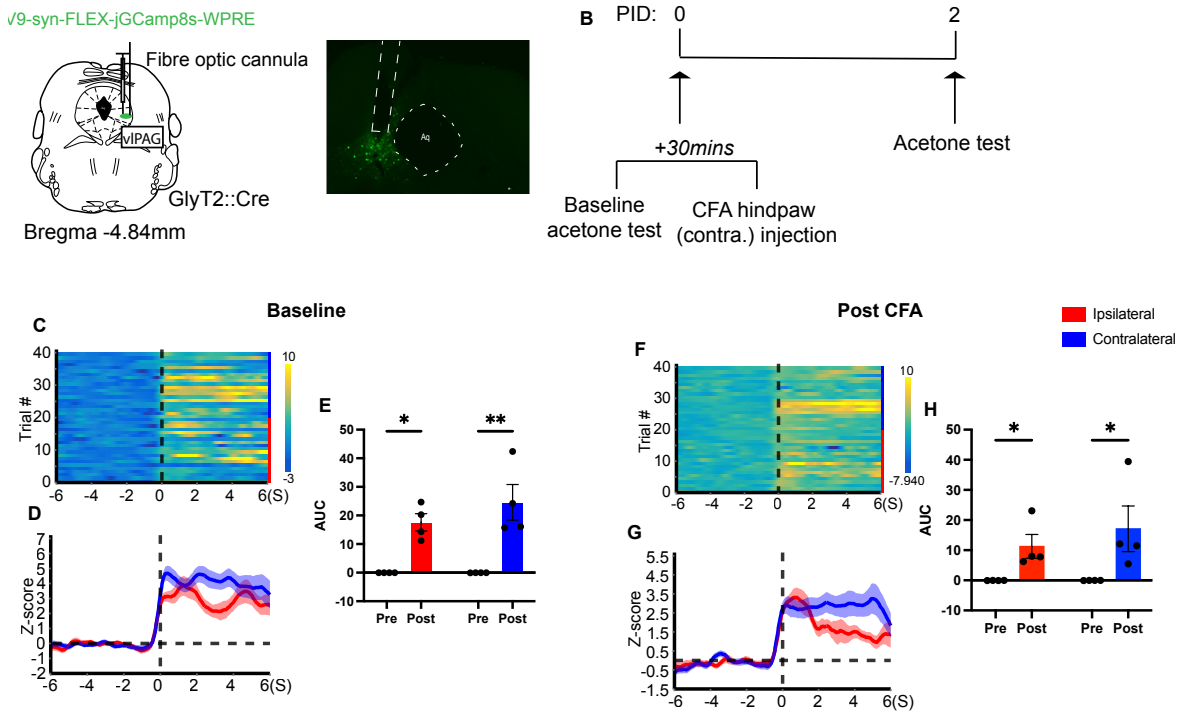


**Figure 5: Calcium dependent fibre photometry reveals that PAG$^{GlyT2}$ neurons are engaged during a cold noxious stimulus before and after CFA hind paw injection**. (A) Schematic depicting unilateral Cre dependent viral vector (jGCamp8s) injection and fibre optic cannula implantation into the vlPAG of GlyT2::Cre mice with representative microscope image (Scale bar = 500$\mu$m). (B) Experimental

timeline. Heatmap (C), average z-score trace (D) and area under the curve of pre and post stimulus of acetone on the ipsilateral (red) or contralateral (blue) paw (pre=-6 to 0s, post=0-6s), before CFA injection (Baseline). The AUC significantly increased post stimulus for both the ipsilateral and contralateral paw. Heatmap (F), average z-score trace (G) and area under the curve of pre and post stimulus of acetone on the ipsilateral (red) or contralateral (blue) paw (pre=-6 to 0s, post=0-6s), after CFA hind paw injection on the contralateral paw (Post CFA). The AUC significantly increased post stimulus for both the ipsilateral and contralateral paw. PID: post injection day, contra: contralateral paw, AUC: Area under the curve. Individual animals presented with bars representing mean ± SEM. n=4/group. *p<0.05, **p<0.01, ***p<0.001, ****p<0.0001

In a preliminary set of experiments in female mice, we also confirmed that the PAG is engaged by CFA hind paw injection. This was achieved by assessing differences in activity using cFos in the vlPAG, particularly in PAG$^{GlyT2}$ neurons, which were identified in GlyT2::crexAi14 mice by their expression of TdTomato (Supplementary Figure 7A). Animals injected with CFA had significantly reduced paw withdrawal threshold compared with animals with saline, confirming the validity of the model (Supplementary Figure 7B). On PID7, there was significantly increased cFos expression in the PAG of CFA-injected animals when compared to saline (Supplementary Figure C-D, Morales-Medina et al. 2023) and approximately 2 vs 10% of these cells are GlyT2+ in control vs CFA animals (Supplementary Figure 7E; not complete due to animal breeding house errors). Therefore, the CFA persistent inflammatory pain model engages the PAG.

To determine if PAG$^{GlyT2}$ neuronal projections to different projection targets might underly this separation of nociceptive, locomotor and anxiety-like responses, we carried out neuronal activity using immunohistochemical detection of the immediate early gene cFos for increases in neuronal activity and phosphorylated pyruvate dehydrogenase (pPDH) for decreases in neuronal activity (Yang et al. 2024, Morales-Medina et al. 2023). We quantified cFos and pPDH signals in tissue from naïve and CFA-model male and female mice expressing hM3Dq following chemogenetic activation of PAG$^{GlyT2}$ neurons with CNO or vehicle control (Figure 6A). As expected, chemogenetic activation of PAG$^{GlyT2}$ neurons with CNO resulted in significantly increased co-expression of cFos in mCherry+ vlPAG neurons compared to vehicle injected animals (Figure 6B-C, Assareh et al., 2023). Similar results were also observed in CFA-model animals (Figure 6D-E). No pPDH staining was observed in the vlPAG.

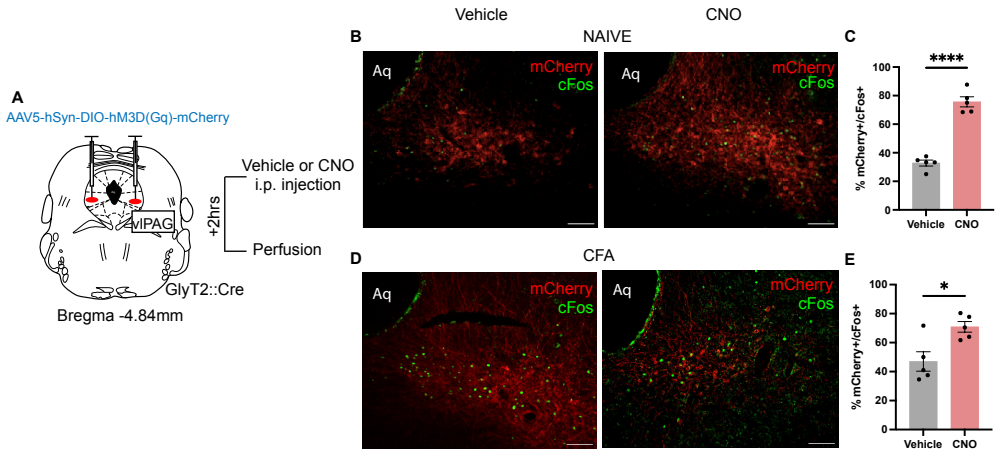


**Figure 6: PAG$^{GlyT2}$ neurons are engaged following chemogenetic activation via CNO in naïve and CFA states.** (A) Schematic showing bilateral stereotaxic injection of the excitatory Cre-dependent DREADD into the vlPAG of GlyT2::Cre mice, targeting PAG$^{GlyT2}$ cells. Two hours following either vehicle or CNO (3mg/kg) intraperitoneal (i.p.) injection, mice underwent cardiac perfusion for neuronal activity mapping. Representative images (B, D) and quantification (C, E) showing increased cFos expression in mCherry+ cells in CNO mice compared to vehicle in both naïve and CFA animals following chemogenetic activation of PAG$^{GlyT2}$ cells. Scale bar= 500$\mu$m. Magnification: 10X. Aq: Cerebral aqueduct. Individual animals presented with bars representing mean ± SEM. n=5/group (Naïve: vehicle=3 females, 2 males, CNO= 3 females, 2 males; CFA: vehicle=3 females, 2 males, CNO= 1 female, 4 males). *p<0.05, **p<0.01, ***p<0.001, ****p<0.0001

We then compared cFos and pPDH labelling at a selection of projection regions that have been reported to modulate pain responses (Ganley et al. 2023, Siemian et al. 2021, Di Li et al. 2025, Taylor & Westlund 2017). In naïve animals, cFos expression was unchanged by chemogenetic PAG$^{GlyT2}$ activation in the RVM and lPBN. On the other hand, cFos expression was significantly increased in PAG$^{GlyT2}$ projection regions including the LC, LH, and PVT when compared to vehicle. However, in CFA animals, cFos expression was significantly increased in only the LC (Figure 7A-B). In naïve animals, pPDH expression in RVM decreased (p=0.0598) but was unchanged in the LC, lPBN, LH and PVT when compared to vehicle controls. In CFA animals, there were no significant changes in pPDH expression in those regions (Figure 7C-D). Together with our behavioural findings, the neuronal activity data suggests that differential engagement of projection regions (RVM, LH and PVT) may contribute the different role of the PAG$^{GlyT2}$ neurons in the CFA state when compared to a naïve state.

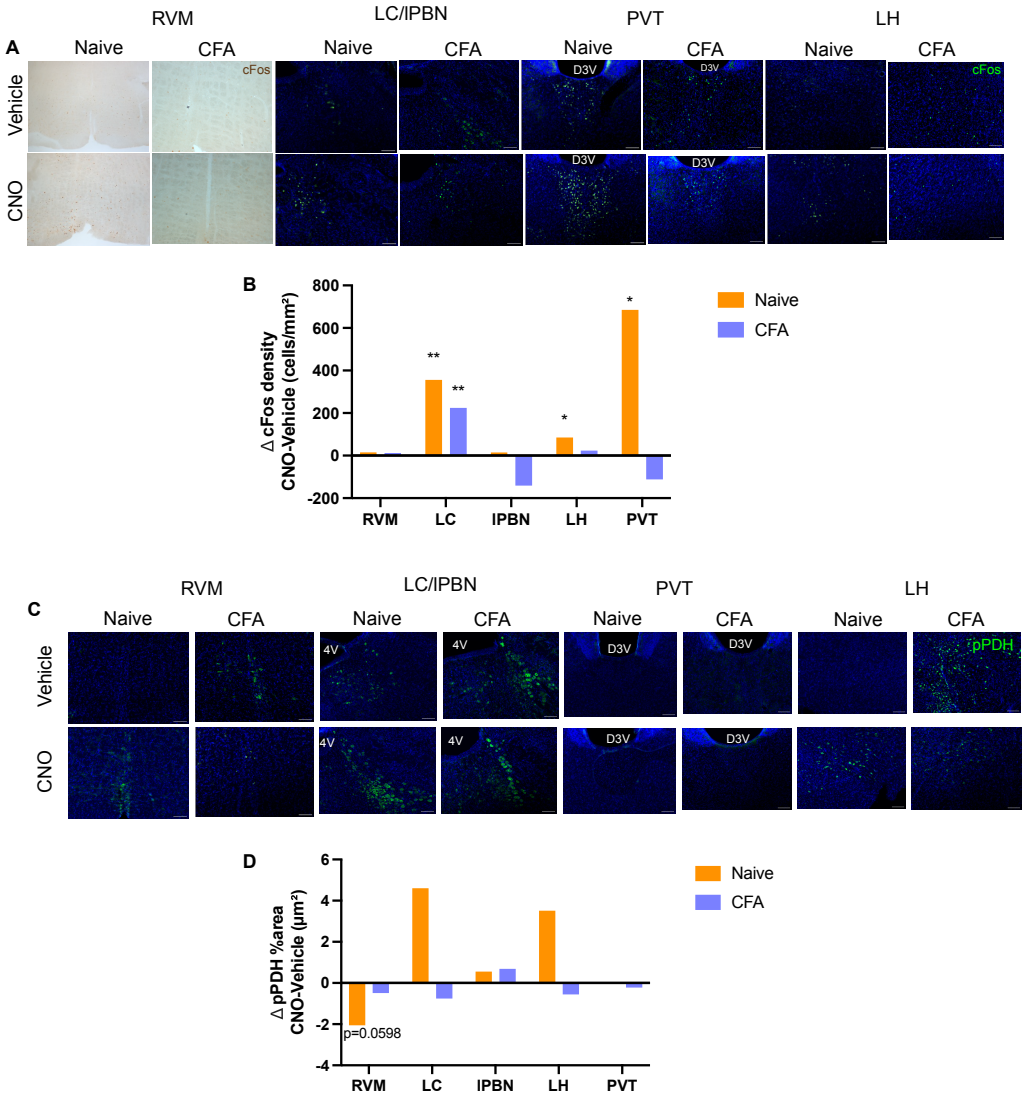


**Figure 7: Neuronal activity marking shows a shift in engagement of projection regions from a naïve to a CFA state.** (A, C) Representative images of cfos density (cells per mm$^2$) or PPDH intensity (percentage of area (µm$^2$) with signal) of vehicle and CNO mice, in both naïve and CFA states, following chemogenetic activation of PAG$^{GlyT2}$ cells in the RVM (-5.6--6mm), LC/lPBN (-5.34mm), PVT (-0.1mm) and LH (-0.1--1.8mm). n=5 animals/group; mean +/SEM. PAG: periaqueductal grey, RVM: rostral ventromedial medulla, pPDH: phosphorylation of pyruvate dehydrogenase, LC: locus coeruleus, PVT: paraventricular thalamus, D3V: third ventricle, LH; lateral hypothalamus, lPBN: lateral parabrachial nucleus, 4V: fourth ventricle.

## 5.5 Discussion

Here we show that in contrast to naïve animals (Chapter 3), in the CFA induced persistent inflammatory pain state, PAG$^{GlyT2}$ neurons are no longer able to modulate nociception but continue to modulate locomotor and anxiety-like behaviours in a sex specific manner (Figure 8). However, using fibre photometry, we found that PAG$^{GlyT2}$ neuronal activation by noxious cold stimulation occurs in this inflammatory persistent pain state, suggesting that these neurons are still receiving noxious information. Lastly, we illustrated using neuronal activity marking that this loss of nociception modulation is accompanied by a reduction in engagement with projections to the RVM, LH and PVT. This suggests that one or more of these projections are responsible for the PAG$^{GlyT2}$ neuronal specific nociceptive response. Overall, PAG$^{GlyT2}$ neuron function reveals an interesting shift in pain circuitry between a naïve and chronic pain state and suggests they are involved in the dysfunctions associated with chronic inflammatory pain.

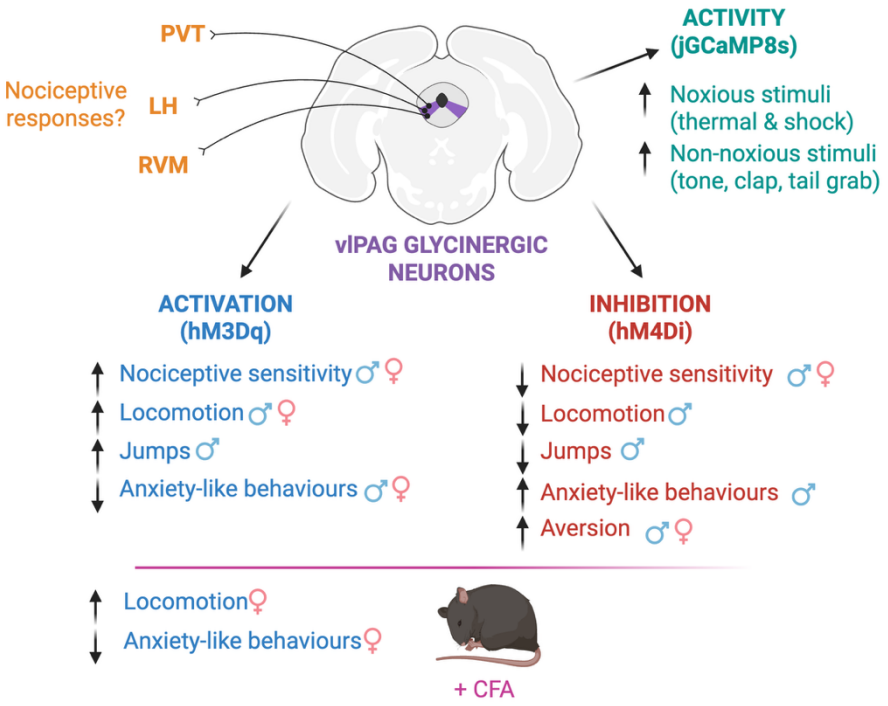


**Figure 8: Summary of the role of PAG$^{GlyT2}$ neurons.** Created with BioRender.

### PAG$^{GlyT2}$ neurons have a different role in naïve and chronic pain states

We initially hypothesised that chemogenetic inhibition of PAG$^{GlyT2}$ neurons would be able to alleviate heightened nociceptive sensitivity following the CFA model, however this was untrue.

It was unexpected to find that these neurons lost the ability to modulate nociception in the CFA state, as many studies have shown a conservation of modulation between naïve and chronic pains states (Samineni et al. 2019, Samineni et al. 2017, Siemian et al. 2021, Yang et al. 2022, Zhang et al. 2023, Bao et al. 2025). This suggests that PAG$^{GlyT2}$ neurons are part of the shift in PAG signalling that occurs in chronic pain states like the CFA model. This differential signalling in the vlPAG could be modulated through endogenous cannabinoids or opioids which have been previously shown to be altered in the vlPAG in the CFA model (Bouchet et al. 2023, Tonsfeldt et al. 2016, Wilson-Poe et al. 2021, Coutens et al. 2025, Kimmey et al. 2025, McPherson et al. 2023, Hurley & Hammond 2000). Indeed, the activity of endogenous opioids and cannabinoids is important for the descending pain pathway so their interaction with PAG$^{GlyT2}$ neurons would be probable.

Differential cannabinoid receptors and signalling have been demonstrated in females and not in males (Jiang et al. 2022, Tonsfeldt et al. 2016). We see a clear sex difference in PAG$^{GlyT2}$ neurons in their ability to modulate locomotor and anxiety-like behaviours only after a CFA state and cannabinoid signalling could be contributing to this. However, we have demonstrated that there are innate differences of the CFA model itself in males and females (Chapter 4) and thus it is hard to conclude if the sex differences reported here are due to PAG$^{GlyT2}$ neuronal modulation or the effects of the CFA model, or a combination of the two. In addition, ethological and anxiety-like behaviours have been reported to differ between sexes (Levy et al. 2023, Meseguer Henarejos et al. 2020, Kaluve et al. 2022) and thus, cannot be ignored. Interestingly, these striking sex differences were not present in naïve animals (Chapter 3). One theory could be that not all PAG$^{GlyT2}$ neurons are targeted by chemogenetic modulation, and the firing state influenced by CNO administration after CFA treatment is not the same as in naïve animals. This may be due to alterations in cell properties, such as firing patterns, thresholds and resting potentials, due to opioid or cannabinoid signalling. To test whether endogenous opioid or cannabinoid signalling could be influencing the activity of PAG$^{GlyT2}$ neurons, future experiments could use electrophysiology, to investigate signalling in PAG$^{GlyT2}$ neurons in a CFA state.

### PAG$^{GlyT2}$ neurons are not a functionally homogenous group of cells

In addition to the interaction of different neuromodulators within the PAG, the influence of differential engagement of projection regions may be contributing to the shift between the naïve

and CFA state. Our cfos/pPDH data suggests that the projections to the RVM, LH and PVT modulate nociception while the LC projection modulates locomotor and anxiety-like behaviours, an established role of the LC (Morris et al. 2020, McCall et al. 2015, Riga et al. 2025). It should be noted that the cfos/pPDH experiments were conducted in both male and females, so the role of the LC projection is unclear. Unpublished and preliminary data from our lab has also suggested that projections to the LH and PVT are from different PAG subpopulations, so together with the cfos/pPDH data there is possible evidence of different neuronal subpopulations within the $PAG^{GlyT2}$ group of neurons.

In a naïve state, we expected that chemogenetic activation of $PAG^{GlyT2}$ neurons would increase neuronal activity in the descending pain pathway, mainly the RVM (Winters et al. 2022, Lau & Vaughan 2014, Lau et al. 2020), and the reduced pPDH expression suggests this may be the case. We also see engagement of the LH and PVT following chemogenetic activation of $PAG^{GlyT2}$ neurons, both reported to modulate nociception (Siemian et al. 2021, Li et al. 2024, Di Li et al. 2025). Future experiments could use optogenetics to specifically target one of the projections in a CFA state and see the behavioural outcome. In addition, it would be interesting to investigate if these projections can be differentiated by different neurochemical properties of $PAG^{GlyT2}$ neurons. For example, transcriptomic and FISH studies suggest that $PAG^{GlyT2}$ neurons may also be neuropeptide Y(NPY)-positive (Vaughn et al. 2022, Lein et al. 2007, Allen Institute of Brain Science), an interesting theory could be that $PAG^{GlyT2}$ neurons could be separated into NPY positive and negative subpopulations that could differentiate their projections and engagement to these regions. Therefore, $PAG^{GlyT2}$ neurons are not a functionally homogenous group of cells as different projections are responsible for different behavioural outputs, and their projections and function are sensitive to a CFA inflammatory persistent pain state.

**Limitations**

One limitation of this study is the contribution of off-target CNO effects (Gomez et al. 2017, Mahler & Aston-Jones 2018). A small proportion of systemically administered CNO, has been previously shown to reverse-metabolise into clozapine, an antipsychotic drug that not only crosses the blood brain barrier but also more potently binds to DREADDs than CNO and modulates pain and anxiety (Gomez et al. 2017, Mahler & Aston-Jones 2018, Xuan Li et al. 2025, Manvich et al. 2018). As CNO off-target effects were not observed in our naïve study

(Chapter 3), it is unlikely that the contribution of CNO could affect our results, and we see no indication of this in the nociception and locomotor data. However, in the light dark test, we observed a significant increase in time spent in the light zone in females, only when the hM3Dq group was compared to vehicle controls and not when the control mCherry-CNO group was compared directly to the hM3Dq-CNO group. Further elevated plus maze experiments were only conducted on a subset of animals and thus CNO-off target effects may be contributing to this anxiety-like result in females. The addition of a mCherry-vehicle group would be able to determine any CNO-off target effects or the consideration of recently discovered DREADD agonists with improved selectivity such as DCZ and J60 (Nagai et al. 2020, Bonaventura et al. 2019) although off-target effects may still be present and relevant controls are still required (Lawson et al. 2023).

In addition, we used fluorescent cFos expression for all projection region automated analysis however in the RVM (a key region we wanted to investigate) it was unable to be detected. Thus, we used a standard colorimetric immunohistochemistry protocol that was used earlier for our initial PAG study (Assareh et al 2023, Appendix 1). This change in protocol between other regions could contribute to the non-significant result in cFos expression in the RVM and future experiments should optimise fluorescent cFos expression in the RVM to be comparable with the rest of the brain (i.e. using a different cFos primary antibody such as the guinea pig anti-cFos from Synaptic Systems) (Teng et al. 2022, Zhang et al. 2025, Wojick et al. 2025).

## Conclusion

In conclusion, a small subpopulation of glycinergic neurons in the vlPAG is involved in the pain circuitry shift between a naïve and persistent inflammatory pain state. By understanding the role of different subpopulations of neurons and their outputs, we can further understand the complexity of how the central nervous system can compute a range of behaviours. Thus, this novel study reveals new insights into the complexity of chronic pain circuits in the midbrain.

## 5.6 References (Chapter 5)


Anderson, WB et al. 2014, 'Actions of the dual FAAH/MAGL inhibitor JZL195 in a murine inflammatory pain model', *Neuropharmacology*, vol. 81, pp. 224–230, viewed 24 September 2025, <https://www.sciencedirect.com/science/article/pii/S0028390813005960>.

Assareh, N et al. 2023, 'Bidirectional Modulation of Nociception by GlyT2+ Neurons in the Ventrolateral Periaqueductal Gray', *eNeuro*, vol. 10, no. 6, viewed 18 July 2024, <https://www.eneuro.org/content/10/6/ENEURO.0069-23.2023>.

Bailey, KR & Crawley, JN 2009,'Anxiety-Related Behaviors in Mice', in JJ Buccafusco (ed.), *Methods of Behavior Analysis in Neuroscience*, Frontiers in Neuroscience, CRC Press/Taylor & Francis, Boca Raton (FL), viewed 28 July 2025, <http://www.ncbi.nlm.nih.gov/books/NBK5221/>.

Bao, S-T et al. 2025, 'Excitatory projections from the nucleus reuniens to the medial prefrontal cortex modulate pain and depression-like behaviors in mice', *PLOS Biology*, vol. 23, no. 5, p. e3003170, viewed 11 September 2025, <https://journals.plos.org/plosbiology/article?id=10.1371/journal.pbio.3003170>.

Basbaum, AI et al. 2009, 'Cellular and Molecular Mechanisms of Pain', *Cell*, vol. 139, no. 2, pp. 267–284, viewed 24 September 2025, <https://www.sciencedirect.com/science/article/pii/S0092867409012434>.

Bonaventura, J et al. 2019, 'High-potency ligands for DREADD imaging and activation in rodents and monkeys', *Nature Communications*, vol. 10, no. 1, p. 4627, viewed 24 September 2025, <https://www.nature.com/articles/s41467-019-12236-z>.

Bonin, RP, Bories, C, & De Koninck, Y 2014, 'A Simplified Up-Down Method (SUDO) for Measuring Mechanical Nociception in Rodents Using von Frey Filaments', *Molecular Pain*, vol. 10, pp. 1744-8069-10–26, viewed 28 July 2025, <https://doi.org/10.1186/1744-8069-10-26>.

Bouchet, CA et al. 2023, 'Monoacylglycerol Lipase Protects the Presynaptic Cannabinoid 1 Receptor from Desensitization by Endocannabinoids after Persistent Inflammation', *Journal of Neuroscience*, vol. 43, no. 30, pp. 5458–5467, viewed 23 September 2025, <https://www.jneurosci.org/content/43/30/5458>.

Bourin, M & Hascoët, M 2003, 'The mouse light/dark box test', *European Journal of Pharmacology*, vol. 463, no. 1–3, pp. 55–65.

Burek, DJ et al. 2022, 'Behavioral outcomes of complete Freund adjuvant–induced inflammatory pain in the rodent hind paw: a systematic review and meta-analysis', *PAIN*, vol. 163, no. 5, p. 809, viewed 28 August 2024, <https://journals.lww.com/pain/fulltext/2022/05000/behavioral_outcomes_of_complete_freund.3.aspx>.

Coutens, B et al. 2025, 'Corticosterone stimulates synthesis of 2-arachidonoylglycerol via putative membrane-bound glucocorticoid receptors and inhibits GABA release via CB1 cannabinoid receptors in the ventrolateral periaqueductal gray', *Molecular Pharmacology*, vol. 107, no. 8, p. 100058, viewed 24 September 2025, <https://www.sciencedirect.com/science/article/pii/S0026895X25153182>.

Denk, F, McMahon, SB, & Tracey, I 2014, 'Pain vulnerability: a neurobiological perspective', *Nature Neuroscience*, vol. 17, no. 2, pp. 192–200, viewed 24 September 2025, <https://www.nature.com/articles/nn.3628>.

Dworkin, RH et al. 2010, 'Recommendations for the Pharmacological Management of Neuropathic Pain: An Overview and Literature Update', *Mayo Clinic Proceedings*, vol. 85, no. 3 Suppl, pp. S3–S14, viewed 10 September 2025, <https://www.ncbi.nlm.nih.gov/pmc/articles/PMC2844007/>.

Espejo, EF et al. 1994, 'Effects of morphine and naloxone on behaviour in the hot plate test: an ethopharmacological study in the rat', *Psychopharmacology*, vol. 113, no. 3, pp. 500–510, viewed 24 September 2025, <https://doi.org/10.1007/BF02245230>.

François, A et al. 2017, 'A Brainstem-Spinal Cord Inhibitory Circuit for Mechanical Pain Modulation by GABA and Enkephalins', *Neuron*, vol. 93, no. 4, pp. 822-839.e6, viewed 24 September 2025, <https://www.sciencedirect.com/science/article/pii/S0896627317300107>.

Ganley, RP et al. 2023, 'Descending GABAergic Neurons of the RVM That Mediate Widespread Bilateral Antinociception', , p. 2023.04.29.538824, viewed 23 September 2025, <https://www.biorxiv.org/content/10.1101/2023.04.29.538824v1>.

Goldberg, DS & McGee, SJ 2011, 'Pain as a global public health priority', *BMC Public Health*, vol. 11, no. 1, p. 770, viewed 24 September 2025, <https://doi.org/10.1186/1471-2458-11-770>.

Gomez, JL et al. 2017, 'Chemogenetics revealed: DREADD occupancy and activation via converted clozapine', *Science*, vol. 357, no. 6350, pp. 503–507, viewed 24 September 2025, <https://www.science.org/doi/10.1126/science.aan2475>.

Hurley, RW & Hammond, DL 2000, 'The Analgesic Effects of Supraspinal μ and δ Opioid Receptor Agonists Are Potentiated during Persistent Inflammation', *Journal of Neuroscience*, vol. 20, no. 3, pp. 1249–1259, viewed 24 September 2025, <https://www.jneurosci.org/content/20/3/1249>.

Jiang, Z et al. 2022, 'Sex-specific cannabinoid 1 receptors on GABAergic neurons in the ventrolateral periaqueductal gray mediate analgesia in mice', *Journal of Comparative Neurology*, vol. 530, no. 13, pp. 2315–2334, viewed 11 September 2025, <https://onlinelibrary.wiley.com/doi/abs/10.1002/cne.25334>.

Kaluve, AM, Le, JT, & Graham, BM 2022, 'Female rodents are not more variable than male rodents: A meta-analysis of preclinical studies of fear and anxiety', *Neuroscience & Biobehavioral Reviews*, vol. 143, p. 104962, viewed 24 September 2025, <https://www.sciencedirect.com/science/article/pii/S0149763422004511>.

Kimmey, BA et al. 2025, 'Convergent state-control of endogenous opioid analgesia', *bioRxiv*, p. 2025.01.03.631111, <http://biorxiv.org/content/early/2025/01/04/2025.01.03.631111.abstract>.

Knight, B et al. 1992, 'Induction of adjuvant arthritis in mice.', *Clinical and Experimental Immunology*, vol. 90, no. 3, pp. 459–465, viewed 25 July 2025, <https://www.ncbi.nlm.nih.gov/pmc/articles/PMC1554568/>.

Lau, BK & Vaughan, CW 2014, 'Descending modulation of pain: the GABA disinhibition hypothesis of analgesia', *Current Opinion in Neurobiology*, vol. 29, pp. 159–164, viewed 24 September 2025, <https://www.sciencedirect.com/science/article/pii/S0959438814001378>.

Lau, BK, Winters, BL, & Vaughan, CW 2020, 'Opioid presynaptic disinhibition of the midbrain periaqueductal grey descending analgesic pathway', *British Journal of Pharmacology*, vol. 177, no. 10, pp. 2320–2332, viewed 23 September 2025, <https://onlinelibrary.wiley.com/doi/abs/10.1111/bph.14982>.

Lawson, KA, Ruiz, CM, & Mahler, SV 2023, 'A head-to-head comparison of two DREADD agonists for suppressing operant behavior in rats via VTA dopamine neuron inhibition', *Psychopharmacology*, vol. 240, no. 10, pp. 2101–2110, viewed 24 September 2025, <https://pmc.ncbi.nlm.nih.gov/articles/PMC10794001/>.

Lein, ES et al. 2007, 'Genome-wide atlas of gene expression in the adult mouse brain', *Nature*, vol. 445, no. 7124, pp. 168–176.

Levy, DR et al. 2023, 'Mouse spontaneous behavior reflects individual variation rather than estrous state', *Current biology: CB*, vol. 33, no. 7, pp. 1358-1364.e4.

Li, D et al. 2024, 'A neural circuit from thalamic paraventricular nucleus via zona incerta to periaqueductal gray for the facilitation of neuropathic pain', *Neurobiology of Disease*, vol. 202, p. 106699, viewed 11 September 2025, <https://www.sciencedirect.com/science/article/pii/S0969996124002997>.

Li, Di et al. 2025, 'The paraventricular thalamus mediates visceral pain and anxiety-like behaviors via two distinct pathways', *Neuron*, vol. 113, no. 14, pp. 2310-2324.e7, viewed 30 July 2025, <https://www.sciencedirect.com/science/article/pii/S0896627325003022>.

Li, Xuan et al. 2025, 'Off-targets effects of CNO on somatosensory and anxiety-related behaviors in rats', *Brain Research Bulletin*, vol. 229, p. 111474, viewed 24 September 2025, <https://www.sciencedirect.com/science/article/pii/S0361923025002862>.

Mahler, SV & Aston-Jones, G 2018, 'CNO Evil? Considerations for the Use of DREADDs in Behavioral Neuroscience', *Neuropsychopharmacology*, vol. 43, no. 5, pp. 934–936, viewed 24 September 2025, <https://pmc.ncbi.nlm.nih.gov/articles/PMC5854815/>.

Manvich, DF et al. 2018, 'The DREADD agonist clozapine N-oxide (CNO) is reverse-metabolized to clozapine and produces clozapine-like interoceptive stimulus effects in rats and mice', *Scientific Reports*, vol. 8, no. 1, p. 3840, viewed 24 September 2025, <https://www.nature.com/articles/s41598-018-22116-z>.

McCall, JG et al. 2015, 'CRH Engagement of the Locus Coeruleus Noradrenergic System Mediates Stress-Induced Anxiety', *Neuron*, vol. 87, no. 3, pp. 605–620.

McPherson, KB et al. 2023, 'Persistent inflammation selectively activates opioid-sensitive phasic-firing neurons within the vlPAG', *Journal of Neurophysiology*, vol. 129, no. 5, pp. 1237–1248, viewed 24 September 2025, <https://journals.physiology.org/doi/full/10.1152/jn.00016.2023>.

Meseguer Henarejos, AB et al. 2020, 'Sex and Time-of-Day Impact on Anxiety and Passive Avoidance Memory Strategies in Mice', *Frontiers in Behavioral Neuroscience*, vol. 14, viewed 24 September 2025, <https://www.frontiersin.org/journals/behavioral-neuroscience/articles/10.3389/fnbeh.2020.00068/full>.

Mitchell, VA et al. 2021, 'Oral efficacy of Δ(9)-tetrahydrocannabinol and cannabidiol in a mouse neuropathic pain model', *Neuropharmacology*, vol. 189, p. 108529.

Morales-Medina, JC et al. 2023, 'Persistent peripheral inflammation and pain induces immediate early gene activation in supraspinal nuclei in rats', *Behavioural Brain Research*, vol. 446, p. 114395, viewed 24 September 2025, <https://www.sciencedirect.com/science/article/pii/S0166432823001134>.

Morris, LS et al. 2020, 'The role of the locus coeruleus in the generation of pathological anxiety', *Brain and Neuroscience Advances*, vol. 4, p. 2398212820930321.

Nagai, Y et al. 2020, 'Deschloroclozapine, a potent and selective chemogenetic actuator enables rapid neuronal and behavioral modulations in mice and monkeys', *Nature Neuroscience*, vol. 23, no. 9, pp. 1157–1167.

Paxinos, G & Franklin, K 2001, *The mouse brain in stereotaxic coordinates*, 2nd Edition, Academic Press, San Diego.

Philipsberg, PA et al. 2023, 'Chronotate: An open-source tool for manual timestamping and quantification of animal behavior', *Neuroscience Letters*, vol. 814, p. 137461, viewed 24 September 2025, <https://www.sciencedirect.com/science/article/pii/S0304394023004202>.

Pitzer, C et al. 2019, 'Inflammatory and neuropathic pain conditions do not primarily evoke anxiety-like behaviours in C57BL/6 mice', *European Journal of Pain*, vol. 23, no. 2, pp. 285–306, viewed 10 September 2024, <https://onlinelibrary.wiley.com/doi/abs/10.1002/ejp.1303>.

Riebe, CJ & Wotjak, CT 2012,'A Practical Guide to Evaluating Anxiety-Related Behavior in Rodents', in A Szallasi & T Bíró (eds), *TRP Channels in Drug Discovery: Volume II*, Humana Press, Totowa, NJ, pp.167–185, viewed 11 August 2025, <https://doi.org/10.1007/978-1-62703-095-3_10>.

Riga, D et al. 2025, 'Neuropeptide Y neurons surrounding the locus coeruleus inhibit noradrenergic system activity to reduce anxiety', *Science Advances*, vol. 11, no. 30, p. eadq0011, viewed 24 September 2025, <https://www.science.org/doi/10.1126/sciadv.adq0011>.

Samineni, VK et al. 2017, 'Divergent Modulation of Nociception by Glutamatergic and GABAergic Neuronal Subpopulations in the Periaqueductal Gray', *eNeuro*, vol. 4, no. 2, viewed 11 September 2025, <https://www.eneuro.org/content/4/2/ENEURO.0129-16.2017>.

Samineni, VK et al. 2019, 'Cell type-specific modulation of sensory and affective components of itch in the periaqueductal gray', *Nature Communications*, vol. 10, no. 1, p. 4356, viewed 18 November 2024, <https://www.nature.com/articles/s41467-019-12316-0>.

Schmidt, U et al. 2018,'Cell Detection with Star-Convex Polygons', in AF Frangi et al. (eds), *Medical Image Computing and Computer Assisted Intervention – MICCAI 2018*, Springer International Publishing, Cham, pp.265–273.

Siemian, JN et al. 2021, 'An excitatory lateral hypothalamic circuit orchestrating pain behaviors in mice', *eLife*, vol. 10, p. e66446, viewed 18 November 2024, <https://doi.org/10.7554/eLife.66446>.

Stein, C, Millan, MJ, & Herz, A 1988, 'Unilateral inflammation of the hindpaw in rats as a model of prolonged noxious stimulation: Alterations in behavior and nociceptive thresholds', *Pharmacology Biochemistry and Behavior*, vol. 31, no. 2, pp. 445–451, viewed 18 July 2024, <https://www.sciencedirect.com/science/article/pii/0091305788903723>.

Taylor, BK & Westlund, KN 2017, 'The Noradrenergic Locus Coeruleus as a Chronic Pain Generator', *Journal of neuroscience research*, vol. 95, no. 6, pp. 1336–1346, viewed 24 September 2025, <https://pmc.ncbi.nlm.nih.gov/articles/PMC5374049/>.

Teng, S et al. 2022, 'Control of non-REM sleep by ventrolateral medulla glutamatergic neurons projecting to the preoptic area', *Nature Communications*, vol. 13, no. 1, p. 4748, viewed 24 September 2025, <https://www.nature.com/articles/s41467-022-32461-3>.

Tonsfeldt, KJ et al. 2016, 'Sex Differences in GABAA Signaling in the Periaqueductal Gray Induced by Persistent Inflammation', *Journal of Neuroscience*, vol. 36, no. 5, pp. 1669–1681, viewed 23 September 2025, <https://www.jneurosci.org/content/36/5/1669>.

Treede, R-D et al. 2019, 'Chronic pain as a symptom or a disease: the IASP Classification of Chronic Pain for the International Classification of Diseases (ICD-11)', *PAIN*, vol. 160, no. 1, p. 19, viewed 10 September 2025, <https://journals.lww.com/pain/fulltext/2019/01000/chronic_pain_as_a_symptom_or_a_disease__the_iasp.3.aspx>.

Vaughn, E et al. 2022, 'Three-dimensional Interrogation of Cell Types and Instinctive Behavior in the Periaqueductal Gray', , p. 2022.06.27.497769, viewed 24 September 2025, <https://www.biorxiv.org/content/10.1101/2022.06.27.497769v2>.

Wei, N et al. 2025, 'A systematic review of the pain-related emotional and cognitive impairments in chronic inflammatory pain induced by CFA injection and its mechanism', *IBRO Neuroscience Reports*, vol. 18, pp. 414–431, viewed 27 March 2025, <https://www.sciencedirect.com/science/article/pii/S2667242125000338>.

Wilson-Poe, AR et al. 2021, 'Effects of inflammatory pain on CB1 receptor in the midbrain periaqueductal gray', *PAIN Reports*, vol. 6, no. 1, p. e897, viewed 15 September 2025, <https://journals.lww.com/painrpts/fulltext/2021/01000/effects_of_inflammatory_pain_on_cb1_receptor_in.25.aspx>.

Winters, BL, Lau, BK, & Vaughan, CW 2022, 'Cannabinoids and Opioids Differentially Target Extrinsic and Intrinsic GABAergic Inputs onto the Periaqueductal Grey Descending Pathway', *Journal of Neuroscience*, vol. 42, no. 41, pp. 7744–7756, viewed 11 September 2025, <https://www.jneurosci.org/content/42/41/7744>.

Wojick, JA et al. 2025, 'A nociceptive amygdala-striatal pathway modulating affective-motivational pain', *Science Advances*, vol. 11, no. 30, p. eado2837, viewed 24 September 2025, <https://www.science.org/doi/10.1126/sciadv.ado2837>.

Xie, L et al. 2023, 'Divergent modulation of pain and anxiety by GABAergic neurons in the ventrolateral periaqueductal gray and dorsal raphe', *Neuropsychopharmacology*, vol. 48, no. 10, pp. 1509–1519, viewed 11 September 2025, <https://www.nature.com/articles/s41386-022-01520-0>.

Yang, D et al. 2024, 'Phosphorylation of pyruvate dehydrogenase inversely associates with neuronal activity', *Neuron*, vol. 112, no. 6, pp. 959-971.e8, viewed 24 September 2025, <https://www.cell.com/neuron/abstract/S0896-6273(23)00974-1>.

Yang, L et al. 2022, 'Ventrolateral Periaqueductal Gray Astrocytes Regulate Nociceptive Sensation and Emotional Motivation in Diabetic Neuropathic Pain', *Journal of Neuroscience*, vol. 42, no. 43, pp. 8184–8199, viewed 11 September 2025, <https://www.jneurosci.org/content/42/43/8184>.

Yoon, C et al. 1994, 'Behavioral signs of ongoing pain and cold allodynia in a rat model of neuropathic pain', *PAIN*, vol. 59, no. 3, p. 369, viewed 28 July 2025, <https://journals.lww.com/pain/abstract/1994/12000/behavioral_signs_of_ongoing_pain_and_cold.7.aspx>.

Zhang, M et al. 2025, 'A neural circuit for sex-dependent conditioned pain hypersensitivity in mice', *Nature Communications*, vol. 16, no. 1, p. 3639.

Zhang, Y et al. 2023, 'Somatostatin Neurons from Periaqueductal Gray to Medulla Facilitate Neuropathic Pain in Male Mice', *The Journal of Pain*, vol. 24, no. 6, pp. 1020–1029, viewed 11 September 2025, <https://www.sciencedirect.com/science/article/pii/S152659002300010X>.

Zhu, X et al. 2024, 'Modulation of Comorbid Chronic Neuropathic Pain and Anxiety-Like Behaviors by Glutamatergic Neurons in the Ventrolateral Periaqueductal Gray and the Analgesic and Anxiolytic Effects of Electroacupuncture', *eNeuro*, vol. 11, no. 8, p. ENEURO.0454-23.2024, viewed 11 September 2025, <https://www.ncbi.nlm.nih.gov/pmc/articles/PMC11360982/>.

## 5.7 Supplementary Data

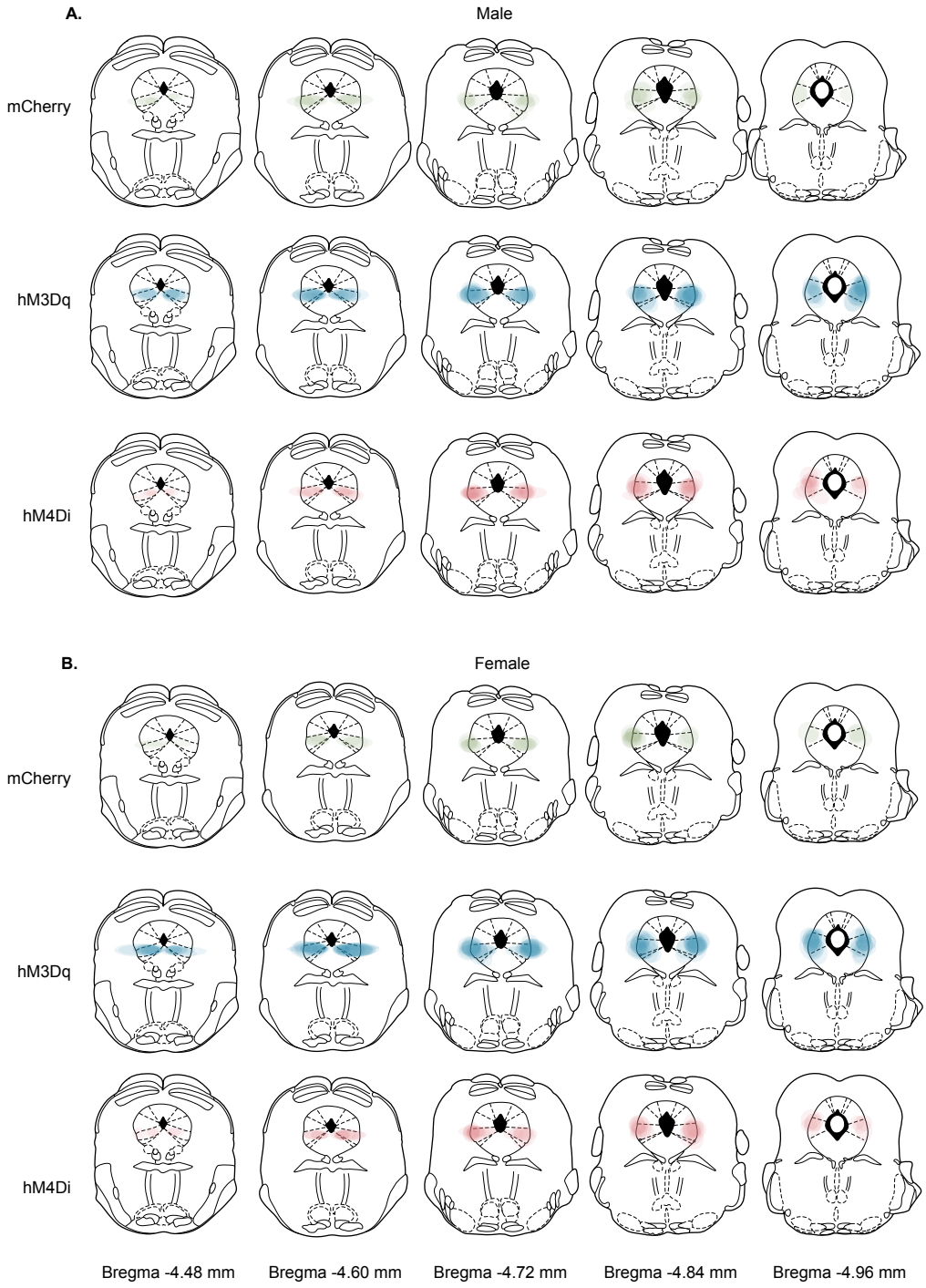


**Supplementary Figure 1: AAV5 viral vector expression.** Schematic showing viral vector expression of across all male (A) and female (B) mice for control (mCherry; green), hM3Dq (blue) and hM4Di (red) groups, with 10% opacity for expression spread per bregma section for each animal.

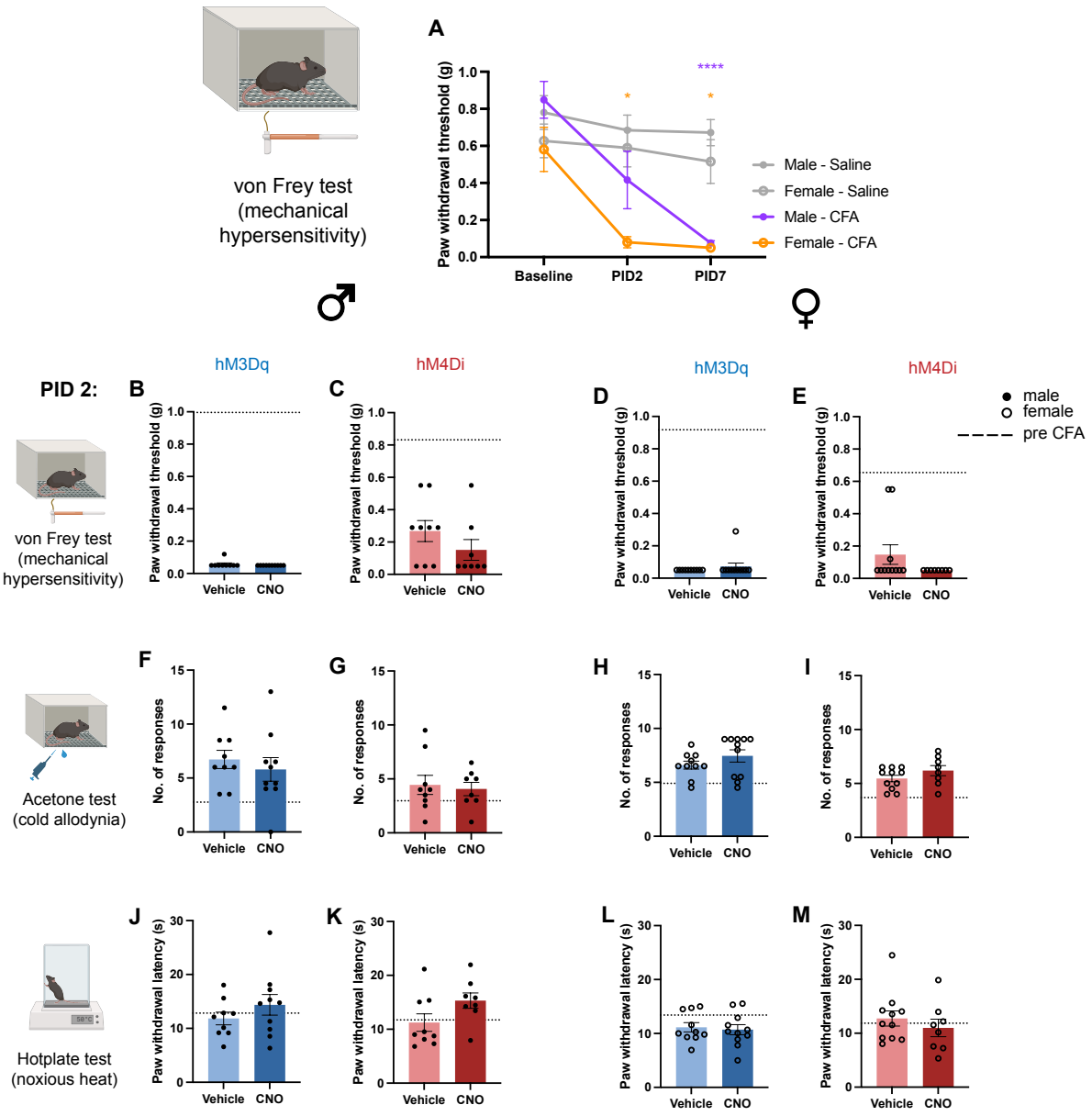


**Supplementary Figure 2: Chemogenetic modulation of PAG$^{GlyT2}$ neurons does not alter nociceptive responses in the CFA model of persistent inflammatory pain at PID 2**. (A) von Frey testing at baseline, PID2 and PID 7 (before vehicle or CNO), confirmed mechanical hypersensitivity in females at PID2 and PID7, and males at PID7. At PID2, there were no significant differences in paw withdrawal threshold, number of responses to acetone or paw withdrawal latency between vehicle and CNO for male (closed circle) and female (open circle) mice (B-M). Individual animals presented with bars representing mean ± SEM. n=7-11/group. Dotted line represents average of baseline values for the groups presented. *p<0.05, **p<0.01, ***p<0.001, ****p<0.0001.

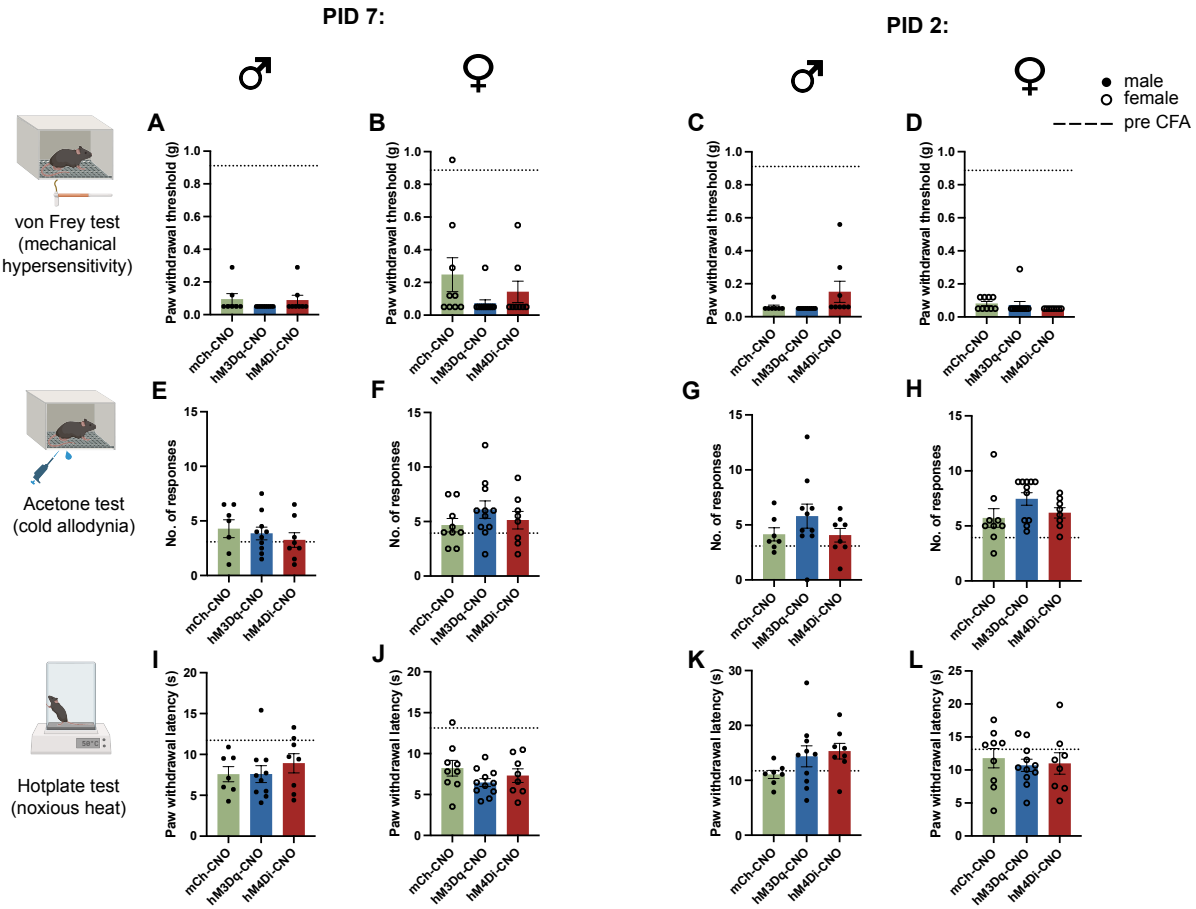


**Supplementary Figure 3: Chemogenetic modulation of PAG$^{GlyT2}$ neurons does not alter nociceptive responses in the CFA model of persistent inflammatory pain.** At PID 2 and 7, there were no significant differences there were no significant differences in paw withdrawal threshold, number of responses to acetone or paw withdrawal latency between CNO injected groups for male (closed circle) and female (open circle) mice (B-M). Individual animals presented with bars representing mean ± SEM. n=7-11/group. Dotted line represents average of baseline values for the groups presented. *p<0.05, **p<0.01, ***p<0.001, ****p<0.0001.

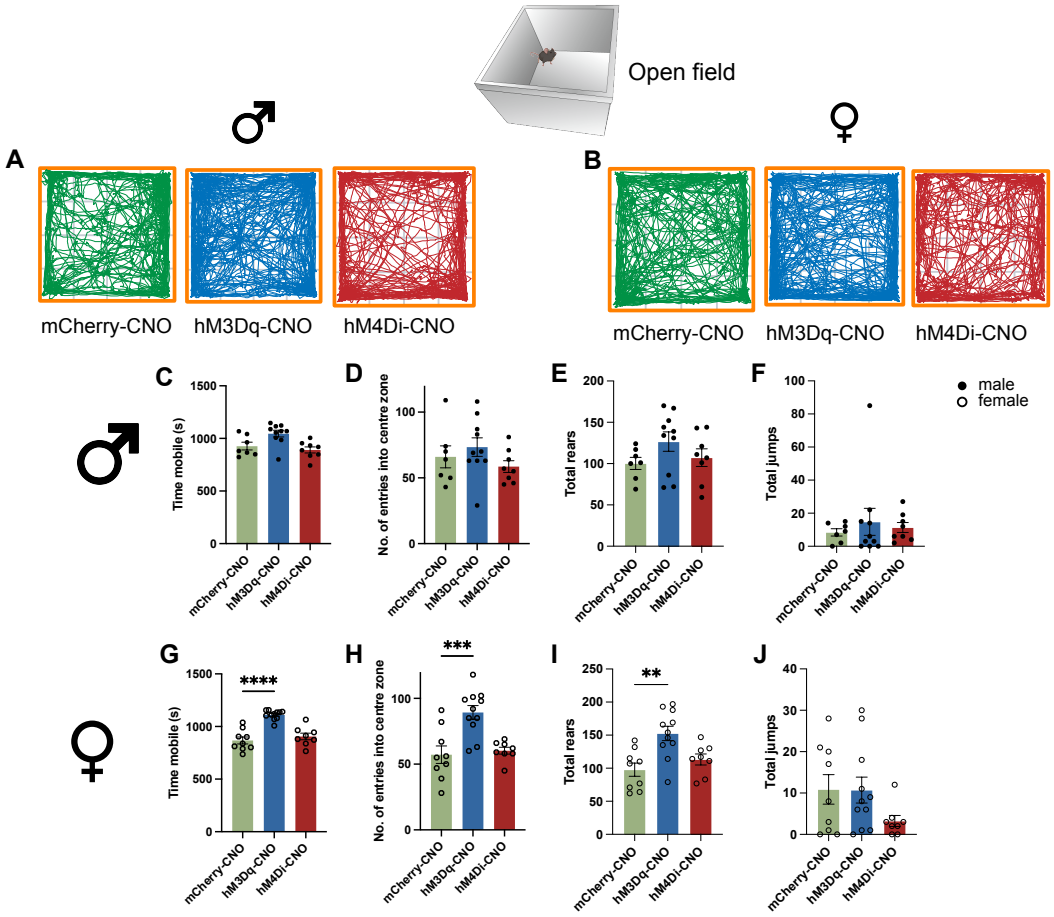


**Supplementary Figure 4: Chemogenetic modulation of PAG$^{GlyT2}$ neurons does not alter locomotor behaviours in males but does in females.** Track plot of the centre point of male (A) and female (B) mice during the 20-minute open field test. Chemogenetic modulation resulted in no significant difference in mobility time, number of entries into the centre zone, rearing and jumping in the open field for males (closed circles; C-F). In females, chemogenetic activation resulted in significantly increased mobility, number of centre zone entries and rearing and jumping compared to other CNO groups (open circles; G-I). Chemogenetic modulation resulted in no significant differences in jumping responses when compared to other CNO groups (J). Individual animals presented with bars representing mean ± SEM. n=7-11/group. Dotted line represents average of baseline values for the groups presented. *p<0.05, **p<0.01, ***p<0.001, ****p<0.0001.

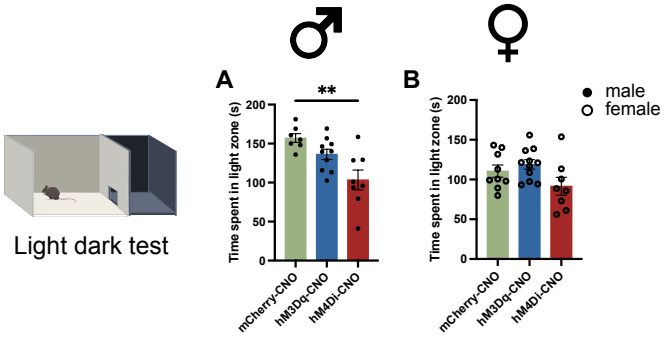


**Supplementary Figure 5: Chemogenetic modulation of PAG$^{GlyT2}$ neurons alters anxiety-like behaviours in only male mice, when compared to mCherry-CNO control group**. Chemogenetic modulation of PAG$^{GlyT2}$ neurons resulted in a significant decrease in time spent in the light zone in the light dark test in hM4Di-CNO male mice compared to mCherry-CNO (closed circles; A). In females, chemogenetic modulation did not change time spent in the light zone compared to the mCherry-CNO group (open circles; B). Individual animals presented with bars representing mean ± SEM. n=7-11/group. Dotted line represents average of baseline values for the groups presented. *p<0.05, **p<0.01, ***p<0.001, ****p<0.0001.

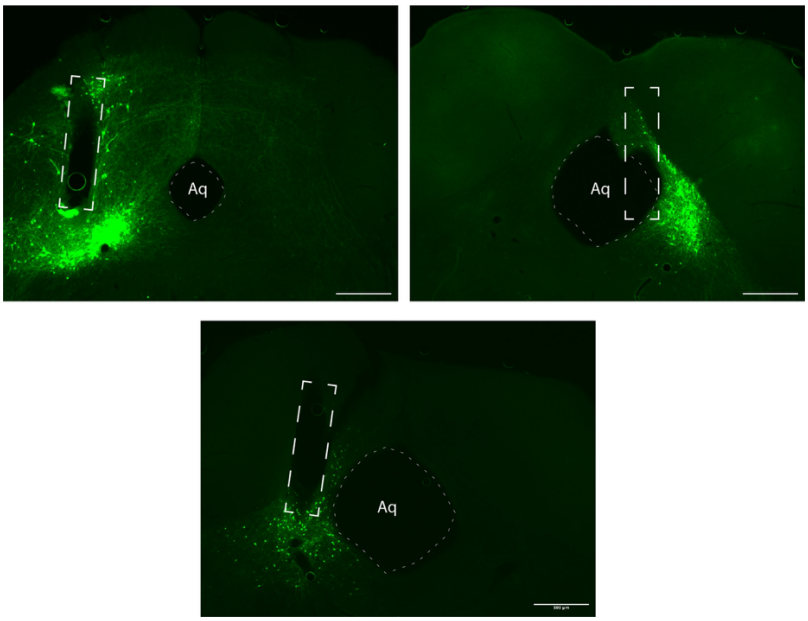


**Supplementary Figure 6: Fibre and injection placement for *in vivo* fibre photometry experiment.** Representative microscope image showing middle of injection expression and fibre optic cannula placement for fibre photometry experiment. n=1 animal unable to obtain image. Scale bar= 500$\mu$m. Magnification: 2.5X. Aq: Cerebral aqueduct.

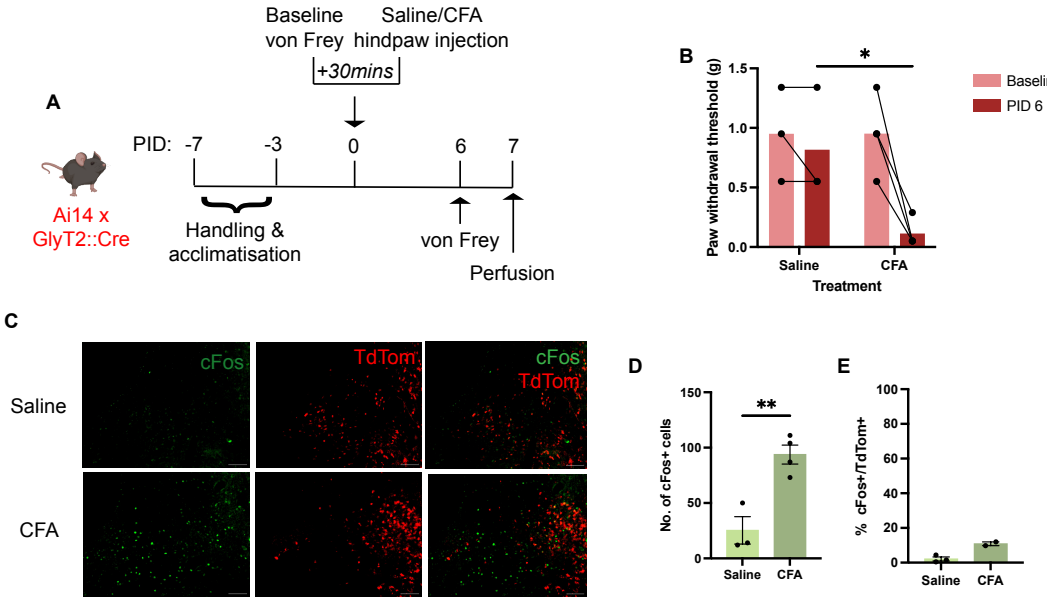


**Supplementary Figure 7: The PAG is engaged following a CFA induced persistent inflammatory pain state.** (A) Schematic showing experimental timeline of GlyT2::Cre reporter animals (Ai14 x GlyT2::Cre) receiving a von Frey test before and after saline or CFA hind paw injection, followed by perfusion on the 7th day post CFA injection. (B) Animals injected with CFA had significantly reduced paw withdrawal thresholds when compared to saline injected animals on PID6. (C) Representative microscope images of cFos and TdTomato expression in the vlPAG of saline and CFA injected mice, scale bar= 500$\mu$m. (D) Total number of cFos+ cells in the vlPAG of saline and CFA injected mice. (E) Percentage of cFos+ cells colocalised with TdTom expression in the vlPAG of saline and CFA injected mice. PID: post injection day. Individual animals presented with bars representing mean ± SEM. Saline: n=3 females, CFA: n=2-4 females. *p<0.05, **p<0.01, ***p<0.001, ****p<0.0001.

## Supplementary Table 1: Statistical analysis details

| Figure | Experiment | Sex | n/group | mean +/- SEM | Test | Main effect | F (DFn, DFd) | *p* value | Post-hoc | Multiple comparison | *p* value |
|---|---|---|---|---|---|---|---|---|---|---|---|
| 2A | von Frey-PID comparison | Male and female | 7-11 mice | | RM two-way ANOVA with Geisser Greenhouse correction | Time x Treatment | F (5.612, 56.12) = 4.005 | P=0.0026 | Bonferroni | PID2: Male-Saline vs Male- CFA | 0.9303 |
| | | | | | | Time | F (1.871, 56.12) = 19.54 | P<0.0001 | | PID2: Female-Saline vs Female- CFA | 0.0122 |
| | | | | | | Treatment | F (3, 30) = 13.66 | P<0.0001 | | PID7: Male-Saline vs Male-CFA | <0.0001 |
| | | | | | | | | | | PID7: Female-Saline vs Female-CFA | 0.0449 |
| 2B | von Frey-hM3D | Male | 9 vehicle, 10 CNO | Vehicle (0.05 ± 0) CNO (0.05 ± 0) | N/A *all values are identical | | | | | | |
| 2C | von Frey-hM3D | Male | 9 vehicle, 8 CNO | Vehicle (0.3144 ± 0.1051) CNO (0.08875 ± 0.03003) | Unpaired t-test | | t=1.955, df=15 | 0.0694 | | | |
| 2D | von Frey-hM4D | Female | 10 vehicle, 11 CNO | Vehicle (0.1050 ± 0.03160) CNO (0.07182 ± 0.02182) | Unpaired t-test | | t=0.8778, df=19 | 0.391 | | | |
| 2E | von Frey-hM4D | Female | 11 vehicle, 8 CNO | Vehicle (0.07818 ± 0.02211) CNO (0.1425 ± 0.06535) | Unpaired t-test | | t=1.055, df=17 | 0.3064 | | | |

| | | | | | | | |
|---|---|---|---|---|---|---|---|
| 2F | acetone-hM3D | Male | 9 vehicle, 10 CNO | Vehicle (4.444 ± 0.5860)<br>CNO (3.850 ± 0.5776) | Unpaired t-test | t=0.7209, df=17 | 0.4807 |
| 2G | acetone-hM4D | Male | 9 vehicle, 8 CNO | Vehicle (3.500 ± 0.4859)<br>CNO (3.250 ± 0.6682) | Unpaired t-test | t=0.3075, df=15 | 0.7627 |
| 2H | acetone-hM3D | Female | 10 vehicle, 11 CNO | Vehicle (5.55 ± 0.1893)<br>CNO (6.091 ± 0.8029) | Unpaired t-test | t=0.6267, df=19 | 0.5383 |
| 2I | acetone-hM4D | Female | 11 vehicle, 8 CNO | Vehicle (4.727 ± 0.6006)<br>CNO (5.125 ± 0.8059) | Unpaired t-test | t=0.4047, df=17 | 0.6908 |
| 2J | hotplate-hM3D | Male | 9 vehicle, 10 CNO | Vehicle (8.037 ± 0.6900)<br>CNO (7.593 ± 1.035) | Unpaired t-test | t=0.3482, df=17 | 0.7319 |
| 2K | hotplate-hM4D | Male | 9 vehicle, 8 CNO | Vehicle (8.644 ± 1.211)<br>CNO (8.917 ± 1.170) | Unpaired t-test | t=0.1607, df=15 | 0.8745 |
| 2L | hotplate-hM3D | Female | 10 vehicle, 11 CNO | Vehicle (8.117 ± 0.8965)<br>CNO (6.455 ± 0.4851) | Unpaired t-test | t=1.673, df=19 | 0.1107 |
| 2M | hotplate-hM4D | Female | 11 vehicle, 8 CNO | Vehicle (7.773 ± 0.6725)<br>CNO (7.304 ± 0.8323) | Unpaired t-test | t=0.4419, df=17 | 0.6641 |

| | | | | | | | |
|---|---|---|---|---|---|---|---|
| S2-B | von Frey-hM3D | Male | 9 vehicle, 10 CNO | Vehicle (0.05778 ± 0.007778) CNO (0.05000 ± 0.000) | Unpaired t-test | t=1.058, df=17 | 0.3051 |
| S2-C | von Frey-hM3D | Male | 9 vehicle, 8 CNO | Vehicle (0.2678 ± 0.06493) CNO (0.1513 ± 0.06415) | Unpaired t-test | t=1.271, df=15 | 0.2231 |
| S2-D | von Frey-hM4D | Female | 10 vehicle, 11 CNO | Vehicle (0.05000 ± 0.000) CNO (0.07182 ± 0.02182) | Unpaired t-test | t=0.9512, df=19 | 0.3535 |
| S2-E | von Frey-hM4D | Female | 11 vehicle, 8 CNO | Vehicle (0.1473 ± 0.06036) CNO (0.05000 ± 0.000) | Unpaired t-test | t=1.363, df=17 | 0.1906 |
| S2-F | acetone-hM3D | Male | 9 vehicle, 10 CNO | Vehicle (6.722 ± 0.8462) CNO (5.800 ± 1.088) | Unpaired t-test | t=0.6581, df=17 | 0.5193 |
| S2-G | acetone-hM4D | Male | 9 vehicle, 8 CNO | Vehicle (4.444 ± 0.8915) CNO (4.063 ± 0.6228) | Unpaired t-test | t=0.3426, df=15 | 0.7366 |
| S2-H | acetone-hM3D | Female | 10 vehicle, 11 CNO | Vehicle (6.600 ± 0.3712) CNO (7.455 ± 0.5699) | Unpaired t-test | t=1.229, df=19 | 0.2341 |
| S2-I | acetone-hM4D | Female | 11 vehicle, 8 CNO | Vehicle (5.455 ± 0.2974) CNO (6.188 ± 0.4719) | Unpaired t-test | t=1.380, df=17 | 0.1853 |

| | | | | | | | | | | | |
|---|---|---|---|---|---|---|---|---|---|---|---|
| S2-J | hotplate-hM3D | Male | 9 vehicle, 10 CNO | Vehicle (11.83 ± 1.172) CNO (14.37 ± 1.918) | Unpaired t-test | | t=1.099, df=17 | 0.2871 | | | |
| S2-K | hotplate-hM4D | Male | 9 vehicle, 8 CNO | Vehicle (11.24 ± 1.621) CNO (15.31 ± 1.433) | Unpaired t-test | | t=1.861, df=15 | 0.0825 | | | |
| S2-L | hotplate-hM3D | Female | 10 vehicle, 11 CNO | Vehicle (11.14 ± 0.8669) CNO (10.71 ± 0.9349) | Unpaired t-test | | t=0.3409, df=19 | 0.737 | | | |
| S2-M | hotplate-hM4D | Female | 11 vehicle, 8 CNO | Vehicle (12.74 ± 1.404) CNO (10.99 ± 1.625) | Unpaired t-test | | t=0.8154, df=17 | 0.4261 | | | |
| S3-A | PID7 von Frey-CNO groups | Male | 7 mCherry, 10 hM3D, 9 hM4D | mCh (0.09429 ± 0.03408), hM3D (0.05000 ± 0.000), hM4D (0.08875 ± 0.03003) | One-way ANOVA | Treatment | F (2, 22) = 1.149 | P=0.3354 | Bonferroni | mCh-CNO vs. hM3D q-CNO | 0.3892 |
| | | | | | | | | | | mCh-CNO vs. hM4D i-CNO | >0.9999 |
| S3-B | PID7 von Frey-CNO groups | Female | 9 mCherry, 11 hM3D, 8 hM4D | mCh (0.2478 ± 0.1038), hM3D (0.07182 ± 0.02182), hM4D (0.1425 ± 0.06535) | One-way ANOVA | Treatment | F (2, 25) = 1.801 | P=0.1860 | Bonferroni | mCh-CNO vs. hM3D q-CNO | 0.1394 |

| | | | | | | | | | | | |
|---|---|---|---|---|---|---|---|---|---|---|---|
| | | | | | | | | | | mCh-CNO vs. hM4Di-CNO | 0.6086 |
| S3-C | PID2 von Frey-CNO groups | Male | 7 mCherry, 10 hM3D, 9 hM4D | mCh (0.06000 ± 0.01000), hM3D (0.05000 ± 0.000), hM4D (0.1513 ± 0.06415) | One-way ANOVA | Treatment | F (2, 22) = 2.425 | P=0.1118 | Bonferroni | mCh-CNO vs. hM3Dq-CNO | >0.9999 |
| | | | | | | | | | | mCh-CNO vs. hM4Di-CNO | 0.2038 |
| S3-D | PID2 von Frey-CNO groups | Female | 9 mCherry, 11 hM3D, 8 hM4D | mCh (0.08111 ± 0.01230), hM3D (0.07182 ± 0.02182), hM4D (0.05000 ± 0.000) | One-way ANOVA | Treatment | F (2, 25) = 0.8479 | P=0.4403 | Bonferroni | mCh-CNO vs. hM3Dq-CNO | >0.9999 |
| | | | | | | | | | | mCh-CNO vs. hM4Di-CNO | 0.4295 |
| S3-E | PID7 acetone-CNO groups | Male | 7 mCherry, 10 hM3D, 9 hM4D | mCh (4.286 ± 0.8227), hM3D (3.850 ± 0.5776), hM4D (3.250 ± 0.6682) | One-way ANOVA | Treatment | F (2, 22) = 0.5386 | P=0.5910 | Bonferroni | mCh-CNO vs. hM3Dq-CNO | >0.9999 |

| | | | | | | | | | | | |
|---|---|---|---|---|---|---|---|---|---|---|---|
| | | | | | | | | | | mCh-CNO vs. hM4D i-CNO | 0.6307 |
| S3-F | PID7 acetone-CNO groups | Female | 9 mCherry, 11 hM3D, 8 hM4D | mCh (4.667 ± 0.6180), hM3D (6.091 ± 0.8029), hM4D (5.125 ± 0.8059) | One-way ANOVA | Treatment | F (2, 25) = 0.9872 | P=0.3867 | Bonferroni | mCh-CNO vs. hM3D q-CNO | 0.369 |
| | | | | | | | | | | mCh-CNO vs. hM4D i-CNO | >0.9999 |
| S3-G | PID2 acetone-CNO groups | Male | 7 mCherry, 10 hM3D, 9 hM4D | mCh (4.143 ± 0.5948), hM3D (5.800 ± 1.088), hM4D (4.063 ± 0.6228) | One-way ANOVA | Treatment | F (2, 22) = 1.334 | P=0.2839 | Bonferroni | mCh-CNO vs. hM3D q-CNO | 0.402 |
| | | | | | | | | | | mCh-CNO vs. hM4D i-CNO | >0.9999 |
| S3-H | PID2 acetone-CNO groups | Female | 9 mCherry, 11 hM3D, 8 hM4D | mCh (5.722 ± 0.8462), hM3D (7.455 ± 0.5699), hM4D (6.188 ± 0.4719) | One-way ANOVA | Treatment | F (2, 25) = 2.032 | P=0.1522 | Bonferroni | mCh-CNO vs. hM3D q-CNO | 0.1302 |

| | | | | | | | | | | | |
|---|---|---|---|---|---|---|---|---|---|---|---|
| | | | | | | | | | | mCh-CNO vs. hM4Di-CNO | >0.9999 |
| S3-I | PID7 hotplate-CNO groups | Male | 7 mCherry, 10 hM3D, 9 hM4D | mCh (7.581 ± 0.9229), hM3D (7.593 ± 1.035), hM4D (8.917 ± 1.170) | One-way ANOVA | Treatment | F (2, 22) = 0.5055 | P=0.6100 | Bonferroni | mCh-CNO vs. hM3Dq-CNO | >0.9999 |
| | | | | | | | | | | mCh-CNO vs. hM4Di-CNO | 0.8226 |
| S3-J | PID7 hotplate-CNO groups | Female | 9 mCherry, 11 hM3D, 8 hM4D | mCh (8.219 ± 0.9626), hM3D (6.455 ± 0.4851), hM4D (7.304 ± 0.8323) | One-way ANOVA | Treatment | F (2, 25) = 1.467 | P=0.2498 | Bonferroni | mCh-CNO vs. hM3Dq-CNO | 0.1986 |
| | | | | | | | | | | mCh-CNO vs. hM4Di-CNO | 0.839 |
| S3-K | PID2 hotplate-CNO groups | Male | 7 mCherry, 10 hM3D, 9 hM4D | mCh (11.07 ± 0.7377), hM3D (14.37 ± 1.918), hM4D (15.31 ± 1.433) | One-way ANOVA | Treatment | F (2, 22) = 1.724 | P=0.2015 | Bonferroni | mCh-CNO vs. hM3Dq-CNO | 0.3218 |

| | | | | | | | | | | | |
|---|---|---|---|---|---|---|---|---|---|---|---|
| | | | | | | | | | | mCh-CNO vs. hM4D i-CNO | 0.1802 |
| S3-L | PID2 hotplate-CNO groups | Female | 9 mCherry, 11 hM3D, 8 hM4D | mCh (11.79 ± 1.475), hM3D (10.71 ± 0.9349), hM4D (10.99 ± 1.625) | One-way ANOVA | Treatment | F (2, 25) = 0.1886 | P=0.8293 | Bonferroni | mCh-CNO vs. hM3D q-CNO<br>mCh-CNO vs. hM4D i-CNO | >0.9999<br>>0.9999 |
| 3C | open field-mobility-hM3D | Male | 9 Vehicle, 10 CNO | Vehicle (1019 ± 10.52) CNO (1046 ± 31.55) | Unpaired t-test | | t=0.7880, df=17 | 0.4415 | | | |
| 3D | open field-mobility-hM4D | Male | 9 Vehicle, 8 CNO | Vehicle (946.3 ± 27.83) CNO (891.0 ± 28.76) | Unpaired t-test | | t=1.378, df=15 | 0.1883 | | | |
| 3E | open field-mobility-hM3D | Female | 10 Vehicle, 11 CNO | Vehicle (976.6 ± 18.38) CNO (1110 ± 13.37) | Unpaired t-test | | t=5.967, df=19 | <0.0001 | | | |
| 3F | open field-mobility-hM4D | Female | 11 Vehicle, 8 CNO | Vehicle (912.7 ± 34.82) CNO (905.7 ± 31.72) | Unpaired t-test | | t=0.1432, df=17 | 0.8878 | | | |
| 3G | open field-centre-hM3D | Male | 9 Vehicle, 10 CNO | Vehicle (85.11 ± 6.791) CNO (73.40 ± 7.037) | Unpaired t-test | | t=1.192, df=17 | 0.2498 | | | |

| | | | | | | | |
|---|---|---|---|---|---|---|---|
| 3H | open field-centre-hM4D | Male | 9 Vehicle, 8 CNO | Vehicle (62.44 ± 5.826) CNO (58.63 ± 4.468) | Unpaired t-test | t=0.5101, df=15 | 0.6174 |
| 3I | open field-centre-hM3D | Female | 10 Vehicle, 11 CNO | Vehicle (57.80 ± 3.826) CNO (89.36 ± 5.198) | Unpaired t-test | t=4.807, df=19 | 0.0001 |
| 3J | open field-centre-hM4D | Female | 11 Vehicle, 8 CNO | Vehicle (54.55 ± 4.450) CNO (60.25 ± 2.603) | Unpaired t-test | t=1.001, df=17 | 0.331 |
| 3K | open field-rears-hM3D | Male | 9 Vehicle, 10 CNO | Vehicle (108.6 ± 4.849) CNO (126.6 ± 11.74) | Unpaired t-test | t=1.224, df=15 | 0.2398 |
| 3L | open field-rears-hM4D | Male | 9 Vehicle, 8 CNO | Vehicle (133.6 ± 8.906) CNO (107.3 ± 10.73) | Unpaired t-test | t=1.902, df=15 | 0.0765 |
| 3M | open field-rears-hM3D | Female | 10 Vehicle, 11 CNO | Vehicle (94.20 ± 3.820) CNO (152.6 ± 10.78) | Unpaired t-test | t=4.911, df=19 | <0.0001 |
| 3N | open field-rears-hM4D | Female | 11 Vehicle, 8 CNO | Vehicle (109.5 ± 8.272) CNO (113.3 ± 8.300) | Unpaired t-test | t=0.3081, df=17 | 0.7618 |
| 3O | open field-jumps-hM3D | Male | 9 Vehicle, 10 CNO | Vehicle (13.14 ± 5.422) CNO (14.80 ± 8.161) | Unpaired t-test | t=0.1532, df=15 | 0.8803 |

| | | | | | | | | | | | |
|---|---|---|---|---|---|---|---|---|---|---|---|
| 3P | open field-jumps-hM4D | Male | 9 Vehicle, 8 CNO | Vehicle (9.889 ± 4.234) CNO (11.38 ± 3.035) | Unpaired t-test | | t=0.2787, df=15 | 0.7843 | | | |
| 3Q | open field-jumps-hM3D | Female | 10 Vehicle, 11 CNO | Vehicle (2.600 ± 1.267) CNO (10.73 ± 3.137) | Unpaired t-test | | t=2.315, df=19 | 0.032 | | | |
| 3R | open field-jumps-hM4D | Female | 11 Vehicle, 8 CNO | Vehicle (1.727 ± 0.7639) CNO (3.250 ± 1.346) | Unpaired t-test | | t=1.050, df=17 | 0.3085 | | | |
| S4-C | open field-mobility-CNO groups | Male | 7 mCherry, 10 hM3D, 8 hM4D | mCh (927.5 ± 36.80), hM3D (1046 ± 31.55), hM4D (891.0 ± 28.76) | One-way ANOVA | Treatment | F (2, 22) = 6.820 | P=0.0050 | Bonferroni | mCherry-CNO vs. hM3D q-CNO | 0.0519 |
| | | | | | | | | | | mCherry-CNO vs. hM4D i-CNO | >0.9999 |
| S4-D | open field-centre-CNO groups | Male | 7 mCherry, 10 hM3D, 8 hM4D | mCh (66.00 ± 8.330), hM3D (73.40 ± 7.037), hM4D (58.63 ± 4.468) | One-way ANOVA | Treatment | F (2, 22) = 1.262 | P=0.3028 | Bonferroni | mCherry-CNO vs. hM3D q-CNO | >0.9999 |
| | | | | | | | | | | mCherry-CNO vs. hM4D i-CNO | >0.9999 |

| | | | | | | | | | | | |
|---|---|---|---|---|---|---|---|---|---|---|---|
| S4-E | open field-rears-CNO groups | Male | 7 mCherry, 10 hM3D, 8 hM4D | mCh (100.3 ± 7.289), hM3D (126.6 ± 11.74), hM4D (107.3 ± 10.73) | One-way ANOVA | Treatment | F (2, 22) = 1.693 | P=0.2070 | Bonferroni | mCherry-CNO vs. hM3D q-CNO | 0.2958 |
| | | | | | | | | | | mCherry-CNO vs. hM4D i-CNO | >0.9999 |
| S4-F | open field-jumps-CNO groups | Male | 7 mCherry, 10 hM3D, 8 hM4D | mCh (8.429 ± 2.192), hM3D (14.80 ± 8.161), hM4D (11.38 ± 3.035) | One-way ANOVA | Treatment | F (2, 22) = 0.2797 | P=0.7587 | Bonferroni | mCherry-CNO vs. hM3D q-CNO | >0.9999 |
| | | | | | | | | | | mCherry-CNO vs. hM4D i-CNO | >0.9999 |
| S4-G | open field-mobility-CNO groups | Female | 9 mCherry, 11 hM3D, 8 hM4D | mCh (867.7 ± 32.95), hM3D (1110 ± 13.37), hM4D (905.7 ± 31.72) | One-way ANOVA | Treatment | F (2, 25) = 27.86 | P<0.0001 | Bonferroni | mCherry-CNO vs. hM3D q-CNO | <0.0001 |
| | | | | | | | | | | mCherry-CNO vs. hM4D i-CNO | 0.9879 |
| S4-H | open field-centre-CNO groups | Female | 9 mCherry, 11 hM3D, 8 hM4D | mCh (57.22 ± 6.666), hM3D (89.36 ± 5.198), hM4D (60.25 ± 2.603) | One-way ANOVA | Treatment | F (2, 25) = 12.10 | P=0.0002 | Bonferroni | mCherry-CNO vs. hM3D q-CNO | 0.0005 |

| | | | | | | | | | | | |
|---|---|---|---|---|---|---|---|---|---|---|---|
| | | | | | | | | | | mCherry-CNO vs. hM4D i-CNO | >0.9999 |
| S4-I | open field-rears-CNO groups | Female | 9 mCherry, 11 hM3D, 8 hM4D | mCh (97.78 ± 10.02), hM3D (152.6 ± 10.78), hM4D (113.3 ± 8.300) | One-way ANOVA | Treatment | F (2, 25) = 8.449 | P=0.0016 | Bonferroni | mCherry-CNO vs. hM3D q-CNO | 0.0017 |
| | | | | | | | | | | mCherry-CNO vs. hM4D i-CNO | 0.9378 |
| S4-J | open field-jumps-CNO groups | Female | 9 mCherry, 11 hM3D, 8 hM4D | mCh (10.89 ± 3.576), hM3D (10.73 ± 3.137), hM4D (3.250 ± 1.346) | One-way ANOVA | Treatment | F (2, 25) = 1.935 | P=0.1654 | Bonferroni | mCherry-CNO vs. hM3D q-CNO | >0.9999 |
| | | | | | | | | | | mCherry-CNO vs. hM4D i-CNO | 0.297 |
| 4A | lightdark-hM3D | Male | 9 Vehicle, 10 CNO | Vehicle (119.6 ± 6.508) CNO (136.2 ± 6.636) | Unpaired t-test | | t=1.778, df=17 | 0.0933 | | | |
| 4B | lightdark-hM4D | Male | 9 Vehicle, 8 CNO | Vehicle (125.9 ± 11.94) CNO (103.4 ± 12.66) | Unpaired t-test | | t=1.297, df=15 | 0.2142 | | | |
| 4C | lightdark-hM3D | Female | 10 Vehicle, 11 CNO | Vehicle (86.08 ± 8.636) CNO (118.9 ± 5.978) | Unpaired t-test | | t=3.171, df=19 | 0.005 | | | |

| | | | | | | | | | | | |
|---|---|---|---|---|---|---|---|---|---|---|---|
| 4D | lightdark-hM4D | Female | 11 Vehicle, 8 CNO | Vehicle (118.0 ± 7.321) CNO (91.50 ± 11.19) | Unpaired t-test | | t=2.067, df=17 | 0.0543 | | | |
| 4F | epm-entries-hM3D | Male | 10 Vehicle, 10 CNO | Vehicle (22.00 ± 3.134) CNO (26.10 ± 3.361) | Unpaired t-test | | t=0.8921, df=18 | 0.3841 | | | |
| 4G | epm-time-hM3D | Male | 10 Vehicle, 10 CNO | Vehicle (64.95 ± 10.38) CNO (84.08 ± 6.665) | Unpaired t-test | | t=1.551, df=18 | 0.1382 | | | |
| 4I | epm-entries-hM3D | Female | 12 Vehicle, 11 CNO | Vehicle (25.00 ± 1.938) CNO (32.45 ± 1.826) | Unpaired t-test | | t=2.786, df=21 | 0.0111 | | | |
| 4J | epm-time-hM3D | Female | 12 Vehicle, 11 CNO | Vehicle (49.91 ± 5.077) CNO (79.21 ± 5.352) | Unpaired t-test | | t=3.974, df=21 | 0.0007 | | | |
| S5-A | lightdark-CNO | Male | 7 mCherry, 10 hM3D, 8 hM4D | mCh (157.2 ± 5.622), hM3D (136.2 ± 6.636), hM4D (103.4 ± 12.66) | One-way ANOVA | Treatment | F (2, 22) = 8.603 | P=0.0017 | Bonferroni | mCherry-CNO vs. hM3D q-CNO | 0.3268 |
| | | | | | | | | | | mCherry-CNO vs. hM4D i-CNO | 0.0015 |
| S5-B | lightdark-CNO | Female | 9 mCherry, 11 hM3D, 8 hM4D | mCh (110.5 ± 7.626), hM3D (118.9 ± 5.978), hM4D (91.50 ± 11.19) | One-way ANOVA | Treatment | F (2, 25) = 2.918 | P=0.0726 | Bonferroni | mCherry-CNO vs. hM3D q-CNO | >0.9999 |

| | | | | | | | | | | |
|---|---|---|---|---|---|---|---|---|---|---|
| | | | | | | | | | mCherry-CNO vs. hM4Di-CNO | 0.3711 |
| 5E | gcamp-baseline | Male | 4 mice | RM two-way ANOVA with Geisser Greenhouse correction | Time | F (1, 3) = 24.00 | P=0.0163 | Bonferroni | Ipsilateral: pre-post | 0.0255 |
| | | | | | Paw | F (1, 3) = 2.248 | P=0.2308 | | Contralateral: pre-post | 0.0099 |
| | | | | | Time x Paw | F (1, 3) = 2.258 | P=0.2300 | | | |
| 5H | gcamp-baseline | Male | 4 mice | RM two-way ANOVA with Geisser Greenhouse correction | Time | F (1, 3) = 6.067 | P=0.0906 | Bonferroni | Ipsilateral: pre-post | 0.0449 |
| | | | | | Paw | F (1, 3) = 2.541 | P=0.2092 | | Contralateral: pre-post | 0.0142 |
| | | | | | Time x Paw | F (1, 3) = 2.520 | P=0.2106 | | | |
| S7-B | vonfrey | Female | 3 Saline, 4 CFA | RM two-way ANOVA with Geisser Greenhouse correction | Treatment x Time | F (1, 5) = 9.225 | P=0.0288 | Bonferroni | Baseline: saline-CFA | >0.9999 |
| | | | | | Treatment | F (1, 5) = 2.479 | P=0.1762 | | PID 6: saline-CFA | 0.0377 |
| | | | | | Time | F (1, 5) = 17.53 | P=0.0086 | | | |

| | | | | | | | |
|---|---|---|---|---|---|---|---|
| S7-D | cFos count | Female | 3 Saline, 4 CFA | Saline (25.33 ± 12.35)<br>CFA (93.75 ± 8.557) | Unpaired t-test | t=4.730, df=5 | 0.0052 |
| S7-E | % cFos+/TdTom+ | Female | 3 Saline, 2 CFA | Saline (2.139 ± 1.163)<br>CFA (10.88 ± 1.076) | N/A *sample size too small | | |
| 6C | %mCherry+/cFos+ Naïve | Male and female | vehicle=3 females, 2 males, CNO= 3 females, 2 males | Vehicle (32.79 ± 2.091)<br>CNO (75.66 ± 3.542) | Unpaired t-test | t=10.42, df=8 | <0.0001 |
| 6E | %mCherry+/cFos+ CFA | Male and female | CFA: vehicle=3 females, 2 males, CNO= 1 female, 4 males | Vehicle (46.99 ± 6.707)<br>CNO (70.86 ± 3.673) | Unpaired t-test | t=3.122, df=8 | 0.0142 |
| 7B | cFos Naïve and CFA | Male and female | See above | | | | |
| | RVM-naïve | | | Vehicle (42.19 ± 9.284)<br>CNO (58.86 ± 7.665) | Unpaired t-test | t=1.399, df=9 | 0.1955 |
| | RVM-CFA | | | Vehicle (47.89 ± 7.117)<br>CNO (55.58 ± 12.94) | Unpaired t-test | t=0.5209, df=8 | 0.6166 |
| | LC-naïve | | | Vehicle (39.61 ± 6.324)<br>CNO (395.0 ± 81.61) | Unpaired t-test | t=4.342, df=8 | 0.0025 |

| | | | | | | | |
|---|---|---|---|---|---|---|---|
| | LC-CFA | | Vehicle (152.5 ± 33.95)<br>CNO (376.1 ± 56.14) | Unpaired t-test | t=3.409, df=8 | 0.0092 | |
| | lPBN-naïve | | Vehicle (73.56 ± 27.05)<br>CNO (86.50 ± 32.33) | Unpaired t-test | t=0.3068, df=8 | 0.7668 | |
| | lPBN-CFA | | Vehicle (261.2 ± 65.16)<br>CNO (120.5 ± 16.61) | Unpaired t-test | t=2.093, df=8 | 0.0697 | |
| | LH-naïve | | Vehicle (162.7 ± 35.94)<br>CNO (291.0 ± 40.47) | Unpaired t-test | t=2.371, df=8 | 0.0452 | |
| | LH-CFA | | Vehicle (148.2 ± 32.35)<br>CNO (170.8 ± 20.81) | Unpaired t-test | t=0.5877, df=8 | 0.573 | |
| | PVT-naïve | | Vehicle (649.9 ± 83.30)<br>CNO (1335 ± 203.8) | Unpaired t-test | t=3.110, df=8 | 0.0145 | |
| | PVT-CFA | | Vehicle (591.3 ± 142.3)<br>CNO (480.3 ± 45.84) | Unpaired t-test | t=0.7427, df=8 | 0.4789 | |
| 7D | pPDH Naïve and CFA | Male and female | See above | | | | |

| | | | | | |
|---|---|---|---|---|---|
| RVM-naïve | | Vehicle (4.611 ± 0.8114) CNO (2.566 ± 0.4616) | Unpaired t-test | t=2.191, df=8 | 0.0598 |
| RVM-CFA | *4 CNO | Vehicle (2.828 ± 0.4162) CNO (2.348 ± 0.5111) | Unpaired t-test | t=0.7371, df=7 | 0.485 |
| LC-naïve | | Vehicle (11.77 ± 1.737) CNO (16.37 ± 2.046) | Unpaired t-test | t=1.711, df=8 | 0.1254 |
| LC-CFA | | Vehicle (10.63 ± 1.316) CNO (9.887 ± 1.656) | Unpaired t-test | t=0.3524, df=8 | 0.7336 |
| lPBN-naïve | | Vehicle (0.04490 ± 0.04428) CNO (0.5876 ± 0.2902) | Unpaired t-test | t=1.849, df=8 | 0.1017 |
| lPBN-CFA | | Vehicle (0.1274 ± 0.08537) CNO (0.8096 ± 0.5552) | Unpaired t-test | t=1.214, df=8 | 0.2592 |
| LH-naïve | | Vehicle (1.869 ± 0.4029) CNO (5.371 ± 1.642) | Unpaired t-test | t=2.072, df=8 | 0.0721 |
| LH-CFA | | Vehicle (3.671 ± 0.9999) CNO (3.124 ± 0.8292) | Unpaired t-test | t=0.4210, df=8 | 0.6849 |
| PVT-naïve | | *No signal | | | |

| | | | | |
|---|---|---|---|---|
| PVT-CFA | Vehicle (0.2234 ± 0.2234) CNO (0.009400 ± 0.006112) | Unpaired t-test | t=0.9576, df=8 | 0.3663 |

# Chapter 6: General Discussion

## 6.1 Summary of findings

As described in **Chapter 1**, chronic pain is a significant health issue and due to its complex nature, current pharmacotherapies are not helpful for many patients. One way to address this problem is to improve the current knowledge on brain circuits that contribute to pain signalling and their role in the development of chronic pain. The midbrain PAG is an established integrator of pain and related behaviours and the activity of glycinergic neurons in the PAG has been shown to bidirectionally modulate nociception. This thesis aimed to expand what is currently known about glycinergic signalling in the brain, and in particular the PAG, and its role in nociception and affective behaviours in both naïve and chronic pain states.

**Chapter 2** examined the current evidence supporting a role for glycine signalling in supraspinal pain modulation in the form of a scoping review. It is well established that glycinergic neurotransmission in the spinal cord plays a very important role in pain signalling, but the scoping review highlighted that glycinergic neurotransmission in the brain is also important. In addition, the newly discovered glycine receptors (mGlyR and eGlyR) expand the potential role of glycinergic neurotransmission. In addition to pain, the review also showed that glycinergic signalling in the brain has been implicated in a wide range of other behaviours, including cardiac function, hearing, orofacial movement and sleep. When thinking of brain circuitry, the review demonstrated that there is ample evidence that the role of glycinergic neurons should not be ignored.

**Chapter 3** defined the distribution of $PAG^{GlyT2}$ neurons to the caudal vlPAG and found that around 80% of these neurons co-localise with GAD2. Unlike the classical characterisation of inhibitory neurons in the vlPAG as interneurons (Winters et al., 2022), we showed through electrophysiology and circuit tracing experiments that $PAG^{GlyT2}$ neurons are projection neurons that project to many regions outside the PAG. They not only project to the DR and LC, but also to the LH, PVT, RVM, and lPBN. I then expanded what is known about the functional role of these neurons by carrying out fibre photometry and chemogenetic behavioural experiments. Not only do $PAG^{GlyT2}$ neurons in the PAG modulate and sense nociception but also affective behaviours and non-noxious stimuli. We found they can modulate anxiety-like behaviours and aversion, contributing more broadly to the pain experience.

I then wanted to investigate the role of $PAG^{GlyT2}$ neurons in a chronic pain state, so first characterised the CFA-induced persistent inflammatory pain model in **Chapter 4.** My results

revealed that the model robustly mimics heightened nociceptive sensitivity but poorly encapsulates the affective dimension of chronic pain like anxiety-like behaviours.

Lastly, in **Chapter 5** I unexpectedly found that chemogenetic modulation of PAG$^{GlyT2}$ neurons in a chronic pain state is different to a naïve condition. I found that in the CFA model, PAG$^{GlyT2}$ neurons are engaged during noxious stimuli but no longer can modulate nociceptive responses. This shift in their role between a naive and a chronic pain state is further supported by neuronal activity marking which suggests that their engagement of the PVT, LH and RVM is lost in a chronic pain state. However, the chemogenetic study also revealed that PAG$^{GlyT2}$ neurons continued to modulate locomotion and anxiety-like behaviours, but this was only the case in females and not males. This demonstrated that in a chronic pain state, the functional role of PAG$^{GlyT2}$ neurons is sex specific.

Overall, my thesis demonstrated that a small, sparse neuronal population can sense and modulate diverse behaviours and expanded the potential for pain circuitry in the brain. Previously it has been demonstrated that glycinergic neurons in the PAG can modulate nociception (Assareh et al., 2023), but the current study not only extended this but gives new insights into the complexity of PAG mediated circuits. Pain is not just a sensory experience, but is a complex biopsychosocial phenomenon, and my thesis establish that these neurons are contributing to that experience. In addition, we found that the role of these neurons in a chronic pain state is shifted, giving insight into how brain circuitry changes in a chronic pain state. Overall, this thesis reveals that PAG$^{GlyT2}$ neurons are an important part of midbrain circuitry, with a complex role in integrating sensory inputs and modulating pain states.

## 6.2 The implications for supraspinal glycinergic neurotransmission

This thesis demonstrated for the first time that glycinergic neurotransmission in the brain can modulate affective and other pain associated responses like aversion. It is well established that glycinergic neurotransmission is important for homeostatic control, regulating cardiac function, respiration, pain and sleep (Fenech et al., 2024), but its ability to modulate complex behaviours, like emotion, is largely undefined. The development of the GlyT2::Cre model (Foster et al., 2015), has allowed the behavioural integration of glycinergic neurotransmission in affective behaviours. Using this model, this thesis therefore expands the potential for supraspinal

glycinergic neurotransmission, demonstrating that it can interact with affective circuits and be an important contributor. The ability of PAG$^{GlyT2}$ neurons to modulate anxiety-like behaviours also gives new insight into anxiety circuitry in the brain. The vlPAG is already implicated in modulating anxiety behaviours (Lowery-Gionta et al., 2018; Taylor et al., 2019; Tovote et al., 2016; Yan & Liu, 2024; Yin et al., 2020; Zhang et al., 2021) but the involvement of PAG$^{GlyT2}$ neurons in anxiety behaviour is a novel finding.

## 6.3 Glycinergic neurons are not just GABAergic neurons

In the adult mammalian brain, the neurotransmitter glycine is often co-released with GABA, due to the expression of the vesicular inhibitory amino acid transporter (VIAAT; Aubrey et al., 2007; Jonas et al., 1998; Vaaga et al., 2014), which concentrates both GABA and glycine into synaptic vesicles. Thus, we initially hypothesised that the role of PAG$^{GlyT2}$ neurons would mostly resemble GABAergic neurons in the PAG. However, this thesis shows they are somewhat unique.

Firstly, PAG$^{GlyT2}$ neurons are not just interneurons. Indeed, the circuit tracing data demonstrates they make local connections; however, the electrophysiology experiments suggest they are mainly projection neurons (although this result may reflect sampling bias rather than the population). The descending analgesic pathway is classically characterised by inhibitory interneurons which can directly inhibit noxious information at the spinal cord via the RVM (Lau & Vaughan, 2014). Originally it was hypothesised that PAG$^{GlyT2}$ neurons also act via this pathway, whereby they can modulate nociception and analgesia and was indeed supported in our previous study using chemogenetics (Assareh et al., 2023). However, this classic dogma of inhibitory interneurons has been challenged. Previously, data has suggested that there are inhibitory projection neurons in the PAG (Chen et al., 2022; Harding et al., 2024; Laurent et al., 2020; Reis et al., 2024; Waung et al., 2019; Zhong et al., 2024) and in fact, glycinergic neurons have been shown to project to the DR, LC and PVN (Rampon et al., 1999; Varga et al., 2019). This thesis expanded on these findings to show that PAG$^{GlyT2}$ neurons project and engage not only descending pain pathway regions like the RVM and lPBN, but also ascending regions such as the LH and PVT. This extended role of inhibitory neurons in the PAG adds to the complexity of not only pain signalling, but also midbrain circuitry as a whole.

In addition, the behavioural role of PAG$^{GlyT2}$ neurons is different to what has been previously demonstrated for the GABAergic neuronal population in the vlPAG. Chemogenetic

modulation of vGAT-positive neurons in the vlPAG has been shown to modulate nociception (Samineni et al., 2017) and anxiety-like behaviours (Lowery-Gionta et al., 2018) similarly to PAG$^{GlyT2}$ neurons, however others have shown no modulation of locomotor activity using optogenetic modulation of GABAergic neurons in the vlPAG (Hao et al., 2019; Reis et al., 2024). The role of this small, sparse neuronal subpopulation may be unique to inhibitory neurons in the vlPAG and combined with the knowledge of glycine's restricted distribution in the brain, compared to GABA, suggests its heightened potential as a drug target for future pharmacotherapies (Harvey & Yee, 2013; Vandenberg et al., 2014; Zeilhofer et al., 2005, 2018).

## 6.4 A novel PAG-mediated circuit

The behavioural and circuit discoveries made about PAG$^{GlyT2}$ neurons in this thesis expand the potential of PAG-mediated circuitry. One major finding is that the role of PAG$^{GlyT2}$ neurons can separately modulate nociception and anxiety behaviours. Previously it has been demonstrated that analgesia and anxiety can be separated, but this was through separate neuronal populations in the vlPAG (dopaminergic and glutamatergic; Taylor et al., 2019). This thesis showed that the same neuronal subpopulation, PAG$^{GlyT2}$ neurons, in female mice, can modulate nociception and anxiety-like behaviours in a naïve state but loses the ability to modulate nociception in a chronic pain state. Neuronal activity marking suggests that this may be due to differential engagement of projection regions, although this needs to be investigated in separate male and female cohorts to strengthen this conclusion. This study adds to the idea that pain and anxiety can be uncoupled in the brain, and therefore, PAG$^{GlyT2}$ neurons, in females, becomes a potential novel anxiolytic target in a chronic pain state.

This thesis also provides more evidence of the PAG's ability to be context dependent. We know that it can adapt behaviour based on its functional columns for different forms of stressors or threats, allowing us to react by 'flight, fight or freeze' when appropriate (Keay & Bandler, 2008). With this framework, vlPAG activation induces a quiescence response and thus activation of the PAG$^{GlyT2}$ neurons should induce quiescence and immobility. However, these findings were a result of bulk activation of the columns, and now with discoveries into vlPAG subpopulations it's more appropriate to categorise the PAG as this integrator of behaviour that tunes different neuronal subpopulations and their connections to adapt complex behaviour in a meaningful way.

It has also been established that the signalling of the PAG changes following chronic pain states, such as endogenous cannabinoid signalling (Bouchet et al., 2023; Wilson-Poe et al., 2021). Our findings demonstrate that the role of $PAG^{GlyT2}$ neurons is changed following a CFA state, and we also found that $PAG^{GlyT2}$ neurons are unable to modulate visceral pain responses (Appendix 2). This may be due to a differential engagement of projection regions, or a change in $PAG^{GlyT2}$ neuronal properties (by opioids or cannabinoids), or a combination of the two. We also found that there are sex differences in $PAG^{GlyT2}$ neurons following a CFA state, and cannabinoid receptors and $GABA_A$ signalling in the PAG has been shown previously to be sex specific (Jiang et al., 2022; Tonsfeldt et al., 2016). The current hypothesis is that there may be different neuronal subpopulations present within the $PAG^{GlyT2}$ neuronal population, aiding the PAG's ability to adapt to different contexts.

## 6.5 Future directions

This thesis expands the current knowledge of the potential of glycinergic neurotransmission and PAG mediated circuitry, but there are additional gaps in knowledge that could be explored. Firstly, Chapter 4 demonstrates that the CFA persistent inflammatory pain model does not robustly model chronic inflammatory pain in humans, and although many preclinical models also share this problem, investigating how the role of $PAG^{GlyT2}$ neurons shifts in different chronic pain contexts such as neuropathic pain could be interesting. As posed previously, the evidence suggests that $PAG^{GlyT2}$ neurons are made up of different neuronal subpopulations, this could be further investigated by using a two-photon miniscope and seeing if there separate neuronal populations engaged during different behaviours. Another future direction would aim to define the projection-specific behavioural function of $PAG^{GlyT2}$ neurons using circuit specific expression of chemo- or optogenetic channels and an expanded array of sensory and emotional behavioural tests. Additionally, the signalling mechanisms of $PAG^{GlyT2}$ neuronal projections could be further investigated using optogenetic activation, anterograde transsynaptic tracing and slice electrophysiology. It would also be interesting to see the molecular signatures of these projection neurons, and this could be achieved by tagging each projection population with newly developed retrograde-TAG vectors, extracting nuclei and performing single-nuclei RNA sequencing. All of these future directions could be with different chronic pain models and in both males and females as we have established that $PAG^{GlyT2}$ neurons are sex specific in a chronic pain state.

## 6.6 Conclusion

In conclusion, this thesis uncovered the role of glycinergic neurons in the periaqueductal grey. We discovered a novel PAG circuit, that modulates nociception and anxiety-like behaviours, expanding what is currently known about pain circuitry and overall midbrain circuitry. By understanding how the brain computes behaviour and how it shifts in chronic pain states, more effective and safer therapies can be designed to help people suffering from chronic pain and other conditions.

## 6.7 References (General Discussion)


Assareh, N., Fenech, C., Power, R., Uddin, M. N., Otsu, Y., & Aubrey, K. R. (2023). Bidirectional Modulation of Nociception by GlyT2+ Neurons in the Ventrolateral Periaqueductal Gray. *eNeuro*, *10*(6). https://doi.org/10.1523/ENEURO.0069-23.2023

Aubrey, K. R., Rossi, F. M., Ruivo, R., Alboni, S., Bellenchi, G. C., Le Goff, A., Gasnier, B., & Supplisson, S. (2007). The transporters GlyT2 and VIAAT cooperate to determine the vesicular glycinergic phenotype. *The Journal of Neuroscience: The Official Journal of the Society for Neuroscience*, *27*(23), 6273–6281. https://doi.org/10.1523/JNEUROSCI.1024-07.2007

Bouchet, C. A., McPherson, K. B., Coutens, B., Janowsky, A., & Ingram, S. L. (2023). Monoacylglycerol Lipase Protects the Presynaptic Cannabinoid 1 Receptor from Desensitization by Endocannabinoids after Persistent Inflammation. *Journal of Neuroscience*, *43*(30), 5458–5467. https://doi.org/10.1523/JNEUROSCI.0037-23.2023

Chen, Z., Lin, M.-T., Zhan, C., Zhong, N.-S., Mu, D., Lai, K.-F., & Liu, M. J. (2022). A descending pathway emanating from the periaqueductal gray mediates the development of cough-like hypersensitivity. *iScience*, *25*(1). https://doi.org/10.1016/j.isci.2021.103641

Fenech, C., Winters, B. L., Otsu, Y., & Aubrey, K. R. (2024). Supraspinal glycinergic neurotransmission in pain: A scoping review of current literature. *Journal of Neurochemistry*, *168*(11), 3663–3684. https://doi.org/10.1111/jnc.16191

Foster, E., Wildner, H., Tudeau, L., Haueter, S., Ralvenius, W. T., Jegen, M., Johannssen, H., Hösli, L., Haenraets, K., Ghanem, A., Conzelmann, K.-K., Bösl, M., & Zeilhofer, H. U. (2015). Targeted Ablation, Silencing, and Activation Establish Glycinergic Dorsal Horn Neurons as Key Components of a Spinal Gate for Pain and Itch. *Neuron*, *85*(6), 1289–1304. https://doi.org/10.1016/j.neuron.2015.02.028

Hao, S., Yang, H., Wang, X., He, Y., Xu, H., Wu, X., Pan, L., Liu, Y., Lou, H., Xu, H., Ma, H., Xi, W., Zhou, Y., Duan, S., & Wang, H. (2019). The Lateral Hypothalamic and BNST GABAergic Projections to the Anterior Ventrolateral Periaqueductal Gray Regulate Feeding. *Cell Reports*, *28*(3), 616-624.e5. https://doi.org/10.1016/j.celrep.2019.06.051

Harding, E. K., Zhang, Z., Canet-Pons, J., Stokes-Heck, S., Trang, T., & Zamponi, G. W. (2024). Expression of GAD2 in excitatory neurons projecting from the ventrolateral periaqueductal gray to the locus coeruleus. *iScience*, *27*(6), 109972. https://doi.org/10.1016/j.isci.2024.109972

Harvey, R. J., & Yee, B. K. (2013). Glycine transporters as novel therapeutic targets in schizophrenia, alcohol dependence and pain. *Nature Reviews. Drug Discovery*, *12*(11), 866–885. https://doi.org/10.1038/nrd3893

Jiang, Z., Wang, Q., Zhao, J., Wang, J., Li, Y., Dai, W., Zhang, X., Fang, Z., Hou, W., & Xiong, L. (2022). Sex-specific cannabinoid 1 receptors on GABAergic neurons in the ventrolateral periaqueductal gray mediate analgesia in mice. *Journal of Comparative Neurology*, *530*(13), 2315–2334. https://doi.org/10.1002/cne.25334

Jonas, P., Bischofberger, J., & Sandkühler, J. (1998). Corelease of two fast neurotransmitters at a central synapse. *Science (New York, N.Y.)*, *281*(5375), 419–424. https://doi.org/10.1126/science.281.5375.419

Keay, K., & Bandler, R. (2008). 5.42—Emotional and Behavioral Significance of the Pain Signal and the Role of the Midbrain Periaqueductal Gray (PAG). In R. H. Masland, T. D. Albright, T. D. Albright, R. H. Masland, P. Dallos, D. Oertel, S. Firestein, G. K. Beauchamp, M. Catherine Bushnell, A. I. Basbaum, J. H. Kaas, & E. P. Gardner (Eds.), *The Senses: A Comprehensive Reference* (pp. 627–634). Academic Press. https://doi.org/10.1016/B978-012370880-9.00184-5

Laboute, T., Zucca, S., Holcomb, M., Patil, D. N., Garza, C., Wheatley, B. A., Roy, R. N., Forli, S., & Martemyanov, K. A. (2023). Orphan receptor GPR158 serves as a metabotropic glycine receptor: mGlyR. *Science*, *379*(6639), 1352–1358. https://doi.org/10.1126/science.add7150

Lau, B. K., & Vaughan, C. W. (2014). Descending modulation of pain: The GABA disinhibition hypothesis of analgesia. *Current Opinion in Neurobiology*, *29*, 159–164. https://doi.org/10.1016/j.conb.2014.07.010

Laurent, R. S., Damonte, V. M., Tsuda, A. C., & Kauer, J. A. (2020). Periaqueductal Gray and Rostromedial Tegmental Inhibitory Afferents to VTA Have Distinct Synaptic Plasticity and Opiate Sensitivity. *Neuron*, *106*(4), 624-636.e4. https://doi.org/10.1016/j.neuron.2020.02.029

Lowery-Gionta, E. G., DiBerto, J., Mazzone, C. M., & Kash, T. L. (2018). GABA neurons of the ventral periaqueductal gray area modulate behaviors associated with anxiety and conditioned fear. *Brain Structure and Function*, *223*(8), 3787–3799. https://doi.org/10.1007/s00429-018-1724-z

Otsu, Y., Darcq, E., Pietrajtis, K., Matyas, F., Schwartz, E., Bessaih, T., Abi Gerges, S., Rousseau, C. V., Grand, T., Dieudonné, S., Paoletti, P., Acsady, L., Agulhon, C., Kieffer, B. L., & Diana, M. A. (2019). Control of aversion by glycine-gated GluN1/GluN3A NMDA receptors in the adult Medial Habenula. *Science (New York, N.Y.)*, *366*(6462), 250–254. https://doi.org/10.1126/science.aax1522

Rampon, C., Peyron, C., Gervasoni, D., Pow, D. V., Luppi, P.-H., & Fort, P. (1999). Origins of the glycinergic inputs to the rat locus coeruleus and dorsal raphe nuclei: A study combining retrograde tracing with glycine immunohistochemistry. *European Journal of Neuroscience*, *11*(3), 1058–1066. https://doi.org/10.1046/j.1460-9568.1999.00511.x

Reis, F. M. C. V., Maesta-Pereira, S., Ollivier, M., Schuette, P. J., Sethi, E., Miranda, B. A., Iniguez, E., Chakerian, M., Vaughn, E., Sehgal, M., Nguyen, D. C. T., Yuan, F. T. H., Torossian, A., Ikebara, J. M., Kihara, A. H., Silva, A. J., Kao, J. C., Khakh, B. S., & Adhikari, A. (2024). Control of feeding by a bottom-up midbrain-subthalamic pathway. *Nature Communications*, *15*(1), 2111. https://doi.org/10.1038/s41467-024-46430-5

Samineni, V. K., Grajales-Reyes, J. G., Copits, B. A., O'Brien, D. E., Trigg, S. L., Gomez, A. M., Bruchas, M. R., & Gereau, R. W. (2017). Divergent Modulation of Nociception by Glutamatergic and GABAergic Neuronal Subpopulations in the Periaqueductal Gray. *eNeuro*, *4*(2). https://doi.org/10.1523/ENEURO.0129-16.2017

Taylor, N. E., Pei, J., Zhang, J., Vlasov, K. Y., Davis, T., Taylor, E., Weng, F.-J., Dort, C. J. V., Solt, K., & Brown, E. N. (2019). The Role of Glutamatergic and Dopaminergic Neurons in the Periaqueductal Gray/Dorsal Raphe: Separating Analgesia and Anxiety. *eNeuro*, *6*(1). https://doi.org/10.1523/ENEURO.0018-18.2019

Tonsfeldt, K. J., Suchland, K. L., Beeson, K. A., Lowe, J. D., Li, M., & Ingram, S. L. (2016). Sex Differences in GABAA Signaling in the Periaqueductal Gray Induced by Persistent Inflammation. *Journal of Neuroscience*, *36*(5), 1669–1681. https://doi.org/10.1523/JNEUROSCI.1928-15.2016

Tovote, P., Esposito, M. S., Botta, P., Chaudun, F., Fadok, J. P., Markovic, M., Wolff, S. B. E., Ramakrishnan, C., Fenno, L., Deisseroth, K., Herry, C., Arber, S., & Lüthi, A. (2016). Midbrain circuits for defensive behaviour. *Nature*, *534*(7606), 206–212. https://doi.org/10.1038/nature17996

Vaaga, C. E., Borisovska, M., & Westbrook, G. L. (2014). Dual-transmitter neurons: Functional implications of co-release and co-transmission. *Current Opinion in Neurobiology*, *0*, 25–32. https://doi.org/10.1016/j.conb.2014.04.010

Vandenberg, R. J., Ryan, R. M., Carland, J. E., Imlach, W. L., & Christie, M. J. (2014). Glycine transport inhibitors for the treatment of pain. *Trends in Pharmacological Sciences*, *35*(8), 423–430. https://doi.org/10.1016/j.tips.2014.05.006

Varga, E., Farkas, E., Zséli, G., Kádár, A., Venczel, A., Kővári, D., Németh, D., Máté, Z., Erdélyi, F., Horváth, A., Szenci, O., Watanabe, M., Lechan, R. M., Gereben, B., & Fekete, C. (2019). Thyrotropin-Releasing-Hormone-Synthesizing Neurons of the Hypothalamic Paraventricular Nucleus Are Inhibited by Glycinergic Inputs. *Thyroid: Official Journal of the American Thyroid Association*, *29*(12), 1858–1868. https://doi.org/10.1089/thy.2019.0357

Waung, M. W., Margolis, E. B., Charbit, A. R., & Fields, H. L. (2019). A Midbrain Circuit that Mediates Headache Aversiveness in Rats. *Cell Reports*, *28*(11), 2739-2747.e4. https://doi.org/10.1016/j.celrep.2019.08.009

Wilson-Poe, A. R., Wiese, B., Kibaly, C., Lueptow, L., Garcia, J., Anand, P., Cahill, C., & Morón, J. A. (2021). Effects of inflammatory pain on CB1 receptor in the midbrain periaqueductal gray. *PAIN Reports*, *6*(1), e897. https://doi.org/10.1097/PR9.0000000000000897

Winters, B. L., Lau, B. K., & Vaughan, C. W. (2022). Cannabinoids and Opioids Differentially Target Extrinsic and Intrinsic GABAergic Inputs onto the Periaqueductal Grey Descending Pathway. *Journal of Neuroscience*, *42*(41), 7744–7756. https://doi.org/10.1523/JNEUROSCI.0997-22.2022

Yan, C., & Liu, Z. (2024). The role of periaqueductal gray astrocytes in anxiety-like behavior induced by acute stress. *Biochemical and Biophysical Research Communications*, *720*, 150073. https://doi.org/10.1016/j.bbrc.2024.150073

Yin, J.-B., Liang, S.-H., Li, F., Zhao, W.-J., Bai, Y., Sun, Y., Wu, Z.-Y., Ding, T., Sun, Y., Liu, H.-X., Lu, Y.-C., Zhang, T., Huang, J., Chen, T., Li, H., Chen, Z.-F., Cao, J., Ren, R., Peng, Y.-N., … Li, Y.-Q. (2020). dmPFC-vlPAG projection neurons contribute to pain threshold maintenance and antianxiety behaviors. *The Journal of Clinical Investigation*, *130*(12), 6555–6570. https://doi.org/10.1172/JCI127607

Zeilhofer, H. U. (2005). The glycinergic control of spinal pain processing. *Cellular and Molecular Life Sciences: CMLS*, *62*(18), 2027–2035. https://doi.org/10.1007/s00018-005-5107-2

Zeilhofer, H. U., Acuña, M. A., Gingras, J., & Yévenes, G. E. (2018). Glycine receptors and glycine transporters: Targets for novel analgesics? *Cellular and Molecular Life Sciences: CMLS*, *75*(3), 447–465. https://doi.org/10.1007/s00018-017-2622-x

Zeilhofer, H. U., Studler, B., Arabadzisz, D., Schweizer, C., Ahmadi, S., Layh, B., Bösl, M. R., & Fritschy, J.-M. (2005). Glycinergic neurons expressing enhanced green fluorescent protein in bacterial artificial chromosome transgenic mice. *The Journal of Comparative Neurology*, *482*(2), 123–141. https://doi.org/10.1002/cne.20349

Zeilhofer, H. U., Werynska, K., Gingras, J., & Yévenes, G. E. (2021). Glycine Receptors in Spinal Nociceptive Control—An Update. *Biomolecules*, *11*(6), 846. https://doi.org/10.3390/biom11060846

Zhang, G.-W., Shen, L., Tao, C., Jung, A.-H., Peng, B., Li, Z., Zhang, L. I., & Tao, H. W. (2021). Medial preoptic area antagonistically mediates stress-induced anxiety and parental behavior. *Nature Neuroscience*, *24*(4), 516–528. https://doi.org/10.1038/s41593-020-00784-3

Zhong, C.-C., Xu, Z., Gan, J., Yu, Y.-M., Tang, H.-M., Zhu, Y., Yang, J.-X., Ding, H.-L., & Cao, J.-L. (2024). Acute Ongoing Nociception Delays Recovery of Consciousness from Sevoflurane Anesthesia via a Midbrain Circuit. *The Journal of Neuroscience*, *44*(34), e0740242024. https://doi.org/10.1523/JNEUROSCI.0740-24.2024

# Appendix 1: Bidirectional modulation of nociception by GlyT2+ neurons in the ventrolateral periaqueductal grey

**Bidirectional modulation of nociception by GlyT2+ neurons in the ventrolateral periaqueductal grey**

Neda Assareh,[1,2] Caitlin Fenech,[1,2,3] Rebecca Power,[1,2] Mohammad N. Uddin,[1] Yo Otsu,[1,2] and Karin R. Aubrey[1,2]

[1]Pain Management Research, Kolling Institute, Royal North Shore Hospital Northern Sydney Local Health District and Faculty of Medicine and Health, University of Sydney, Sydney, New South Wales 2065, Australia

[2]Sydney Pain Consortium, Faculty of Medicine and Health, University of Sydney, Sydney, New South Wales 2006, Australia

[3]School of Medical Sciences, Faculty of Medicine and Health, University of Sydney, Sydney, New South Wales 2006, Australia

Published in **eNeuro.**

Contributions- N.A., Y.O., and K.R.A. designed research; N.A., C.F., R.P., M.N.U., Y.O., and K.R.A. performed research; N.A., C.F., Y.O., and K.R.A. analysed data; N.A. and K.R.A. wrote the paper.

Sensory and Motor Systems

# Bidirectional Modulation of Nociception by GlyT2$^+$ Neurons in the Ventrolateral Periaqueductal Gray

Neda Assareh,[1,2] Caitlin Fenech,[1,2,3] Rebecca Power,[1,2] Mohammad N. Uddin,[1] Yo Otsu,[1,2] and Karin R. Aubrey[1,2]

https://doi.org/10.1523/ENEURO.0069-23.2023

[1]Pain Management Research, Kolling Institute, Royal North Shore Hospital Northern Sydney Local Health District and Faculty of Medicine and Health, University of Sydney, Sydney, New South Wales 2065, Australia, [2]Sydney Pain Consortium, Faculty of Medicine and Health, University of Sydney, Sydney, New South Wales 2006, Australia, and [3]School of Medical Sciences, Faculty of Medicine and Health, University of Sydney, Sydney, New South Wales 2006, Australia

## Abstract

The midbrain periaqueductal gray (PAG), particularly its ventrolateral column (vlPAG), is part of a key descending pathway that modulates nociception, fear and anxiety behaviors in both humans and rodents. It has been previously demonstrated that inhibitory GABAergic neurons within the vlPAG have a major role in this nociceptive modulation. However, the PAG contains a diverse range of neuronal subtypes and the contribution of different subtypes of inhibitory neurons to nociceptive control has not been investigated. Here, we employed a chemogenetic strategy in mice that express Cre recombinase under the promotor for the glycine transporter 2 (GlyT2::cre) to modulate a novel group of glycinergic neurons within the vlPAG and then investigate their role in nociceptive control. We show that activation of GlyT2-PAG neurons enhances cold and noxious heat responses and increases locomotor activity (LMA) in both male and female mice. In contrast, inhibition of GlyT2-PAG neurons reduced nociceptive responses, while locomotor behaviors were unaffected. Our findings demonstrate that GlyT2$^+$ neurons in the vlPAG modulate nociception and suggest that strategies targeting GlyT2-PAG neurons could be used to design novel analgesic therapies.

*Key words:* chemogenetics; glycinergic neurotransmission; GlyT2::Cre mice; nociception; supraspinal glycine; vlPAG

### Significance Statement

Neuronal circuits are composed of diverse collections of cell types, each with a distinct set of synaptic connections that determine their role in specific functions. One challenge in neuropharmacology is to design drugs that interact with the brain circuits required to have the desired therapeutic effect and limit their activity at nearby circuits, thus reducing side effects. The current study shows that a genetically identified subpopulation of GlyT2$^+$ neurons that are concentrated in the ventrolateral periaqueductal gray (vlPAG) can bidirectionally modulate nociceptive responses and alter locomotion behaviors in mice. These findings provided novel insights into the organization of the nociceptive circuitry of the PAG and identify GlyT2-PAG neurons as a potential target for analgesic drug design.

## Introduction

Responding appropriately to pain (or the possibility of pain) requires the integration of nociceptive inputs with motor, autonomic and affective brain circuits (Behbehani, 1995; Benarroch, 2012). A detailed understanding of how each subpopulation of neurons within these regions contributes to shaping different pain aspects is needed to enhance our understanding

Received February 28, 2023; accepted April 27, 2023; First published May 30, 2023.
The authors declare no competing financial interests.

Author contributions: N.A., Y.O., and K.R.A. designed research; N.A., C.F., R.P., M.N.U., Y.O., and K.R.A. performed research; N.A., C.F., Y.O., and K.R.A. analyzed data; N.A. and K.R.A. wrote the paper.

of the cells involved and to develop effective new therapies for pain.

The midbrain periaqueductal gray (PAG) has extensive efferent and afferent connections that help it coordinate behavioral responses to various stressors and threats, including pain (Cameron et al., 1995a,b). A wealth of tracing and neurochemical analyses have demonstrated that the PAG is functionally subdivided into four columns, dorsomedial (dm), dorsolateral (dl), lateral (l), and ventrolateral (vl), each characterized by distinct afferent and efferent connections, molecular profiles, and associated behavior (Brandão et al., 1982; Zhang et al., 1990; Fanselow, 1991; Carrive, 1993; Bandler and Shipley, 1994; K.A. Keay and Bandler, 2015; Vaughn et al., 2022). Electrical and chemical stimulation studies indicate that the vlPAG drives antinociception and is involved in passive behavioral responses (e.g., quiescence and immobility), whereas the dlPAG and lPAG columns are involved in antinociception coupled with active responses (e.g., flight and defensive behaviors; M. Morgan et al., 1998; K.A. Keay et al., 2001; M.M. Morgan and Clayton, 2005; K. Keay and Bandler, 2008). The ability of the vlPAG to modulate nociception is primarily mediated by a key descending pathway that projects through the rostroventromedial medulla to suppress nociceptive transmission in the dorsal horn of the spinal cord (Vaughan and Christie, 1997; Lau and Vaughan, 2014). This descending pathway is also an important target for both endogenous and exogenous opioids (Mohrland and Gebhart, 1980; Cheng et al., 1986; Bagley and Ingram, 2020). Thus, the vlPAG helps shape complex behavioral responses to stressors, contributes to nociceptive control and can drive profound analgesia.

The vlPAG is made up of a diverse array of cell types characterized by their genetic and neurochemical profiles, and more broadly whether they release inhibitory or excitatory neurotransmitters. The distinct nociceptive roles of excitatory and inhibitory signaling within the vlPAG have been investigated using microinjection of specific GABA- or glutamate receptor agonists and antagonists (Moreau and Fields, 1986; Depaulis et al., 1987; Sandkühler et al., 1989). More recently genetic technologies in combination with chemogenetics or optogenetics have examined the specialized roles of vlPAG neuronal cell types (Tovote et al., 2016; Capelli et al., 2017; Samineni et al., 2017, 2019; Hao et al., 2019; Yin et al., 2020; Yu et al., 2021). Collectively, these studies confirm that activating glutamatergic neurons, or suppressing inhibitory GABAergic neurons is antinociceptive, consistent with disinhibition of the descending pain modulatory pathway (Lau and Vaughan, 2014). However, inhibitory neurotransmission can also be mediated by glycinergic neurons (Zeilhofer et al., 2018), although if and how glycinergic neurons contribute to different vlPAG-mediated behaviors is unknown.

Here, we investigate the behavioral outcome of chemogenetically modulating a subpopulation of inhibitory vlPAG neurons identified by their expression of the SLC6A5 gene, encoding the glycine transporter 2 (GlyT2). GlyT2 is an established marker of inhibitory glycinergic neurons and is responsible for accumulating glycine into presynaptic terminals (Zafra et al., 1995; Rampon et al., 1996; Zeilhofer et al., 2005; Aubrey et al., 2007). GlyT2$^+$ neurons are found throughout the mammalian spinal cord and hindbrain (brainstem, cerebellum, and limited populations in the thalamus), but absent from forebrain regions (Rampon et al., 1996; Zeilhofer et al., 2005; Miranda et al., 2022) and in the adult CNS, they often corelease glycine with GABA (Chéry and De Koninck, 1999; Nabekura et al., 2004; Rousseau et al., 2012; Otsu and Aubrey, 2022). While their role in spinal nociceptive circuits have been intensely investigated, little is known about the involvement of glycinergic neurons in supra-medullary brain regions such as the midbrain PAG.

Previous reports have reported that a minority of inhibitory neurons in the vlPAG express GlyT2 (GlyT2-PAG neurons; Rampon et al., 1996; Tanaka and Ezure, 2004; Zeilhofer et al., 2005), but their functional role has never been investigated. Given the importance of the vlPAG in nociceptive responses, we hypothesise that GlyT2-PAG neurons may form part of a PAG microcircuit involved in nociceptive processing.

## Materials and Methods

### Animals

All experiments were conducted in accordance with the Australian Code for the care and use of animals for scientific purposes. A total of 65 adult transgenic mice with Cre-recombinase expressed under the promoter of the glycine transporter, GlyT2 (GlyT2::Cre mice, a gift from H. U. Zeilhofer; Foster et al., 2015) were used in this study. Seventy percent of these animals are included in the analysis after removal of those with a misplaced or lack of AAV delivery. In addition, $n = 5$ cre-negative littermates were used in control experiments to confirm that there were no behavioral effects of AAV5-DIO-hM3Dq cre-independent leak (Botterill et al., 2021). All protocols were approved by the Institutional Animal Ethics committee (Protocol no. RESP 19/66). Animals were bred and housed in the Institute Animal Facility in ventilated cages with a maximum of four mice/cage. Animals were maintained on a 12/12 h light/dark cycle (23°C, 70% humidity) and were provided food and water *ad libitum*. Cages were enriched with a house igloo, tissues for nesting, and straws or paddle pop sticks on alternate weeks.

### Viral constructs and surgery

Stereotaxic injections were performed on adult mice (8–12 weeks; 22 ± 3 g) under anesthesia (1.5–3% isoflurane

This work was supported by an Ernest Heine Family Foundation Grant ABN 29405919488 and a Pain Foundation Grant ABN 87072480123. C.F. is supported by an Australian Government Research Training Postgraduate scholarship.

Acknowledgements: The GlyT2::Cre mouse was a kind gift from the Zeilhofer Laboratory, AAV-vectors were a kind gift from Brian Roth, supplied by Addgene (catalog #44362, #44361, #50459). We thank Chris Vaughan for critical manuscript feedback.

Correspondence should be addressed to Karin R. Aubrey at karin.aubrey@sydney.edu.au.

https://doi.org/10.1523/ENEURO.0069-23.2023

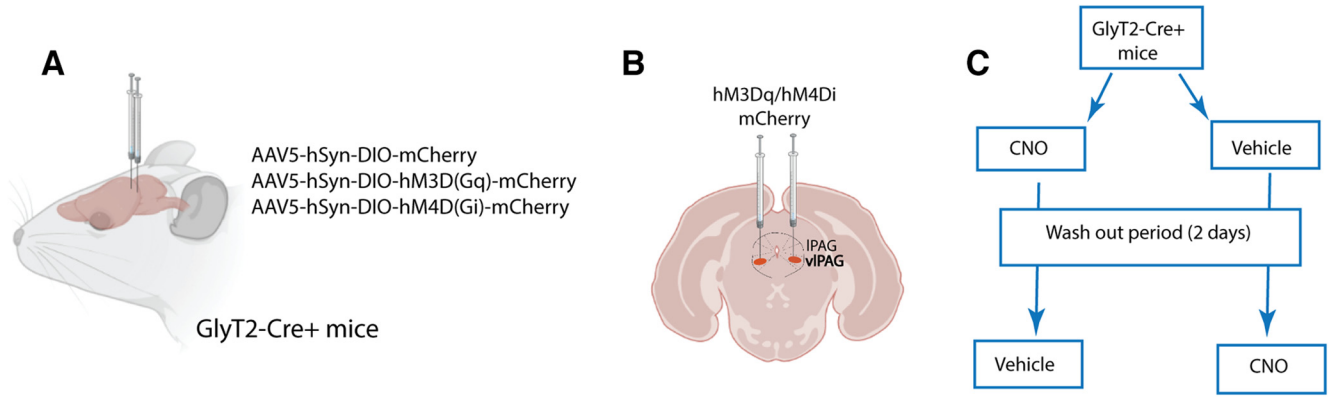


**Figure 1.** Experimental protocol. ***A***, ***B***, Viral vectors AAV5-hSyn-DIO-hM3Dq–mCherry, AAV5-hSyn-DIO-hM4Di–mCherry, and AAV5-hSyn-DIO-mCherry were bilaterally injected into the vlPAG of GlyT2::Cre mice three to four weeks before behavioral tests. ***C***, Behavioral schematic. CNO or vehicle injection (intraperitoneal) took place 1 h before behavioral testing. Test were conducted using a within-subjects crossover design and a 2-d rest period between CNO and vehicle to ensure complete CNO washout.

and 1 l/min $O_2$) using a stereotactic apparatus (Kopf Instruments). Cre dependent expression of control or chemogenetic products was achieved using AAV5-hSyn-DIO-mCherry (8.4e12 vg/ml, Addgene #50459), AAV5-hSyn-DIO-hM3D(Gq)-mCherry (2.3e13 vg/ml, Addgene #44361) and AAV5-hSyn-DIO-hM4D(Gi)-mCherry (2.5e13 vg/ml, Addgene #44362). Vectors were a kind gift from Brian Roth (Addgene catalog #44362, #44361, #50459).

The following coordinates were used to target the vlPAG: bregma Anterior-Posterior (AP), −4.7 to −4.9 mm; Medial-Lateral (ML), ±0.3–0.4 mm; Dorsal-Ventral (DV), 2.7–2.9 mm (Samineni et al., 2017). Injections were made with a motorized microinjector (UMP3T-2 with SMARTouch, WPI) and 200 nl of the vector was infused at the speed of 100 nl/min. Then, the nanovolum needle (SEG Syringe, volume 1 nl, 0.63 mm OD, part #000500) was kept in place for 5 min, retracted 0.1 mm and left for a further 3 min before complete withdrawal. 6–0 black braided silk sutures and iodine sterilization were used to aid in wound healing, and pain relief was administered (buprenorphine 0.05–0.1 μg/g mice, s.c). Following surgery, the mice were individually housed until recovery from the procedure (max 2 d) before being returned to their home cage.

### Chemogenetic manipulation

Three to four weeks after viral injection, mice underwent baseline behavioral testing and were then injected intraperitoneally with clozapine-N-oxide (CNO; diluted in 10% DMSO and saline, 3–5 mg/kg; Sigma-Aldrich) or vehicle control (10% DMSO and saline) and 60 min later behavioral experiments commenced. We used a within-subjects crossover design and animals had a 2-d rest period between CNO and vehicle treatments to ensure complete washout of CNO (Fig. 1). CNO was injected at 3 mg/kg and 5 mg/kg for animals expressing hM3D (Gq) activation and hM4D(Gi) inactivation vectors respectively as previously described (Alexander et al., 2009). Control animals expressing mCherry were administrated 5 mg/kg CNO.

Each animal underwent two (locomotor) or three (nociception) periods of testing following either: baseline (no treatment, nociceptive tests only), CNO or saline treatment. The baseline was determined before the first treatment and the order of CNO, and saline administration was counterbalanced. The researcher was blinded to the treatment group during the behavioral experiments and analysis.

We confirmed that AAV-Cre-independent leak of vectors (Botterill et al., 2021) does not contribute to the CNO-stimulated behavioral changes measured in our model as CNO (3 mg/kg, i.p) had no functional effect (acetone, hotplate, open field tests) in cre-negative littermates injected with AAV5-hSyn-DIO-hM3Dq–mCherry ($n = 5$; Extended Data Fig. 3-1).

### Nociceptive tests

Acute nociception was evaluated by measuring responses to cold (acetone) and hot (hotplate) stimuli applied to the left hind paw (>5 min between tests to ensure results are independent; Anderson et al., 2014; François et al., 2017; Samineni et al., 2017; Mitchell et al., 2021). For the acetone test (Yoon et al., 1994), mice were habituated to adjacent individual testing chambers with a wire-mesh floor for 30 min before testing started. The response to rapid cooling was measured by application of acetone (20 μl) to the plantar surface of the left hind paw with a pipette fitted with a customized tip. The number of licking responses was counted over 20 s and averaged over two trials (5 min between trials). For the hotplate test (Hunskaar et al., 1986; Vermeirsch and Meert, 2004), mice were individually placed in a cylindrical enclosure on a metal surface hotplate at 50°C (for a maximum of 45 s). The time taken to display a nociceptive response, such as licking or shaking of the hind paw, was averaged over three trials (5-min interval between trials). In mice where there was >4-s difference between the three trials, up to two extra trials were conducted and the average response was calculated from the three closest responses (Espejo et al., 1994).

### Locomotor activity

Locomotor activity (LMA) was assessed one week after the sensory testing using the open field test. Mice were

placed in an enclosed open-top arena (50 × 50 × 50 cm) and an overhead camera recorded the behavior of the mice for 20 min (light level = 45 lux). This period allowed for the monitoring of locomotion and anxiety-like behaviors (Bailey and Crawley, 2009). The following characteristics of locomotion were scored; total distance moved, average speed, total time of im/mobility, total line crossing, and total time, distance in the center zone, rearing, and jumping.

### Perfusion and fixation

On the day of perfusion, all mice received a saline or CNO injection (intraperitoneally). Two hours later, mice were deeply anaesthetized with an overdose of Lethabarb (200 mg/kg), and depth of anesthesia was verified by a lack of righting response or paw withdrawal in response to a foot pinch. Then, they were transcardially perfused with 0.9% saline containing 72.5 mM $NaNO_2$ and 3 IU/ml heparin (Sigma), followed by 4% paraformaldehyde (PFA) in 0.13 M PBS (pH 7.4). Brains were removed, postfixed, and refrigerated overnight in the same fixative solution (4% PFA, 4°C). The tissue was washed in PBS and cryoprotected in 30% sucrose in PBS (pH 7.4 at 4°C) for 2 d before being stored at −80°C until cryo-sectioning.

### Viral placement and mCherry/cFos immunohistochemistry

A cryostat (−20°C, Leica Microsystems; Leica 1080) was used to collect serial 40-μm coronal sections of the PAG. These sections were collected in a 1:4 series in 24-well plates as free-floating sections and preserved in 0.1 M phosphate buffer (PB) saline containing 0.1% sodium azide at 4°C. The PAG slices from one series were mounted onto gelatinized glass slides with ProLong mounting media (Thermo Fischer Scientific) and a glass coverslip, allowed to dry, and imaged to confirm stereotaxic AAV-vector placement by visualizing mCherry expression (without amplification).

In a second series of tissue from mice expressing hM3Dq who received either saline or CNO before perfusion, the colocalization of cFos and mCherry was measured by combining cFos DAB-immunohistochemistry (IHC) with immunofluorescent (IF) labeling of mCherry. Sections were washed in 1× Envision FLEX wash buffer (DAKO, catalog #K800721-2, pH 7.6) followed by 50% ethanol and 50% ethanol with 3% hydrogen peroxide in DAKO FLEX wash buffer for 30 min each. Then, sections were incubated in c-Fos (1:5000, New England Biolabs, catalog #2250S) and mCherry primary antibodies (1:1000, Abcam, catalog #ab205402) in DAKO wash buffer for two nights at 4°C. Following washing in DAKO wash buffer, sections were incubated with Envision$^+$ system-HRP-labeled polymer anti-rabbit (DAKO, catalog #K400311-2) at room temperature (RT) for 2 h and peroxidase activity was revealed using liquid DAB$^+$ (DAKO, catalog #K346811-2) for 10 min. The reaction was stopped by the addition milliQ water. Finally, the sections were incubated for 2 h at RT with the secondary antibody for mCherry (goat anti-chicken IgY H + L Alexa Fluor 568 in 1:500, Abcam catalog #Ab175477) in DAKO wash buffer with 10% goat serum and DAPI (1:2000). After a final wash period, slices were mounted on slides using Epredia Lab Vision PermaFluor aqueous mounting medium (Thermo Fisher Scientific, catalog #TA-030-FM).

### Fluorescent and light microscopy

PAG slices were imaged across the rostro-caudal axis on a fluorescent microscope (Zeiss Axio M1) and cFos was imaged using brightfield illumination. The bilateral localization of injection sites centered around the vlPAG was confirmed according to Paxinos and Franklin (2001). Mice with clear evidence of bilateral expression of the injected vector in the PAG were included in the analyses. To create Figures 2*B* and 6*A*, the highest level of viral expression per section was considered and schemed onto PAG templates. In a few animals, sparse labeling of neurons in the superior colliculus was noted near the injection tract.

### Electrophysiology

Four to five weeks after viral infection of PAG neurons, mice were deeply anesthetized with 2% isoflurane (assessed by the rate of breathing, lack of righting reflexes, and lack of response to paw squeeze) and transcardially perfused with ice-cold *N*-methyl-D-glucamine solution (NMDG) containing (in mM): 93 NMDG, 30 NaHCO3, 25 glucose, 5 *N*-acetyl-L-cysteine, 3 Na-pyruvate, 2.5 KCl, 1.2 $NaH_2PO_4$, 20 HEPES, 10 $MgSO_4$, 0.5 $CaCl_2$, 5 sodium ascorbate (~300 mOsm), equilibrated with 95% $O_2$-5% $CO_2$. Mice were then decapitated, 280-μm-thick coronal brain slices (280 mm) including the PAG region were prepared with a vibratome (Leica VT1200S) in the same ice-cold NMDG solution, and then maintained in this solution for 10 min at 34°C. After, they were transferred into the artificial CSF (ACSF; in mM: 126 NaCl, 2.5 KCl, 1.2 $NaH_2PO_4$, 1.2 $MgCl_2$, 2.4 $CaCl_2$, 11 glucose, and 25 NaHCO3, equilibrated with 95% $O_2$ and 5% $CO_2$) and kept at RT until use. For recording, slices were individually transferred to a chamber on an upright fluorescence microscope (Olympus BX51) and superfused continuously with ACSF (33°C, flow rate 2.5 ml $min^{-1}$). PAG neurons were visualized with a 40× water-immersion objective using Dodt gradient contrast optics and mCherry fluorescence was detected using epifluorescent illumination. Whole-cell patch-clamp recordings were performed in the current-clamp configuration. Patch pipettes (3–4 MΩ) were filled with an intracellular solution composed of (in mM): 130 K-gluconate, 0.5 EGTA, 10 HEPES, 10 Na2-phosphocreatine, 5 MgATP, 0.4 NaGTP, and 0.1% biocytin, pH 7.3 with KOH (290–295 mOsm). The liquid junction potential was not corrected. Membrane potential was monitored in the presence of the AMPA/kainate receptor antagonist, 2,3-Dioxo-6-nitro-1,2,3,4-tetrahydrobenzo[f]quinoxaline-7-sulfonamide (NBQX; 5 μM), the NMDA receptor antagonist, d-2-Amino-5-phosphonopentanoic acid (D-AP5; 25 μM), and the $GABA_A$ receptor antagonist picrotoxin (PTX; 100 μM). Loose cell-attached recordings were made using 2–3 MΩ glass pipettes containing normal ACSF at a holding potential at 0 mV in the voltage-clamp configuration under normal ACSF perfusion. Pipettes were gently pushed against the membrane of the mCherry-positive PAG cells (seal

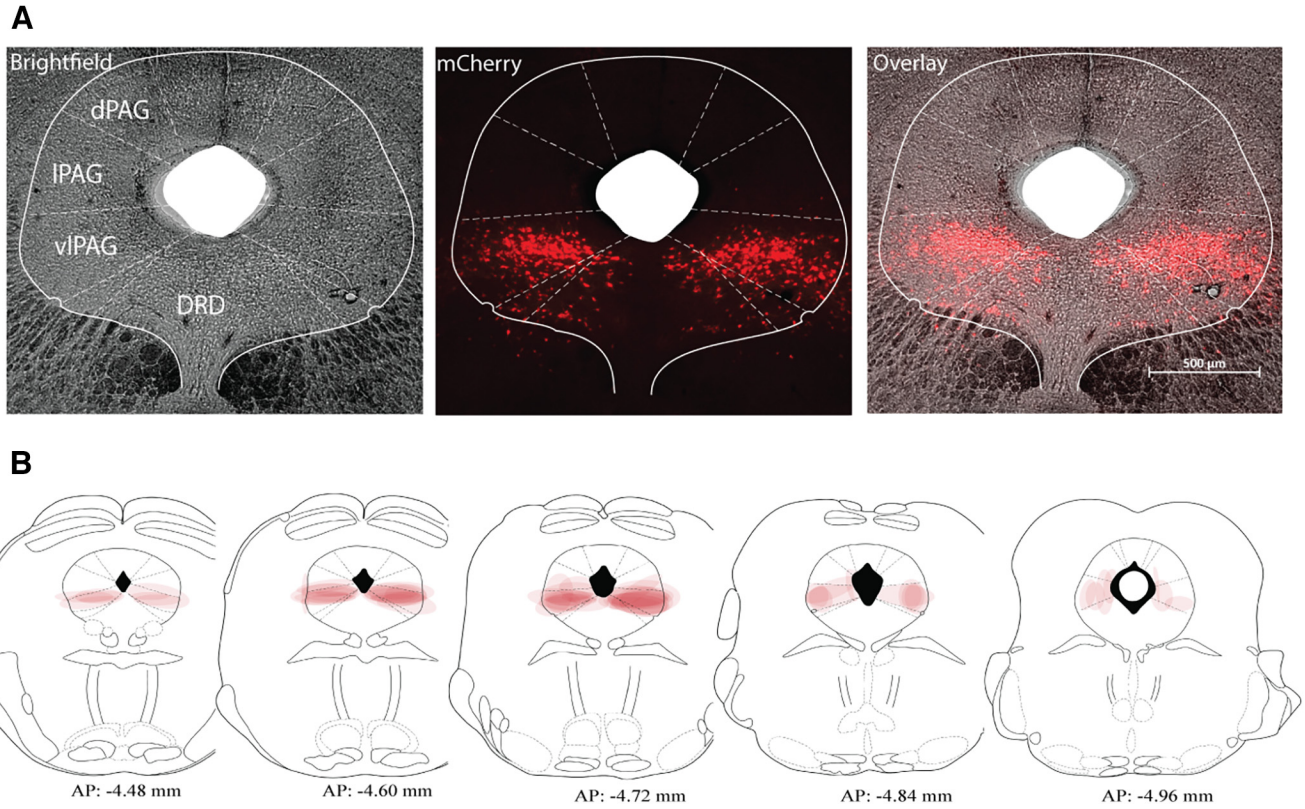


**Figure 2.** GlyT2-PAG neurons in the vlPAG expressed AAV-DREAADs-mCherry. ***A***, Representative microscopic images of coronal sections showing AAV5-hSyn-DIO-hM4D(Gi)-mCherry was largely restricted within the vlPAG: showing the expression of mCherry fluorescence (red), brightfield (gray), and overlayed of mCherry and brightfield images. Scale bars: 500 $\mu$m, Magnification: 2.5×. AP coordinate: −4.72 mm. ***B***, Placement map of AAV5 viral vector expression for all male mice included in the analyses in Figures 4, 5 showing 10% opacity for each animal.

resistance: 5–20 MΩ). We used hM3Dq receptor-expressing cells which had <3-Hz basal frequency to avoid undetectable action potential (AP) currents after the application of CNO. A cell that had 8.8 Hz basal AP frequency reached >50 Hz 1 min after application of CNO. After this time, the AP amplitude became smaller and eventually stopped, presumably suggesting that in cells with a higher baseline AP frequency and a more depolarized membrane potential, that CNO-induced membrane depolarization and inactivates sodium channels. All recordings were filtered (2- to 10-kHz low pass filter) with Multiclamp 700B amplifier (Molecular Device) and digitized at a sampling rate of 10 kHz with an A/D converter (NI USB-6251, National Instruments), and stored using a data acquisition program (AxographX, Axograph Scientific Software). Off-line analysis was performed using Clampfit10 (Molecular Device) and Igor Pro 6 (WaveMetrics).

To visualize cells filled with biocytin during electrophysiology recording, brain slices were fixed in 10% formalin solution (Sigma) and then incubated with streptavidin Alexa-647 (1:1000, Abcam). Slices were rinsed in PBS, mounted with PermaFluor (Epredia), and stored at 4°C. The slices were imaged in a Leica TCS SP5 confocal microscope using a 40× (NA 1.25) objective.

### Drug application

All other drugs were bath applied: NBQX and D-AP5 were from Abcam. Picrotoxin was from Alomone. All other drugs were from Sigma-Aldrich. CNO was dissolved in DMSO for stock solutions (30 mM).

### Data analysis

The experimenter was blinded to the treatment group during data analysis. Statistical analyses were performed using GraphPad Prism (version 9, GraphPad Software). For c-Fos/mCherry colocalization the Student's *t* test was used. For the nociception tests, one-way repeated measures (RM) ANOVA was used to consider interindividual variability within mice in different groups, followed by Bonferroni's multiple comparison test. Normality was assessed by the Shapiro–Wilk test, and outliers were identified by the ROUT method (Q = 1%). If the data from one treatment per group were identified as an outlier, all the dataset for that mouse was removed from RM or Paired analysis. Data that was not normal was analyzed by Friedman ANOVA followed by Dunn's multiple comparison test. Locomotor behavior was analyzed with ANY maze software (version 7.09), except for jumping and rearing behavior which was analyzed manually. Statistics were conducted using paired *t* tests to consider interindividual

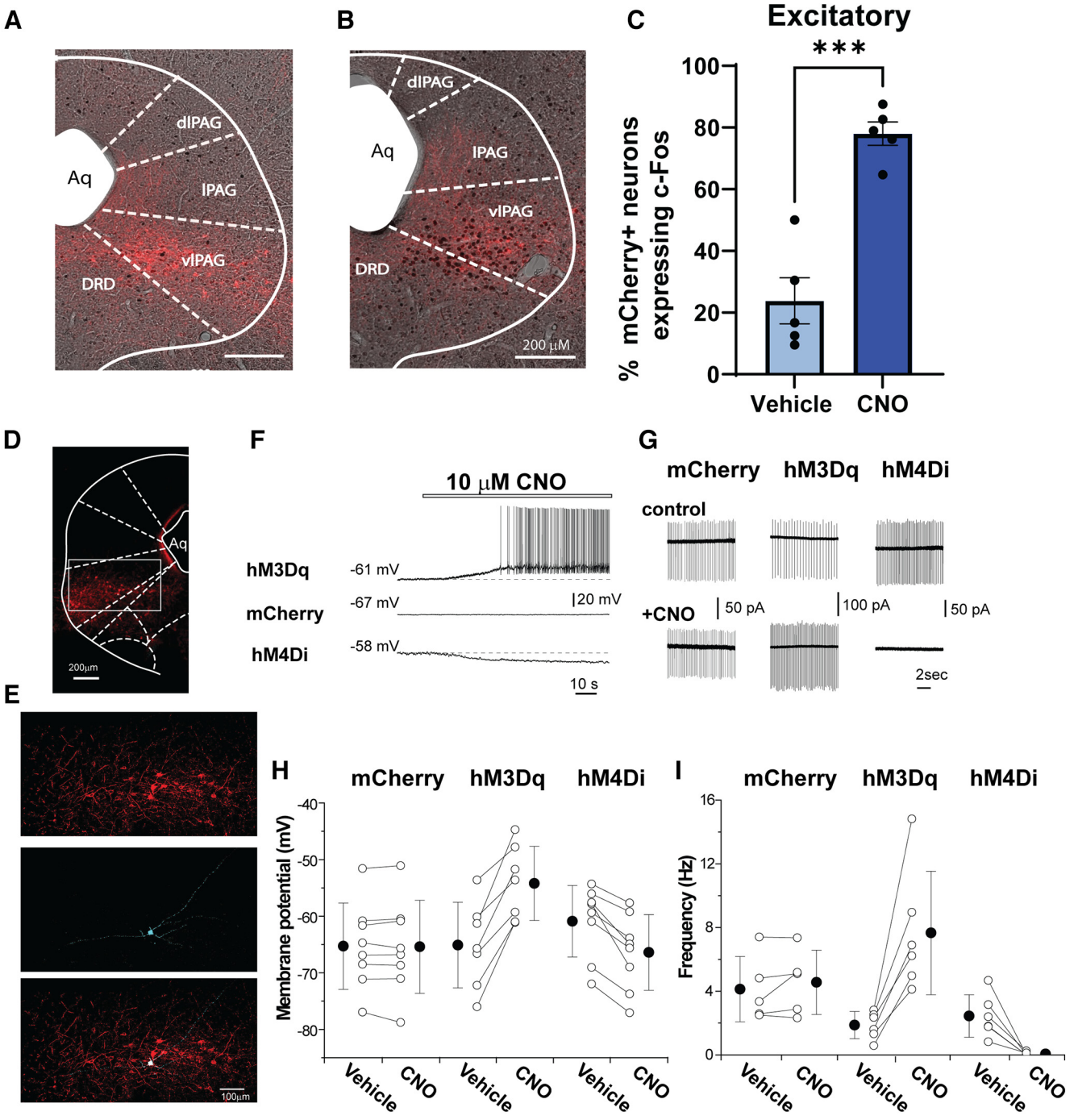


**Figure 3.** Functional characterization of hM3Dq and hM4Di in vlPAG neurons of GlyT2:Cre mice. ***A***, ***B***, c-Fos expression in GlyT2:: cre neurons expressing hM3Dq was enhanced following CNO injection. Representative images of coronal PAG sections showing c-Fos (black spots) is strongly colocalized in DREADD-expressing neurons (mCherry$^+$, red) following CNO (***B***, 3 mg/kg) compared with vehicle (***A***) injection (intraperitoneally). ***C***, Bar graph of the % mCherry$^+$ neurons that were co-labeled with c-Fos following vehicle or CNO injection (24 ± 16.63% vs 78 ± 8.55%, $n = 5$). ***D***, Fluorescent image of vlPAG neurons expressing hM3Di-mCherry and a whole-cell recorded cell. ***E***, Enlarged images (mCherry, streptavidin, merged) of the square region in ***D***. ***F***, Examples of current-clamp recording from hM3Dq, mCherry and hM3Di-expressing vlPAG neurons during bath application of 10 $\mu$M CNO. Dashed lines indicated the membrane potential of the cells before CNO application. ***G***, Quantification of the CNO effect on membrane potential at 3 min after its application. ***H***, Examples of action potential currents from loose-cell attached recordings from mCherry, hM3Dq and hM3Di-expressing vlPAG neurons before and 5 min after 10 $\mu$M CNO application. ***I***, Quantification of the CNO effect on action potential frequency at 5 min after its application. Scale bars in ***D***, ***E***: 100 $\mu$M. *$p < 0.05$. All values are mean ± SEM. A control experiment in Cre-negative littermates is presented in Extended Data Figure 3-1.

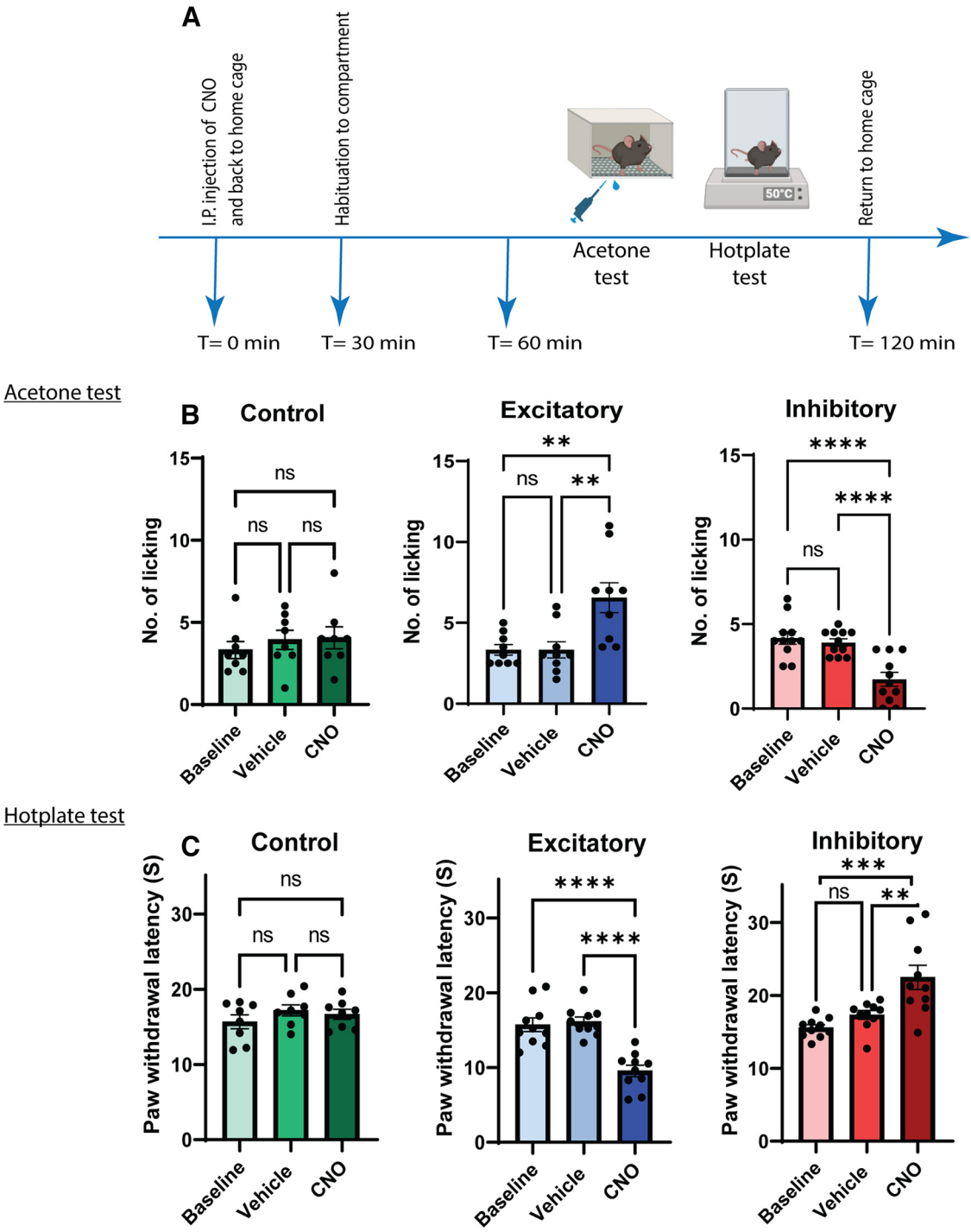


**Figure 4.** Chemogenetic manipulation of vlPAG GlyT2$^+$ neurons bidirectionally modulates acute nociceptive behavior in male mice. ***A***, Schematic of the chemogenetic protocol for assessing acute nociceptive behaviors (acetone and hotplate) in male GlyT2::cre mice. ***B***, ***C***, CNO (3 mg/kg, i.p.) administration resulted in increased hind paw licking and decreased PWL in GlyT2::cre male animals injected with hM3Dq (blue bars). CNO (5 mg/kg, i.p.) administration resulted in decreased hind paw licking and increased PWL in GlyT2::cre animals injected with hM4Di (red bars) compared with vehicle injection. CNO (5 mg/kg, i.p.) administration had no effect on hind paw licking and PWL in GlyT2::cre animals injected with control mCherry vector (green bars). Individual animals are indicated on the graphs ($n = 7$–11) and values are presented as mean ± SEM, and significant results were determined when $^*p < 0.05$.

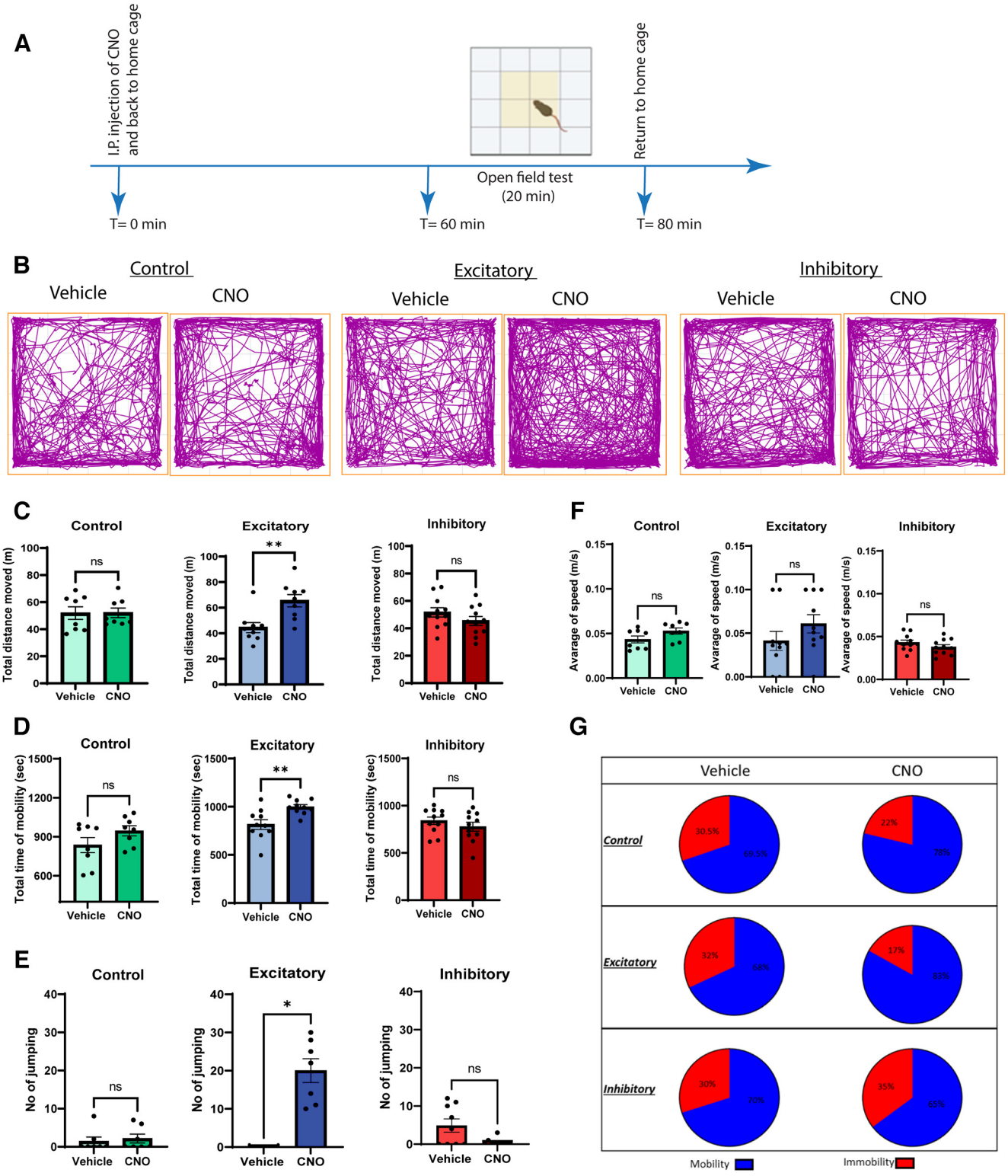


**Figure 5.** Chemogenetic activation of vlPAG GlyT2+ neurons alters locomotion behavior in the open field test in male mice. ***A***, Schematic of the chemogenetic protocol for assessing locomotor behaviors (open field) in male GlyT2::cre mice. ***B***, Plots show the position of the animals' center point for the entire duration of the test. ***C–F***, CNO (3 mg/kg, i.p.) administration resulted in increased total distance moved, increased mobility time, and increased jumping behavior but did not alter the average speed of GlyT2::cre male animals injected with hM3Dq compared with vehicle (blue bars). In contrast, no significant differences were observed in locomotion behavior when CNO (5 mg/kg, i.p.) was administered to GlyT2::cre animals injected with hM4Di compared with vehicle (red bars). In addition, CNO (5 mg/kg, i.p.) had no effect on locomotion behaviors in GlyT2::cre animals injected with the control mCherry vector (green bars). ***G***, Pie charts representing the overall percentage changes in mobility versus immobility in both CNO and

*continued*
vehicle-injected animals expressing control (mCherry), excitatory (hM3Dq) and inhibitory (hM4Di) DREADDS. Individual animals are indicated on the graphs ($n = 7–11$) and values are presented as mean ± SEM and significant results were determined when $^*p < 0.05$.

variability within mice in different groups. If the normality assumption was violated Wilcoxon signed rank test was used.

All data are presented as mean ± SEM and statistically significant results are indicated by an asterisk when $p < 0.05$.A detailed statistical summary can be found in Extended Data Table 1-1.

### Ethics statement

This work was carried out in accordance with the Australian code for the care and use of animals for scientific purposes, and assessed and approved by the Royal North Shore Animal Ethics committee. Genetically modified materials were used and disposed of with the approval of the Royal North Shore Hospital Institutional Biosafety committee.

## Results

### Chemogenetic targeting of GlyT2$^+$ neurons in the PAG

The glycine transporter 2 (GlyT2) is expressed presynaptically in inhibitory neurons that use glycine as a neurotransmitter (McIntire et al., 1997; Sagné et al., 1997; Chaudhry et al., 1998; Dumoulin et al., 1999; Wojcik et al., 2006). Previous reports indicate that a population of GlyT2$^+$ neurons are found in the midbrain PAG, and suggests that these neurons are concentrated in vlPAG (Rampon et al., 1996; Tanaka and Ezure, 2004; Zeilhofer et al., 2005), a region with well-established roles in descending modulation of pain and opioid-mediated analgesia (Behbehani, 1995; K.A. Keay and Bandler, 2015). To better understand the functional role of GlyT2-PAG neurons, we selectively expressed hM3Dq, hM4Di, or control (mCherry) protein in GlyT2-PAG neurons of male or female GlyT2::Cre mice (Foster et al., 2015). Then, we conducted behavioral testing using a within-subject crossover design to deliver the selective DREADD agonist clozapine N-oxide (CNO) or vehicle control (Fig. 1*A–C*).

Adeno-associated viral-vector (AAV5) mediated expression of transgenes in GlyT2::cre mice was strongly concentrated in the vlPAG (Fig. 2*A*,*B*), consistent with previous reports. To confirm that CNO activation of hM3Dq receptor enhanced the neuronal activity of GlyT2-PAG neurons, we combined IHC detection of c-Fos, an immediate early gene that is transiently expressed following neuronal activation (Perrin-Terrin et al., 2016), with IF labeling of hSyn-DIO-hM3Dq-mCherry neurons in mice that were injected with CNO (3 mg/kg, i.p.) or vehicle control 2 h before being killed. c-Fos was strongly colocalized hM3Dq-mCherry expressing vlPAG neurons following CNO-injected compared with vehicle-injected animals (CNO 78 ± 8.55%, vehicle 24 ± 16.63%, $p = 0.0002$, students *t* test, $n = 5$ animals per group; Fig. 3*A–C*).

In addition, we used electrophysiology to directly record DREADD-mediated neuronal modulation in coronal midbrain slices (Fig. 3*D*,*E*) from male and female mice in whole-cell current clamp (Fig. 3*F*) and loose patch configuration (Fig. 3*G*). We compared membrane potential and firing rates from hM3Dq/mCherry$^+$, hM4Di/mCherry$^+$ and mCherry$^+$ control PAG neurons. Bath application of CNO (3–10 $\mu$M) had no significant effect on the membrane potential or firing rate in recordings from mCherry$^+$ control neurons (control vs CNO: −66.0 ± 1.79 vs −66.3 ± 2.10 mV, $p = 0.642$; 3.25 ± 0.85 vs 3.56 ± 0.89 Hz, $p = 0.249$; two tailed paired *t* test, $n = 7–8$ cells; Fig. 3*F–I*). However, CNO significantly depolarized and increased the action potential firing rate of hM3Dq/mCherry$^+$ expressing vlPAG neurons (control vs CNO: −65.1 ± 2.86 vs −54.2 ± 2.48 mV, $p = 0.001$; 1.87 ± 0.35 vs 7.66 ± 1.58 Hz, $p = 008$; two tailed paired *t* test, $n = 6–7$ cells; Fig. 3*F–I*) and significantly hyperpolarized and decreased the action potential firing of hM4Di/mCherry$^+$ vlPAG neurons (control vs CNO: −60.9 ± 2.23 vs −66.4 ± 2.26 mV, $p = 0.001$; 2.44 ± 0.55 vs 0.06 ± 0.04 Hz, $p = 0.008$; two tailed paired *t* test, $n = 6–7$ cells; Fig. 3*F–I*). Together, these findings demonstrate that functional DREADDs are expressed in the vlPAG and that CNO increases and suppresses neuronal excitation in mice expressing hM3Dq and hM4Di respectively.

### Bidirectional control of acute nociceptive behaviors by GlyT2$^+$ neurons in the vlPAG

To test the functional contribution of GlyT2-PAG neurons in acute pain behaviors, we conducted behavioral experiments three to four weeks after stereotaxic injection of AAV5 vectors encoding hM3Dq-mCherry, hM4Di-mCherry, or mCherry control mice (Fig. 4*A*).

Cold responses were measured using the acetone test. In male GlyT2::Cre mice expressing the excitatory DREADDs (hM3Dq; Fig. 4*B*, blue bars), CNO (3 mg/kg, i.p.) significantly increased the number of hind paw licking (No. licking) responses compared with vehicle injection ($F_{(2,16)} = 10.03$, $p < 0.01$, $n = 9$; Fig. 4*B*). In contrast, in GlyT2::Cre animals expressing the inhibitory DREADDs (hM4Di; Fig. 4*B*, red bars), CNO (5 mg/kg, i.p.) significantly decreased the No. licking compared with vehicle injection ($F_{(2,20)} = 22.52$, $p < 0.0001$, $n = 11$; Fig. 4*B*). CNO (5 mg/kg, i.p.) had no effect on No. licking in the mCherry control group ($F_{(2,14)} = 0.54$, $p > 0.05$, $n = 8$; Fig. 4*B*, green bars).

We also investigated the role of GlyT2$^+$ vlPAG neurons on responses to noxious heat, using the hotplate test. In male GlyT2::Cre mice expressing hM3Dq (Fig. 4*C*, blue bars), CNO significantly decreased the paw withdrawal latency (PWL) to noxious thermal stimulation compared with vehicle injection ($F_{(2,18)} = 30.85$, $p < 0.0001$, $n = 10$; Fig. 4*C*). Whereas in the group expressing hM4Di (Fig. 4*C*, red bars), CNO significantly increased the PWL to noxious

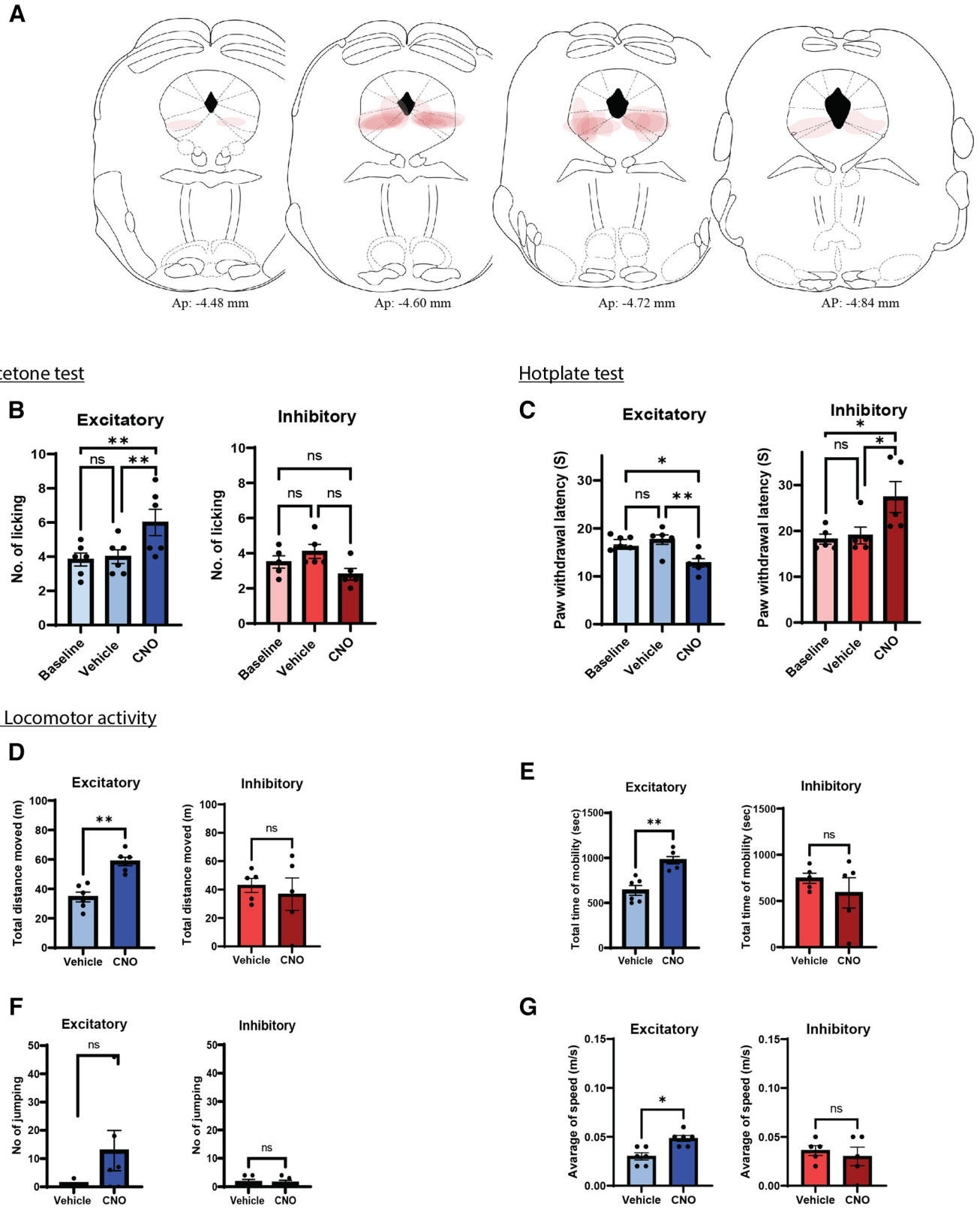


**Figure 6.** Chemogenetic manipulation of vlPAG GlyT2$^{+}$ neurons has bidirectional effects on nociception and increases locomotion in female mice. Female GlyT2::cre mice were tested with the same protocols as shown in Figures 4, 5. ***A***, Placement map of AAV5 viral vectors expression in vlPAG with the injection represented at 10% opacity for each animal. Bar graphs showing the responses to acetone (***B***) and hotplate (***C***) of mice expressing either excitatory (hM3Dq) or inhibitory (hM4Di) DREADDs and following injection with either vehicle or CNO (3–5 mg/kg, i.p., respectively) ***D–G***, Bar graphs of relevant locomotion parameters: total distance (***D***),

*continued*
total time of mobility (***E***), jumping (***F***) and average speed (***G***). Individual animals are indicated on the graphs ($n = 5$–6). Values are presented as mean ± SEM and $^*p < 0.05$.

thermal stimuli compared with vehicle injection ($F_{(2,18)}$ = 14.22, $p \leq 0.001$, $n = 10$; Fig. 4*C*). CNO had no effect on the PWL in the mCherry control group ($F_{(2,14)}$ = 1.47 $p > 0.05$, $n = 8$; Fig. 4*C*, green bars).

As vlPAG modulation of nociception has sex difference (Loyd et al., 2007; Loyd and Murphy, 2014; Rosen et al., 2017; Yu et al., 2021), we also conducted a parallel set of experiments on female GlyT2::Cre mice expressing either the excitatory or inhibitory DREADD under the same conditions. In female GlyT2::Cre mice expressing hM3Dq (Fig. 6*B*, blue bars), CNO significantly increased the No. licking responses compared with vehicle injection ($F_{(2,10)}$ = 13.65, $p < 0.01$, $n = 6$; Fig. 6*B*) and significantly decreased the PWL to noxious thermal stimulation compared with vehicle injection ($F_{(2,10)}$ = 10.91, $p < 0.01$, $n = 6$; Fig. 6*C*). In female GlyT2::Cre animals expressing hM4Di (red bars), CNO did not significantly decrease the No. licking compared with vehicle injection ($F_{(2,8)}$ = 3.024, $p > 0.05$, $n = 5$; Fig. 6*B*) but significantly increased the PWL to noxious thermal stimuli compared with vehicle injection ($F_{(2,8)}$ = 7.221, $p < 0.05$, $n = 6$; Fig. 6*C*). Together, these data indicate that the activity of GlyT2$^+$ neurons in the vlPAG exerts bidirectional nociceptive control in both male and female mice.

Finally, we assessed the locomotor effects of GlyT2$^+$ vlPAG neuronal activity in the open field test over a 20 min test period (Fig. 5*A*). We scored behaviors including total distance traveled, average speed, im/mobility, rearing, jumping, line crossing, center zone entries and total time spent in the center zone.

CNO injection in male GlyT2::cre mice expressing hM3Dq (Fig. 5, blue bars) caused a significant increase in the total distance moved ($p < 0.01$, $n = 9$;Fig. 5*C*), total time of mobility ($p < 0.01$, $n = 10$; Fig. 5*D*), and an associated decrease in immobility time ($p < 0.01$, $n = 10$; Fig. 5*G*). In addition, the total number of line crossings (not shown, $p < 0.05$, $n = 10$), total number of center entries (not shown, $p < 0.05$, $n = 6$), and center zone distance traveled (not shown; $p < 0.05$, $n = 6$), were increased and a dramatic increase in jumping behavior ($p < 0.05$, $n = 7$; Fig. 5*E*) was observed. We did not detect a change in average speed ($p > 0.05$, $n = 10$; Fig. 5*F*), time spent in the center zone (not shown, $p > 0.05$, $n = 9$) or rearing behavior (not shown, $p > 0.05$, $n = 9$) compared with vehicle control.

Comparable locomotor results were measured following CNO injection in hM3Dq expressing female mice (Fig. 6, blue bars), with the exception of jumping behavior, which was not significantly altered ($p > 0.05$, $n = 5$; Fig. 6*F*) and average speed, which increased ($p < 0.05$, $n = 6$; Fig. 6*G*), a finding that is consistent with a previous report (Capelli et al., 2017).

No alteration in locomotor behaviors were detected in hM4Di expressing male or female mice [male: $p > 0.05$, $n = 10$–11 (Fig. 5*C–F*, red bars); female: $p > 0.05$, $n = 5$–6 (Fig. 6*D–G*, red bars)] or in mCherry control mice ($p > 0.05$, $n = 7$–8; Fig. 5*C–F*, green bars) injected with CNO compared with their vehicle controls ($p > 0.05$, $n = 7$–11; Fig. 5*C–F*). These data suggest that activation, but not inhibition of GlyT2$^+$ vlPAG neurons exerts a stimulatory effect on exploratory locomotor behaviors in both male and female mice.

## Discussion

### GlyT2+ neurons have a crucial role in pain modulation

The GlyT2::Cre mouse allows us to selectively manipulate a sparse subset of neurons concentrated primarily in the ventrolateral subdivision of the PAG and to investigate their functional role. We demonstrate that the activity of GlyT2-PAG neurons bidirectionally modulate acute nociceptive responses, and that their activation increases locomotion. These findings can be directly compared with a recent study that used viral vectors to express chemogenetic channels in the vlPAG of male vGAT-Cre mice (Samineni et al., 2017) and monitored nociceptive (but not any other) behaviors. Consistent with our findings, activation of vGAT-PAG neurons was pronociceptive and inhibition was antinociceptive. As the vesicular transporter vGAT is responsible for concentrating both GAD-synthesized GABA and GlyT2-supplied glycine into synaptic vesicles (Burger et al., 1991; McIntire et al., 1997; Wojcik et al., 2006; Aubrey et al., 2007), and because GlyT2 has been shown to be strongly colocalized with GABAergic neurons in the PAG (Tanaka and Ezure, 2004; Vaughn et al., 2022), we consider that the GlyT2-PAG population are a minority subset of all the inhibitory neurons manipulated by Samineni et al. (2017). Thus, our study demonstrates that the activity of a small population of inhibitory neurons, whose cell bodies are confined within the vlPAG (Figs. 2, 6; Rampon et al., 1996; Zeilhofer et al., 2005), can effectively control acute nociceptive responses. Further, as GlyT2-PAG neurons bidirectionally modulate acute nociceptive responses, their baseline activity likely contributes to setting heat and cold sensitivity thresholds. Interestingly, we found that despite their relative scarcity, the scale of the nociception change achieved by manipulating GlyT2-PAG neurons was similar to that reported by Samineni et al. (2017). For example, we report that inhibition of GlyT2-PAG neurons increased PWL (noxious heat) by 130.2%, whereas inhibition of vGAT-PAG neurons led to a 136.3% increase in PWL. Given the relative density of GlyT2 neurons is small (Tanaka and Ezure, 2004; Vaughn et al., 2022), this observation could be explained if GlyT2-PAG neurons exert a more targeted control of the descending pain modulatory pathways than the vGAT$^+$ population, or that the net behavioral output measured following manipulation of all vlPAG vGAT$^+$ neurons reflect a composite behavioral output that is not maximal. In any case, these findings demonstrate that GlyT2-PAG neurons can robustly modulate acute nociception and suggests that treatments designed to selectively inhibit GlyT2-PAG neurons may be effective analgesics. An advantage of this type of modulation is that it would preserve GABAergic inhibitory function in the PAG and indeed in cortical regions, as there are no

GlyT2$^+$ neurons in the cortex (Rampon et al., 1996; Zeilhofer et al., 2005). Interestingly, we were also able to detect significant changes in nociceptive responses in a small group of animals that received a unilateral injection of hM3Dq [data not shown; $p = 0.02$ (acetone), $p = 0.04$ (hot-plate), $n = 5$], suggesting partial engagement of this neuronal population is sufficient to alter behavior.

### Interpretation of locomotor behaviors

The data show that activation of GlyT2-PAG neurons increased locomotor activity in male and female mice. The open-field test allows a systematic assessment of rodent exploration and general locomotor behavior that can be used for the initial screening of anxiety-like behaviors; as the open-field environment is a novel, exposed, white-lit space that temporarily isolates the animal from its cage mates (Bailey and Crawley, 2009). In response to stress, animals generally employ two main coping strategies that depend to a large extent on their state and the environmental context. Either an active (increases in mobility behavior, running or jumping behavior) or a passive (increases in immobility or freezing) fear response. Our finding that chemogenetic activation of GlyT2-PAG neurons expressing hM3Dq increased total distance moved, mobility and jumping behavior in male mice, and total distance moved, mobility and speed in female mice, are consistent with active fear-coping responses that are beyond exploratory behavior. This suggests that GlyT2-PAG neurons may influence neuronal circuits involved in both nociception and anxiety-like behaviors. We did not observe any changes in the time spent in the center zone, which has been associated with increased anxiety/stress in mice and increased locomotor activity in escapable environments (Korte et al., 1999). However, mobility and center zone times are not always correlated, and conclusively determining a role for GlyT2-PAG neurons in anxiety requires more specific tests such as the elevated plus maze and the light dark test (Korte et al., 1999; Bourin and Hascoët, 2003) .

### The vlPAG contains several distinct effector circuits

In addition to the well-described descending pain modulatory pathway which connects the vlPAG to the dorsal horn of the spinal cord via the RVM, the vlPAG houses other descending and ascending projection neurons that are involved in coordinating a host of other threat responses (Cameron et al., 1995b; K.A. Keay and Bandler, 2001). Recent studies have started to unravel the organization and describe distinct functions for these circuits (De Luca-Vinhas et al., 2006; Tovote et al., 2015; Koutsikou et al., 2017). For instance, both PAG-CCK expressing glutamatergic PAG neurons and low-dose NMDA injections influence different aspects of defensive behaviors and nociception (de Mello Rosa et al., 2022; La-Vu et al., 2022). On the other hand, vlPAG neurons that project to the medullary magnocellular nucleus (Mc) are responsible for freezing, locomotion, and coordinating defensive responses, but do not affect thermal nociception (Tovote et al., 2016; Capelli et al., 2017). Our research showing that activation of GlyT2-PAG neurons increases locomotion, aligns with the proposed function of the vlPAG-Mc pathway. However, GlyT2-PAG inhibition did not significantly reduce locomotion as expected and their activation is also linked with increased nociceptive behaviors, suggesting that another independent pathway may be involved.

### Glyt2-PAG neurons modulate nociception and locomotion in male and female mice

It is clear that the anatomy and physiology of pain modulation in male and female animals are distinctive (Loyd and Murphy, 2014; Rosen et al., 2017), and that signaling in the vlPAG contributes to these differences (Loyd et al., 2007; Capelli et al., 2017; Doyle et al., 2017; Yu et al., 2021; Llorente-Berzal et al., 2022). We conducted experiments in both male and female mice and found that GlyT2-PAG neurons similarly modulate the nociceptive and locomotive behaviors tested. However, we found that the quality of locomotor response triggered by GlyT2-PAG neuronal activation was qualitatively different between the sexes, with the increased mobility observed accompanied by jumping behaviors in male mice, and increased speed in female mice. These findings support a role for GlyT2-PAG neurons in modulating pain responses in both sexes and highlight the need to carefully consider and report appropriate behavioral outcomes for mice of different sexes.

### Technical considerations

The chemogenetic DREADDs approach provides a powerful and precise technique to selectively manipulate a particular subpopulation of neurons in neural circuits. The advantage of this method is that it gives researchers the possibility to modulate specific neuronal populations in isolation and observe the resultant behavioral consequences. However, chemogenetic modulation of circuits is not physiological, as it depolarizes or hyperpolarizes target neurons over a sustained period (a few hours), and the effect of prolonged DREADD activation on neuronal firing will be determined by each neuron type, dependent on the types of channels it expresses and its repolarisation capability (Smith et al., 2016). Experiments using optogenetics to achieve a faster and more phasic engagement of these cells will mitigate this problem and could potentially reveal a more nuanced view of GlyT2-PAG modulation of nociception and locomotion. Another advantage of optogenetics is that specific projection pathways can be targeted using precise stereotaxic injection of the viral vector expressing opsin and placement of the optic fiber or intersectional viral approaches strategies. As with all techniques that rely on viral vectors and genetic technologies, alterations in circuit organization, synaptic transmission properties and axonal morphology because of the use of vector-mediated protein expression and foreign protein expression/activation must also be considered (Miyashita et al., 2013; Jackman et al., 2014; Owen et al., 2019).

CNO can have off-target biological effects (Goutaudier et al., 2019). To minimize this possibility, we have used low-medium doses of CNO, which do not cause demonstrable off-target behavioral activity in control DIO-mCherry mice (MacLaren et al., 2016; Gomez et al., 2017;

Bærentzen et al., 2019). Furthermore, in our electrophysiological experiments, changes in the membrane potential and firing rate of vlPAG neurons expressing hM3Dq and hM4Dq were always recorded in response to CNO application, whereas no change was detected in mCherry-expressing midbrain neurons. Finally, in cre-negative littermates of GlyT2::cre mice injected with AAV-DIO- hM3Dq vectors, CNO had no measurable behavioral effect. For these reasons, we are confident the reported effects are correlated with the expected changes in GlyT2-PAG activity.

### Future directions

Future studies should investigate how and with whom GlyT2-PAG neurons communicate. Although the behavioral outcomes of altering GlyT2-PAG neuron activity are consistent with them being a subpopulation of inhibitory GABAergic neurons, their potential to release glycine means that their signaling mechanisms are likely to be distinct. Within the PAG, glycine could alter network activity by interacting with inhibitory glycine receptors or excitatory NMDA receptors (Ahmadi et al., 2003; Lynch, 2009).

A possible role for postsynaptic glycine receptors is suggested by experiments using electrophysiology to record evoked IPSCs in the ventrolateral PAG, where inhibitory currents with a glycine receptor-mediated component are occasionally detected. Indeed, this is the reason for the inclusion of strychnine (the specific glycine receptor antagonist) in slice recordings of the PAG (Tonsfeldt et al., 2016; Aubrey et al., 2017; Winters et al., 2022; Natale et al., 2023). In addition, glycine may be stimulating PAG activity. First, glycine activation of presynaptic glycine receptors expressed on glutamate-releasing neurons has been shown to increase the frequency of spontaneous EPSCs in acutely dissociated PAG neurons (Choi et al., 2013). Second, the modulation of nociceptive behavior by intra-PAG microinjections of glycine is sensitive to the glycine-site NMDA receptor antagonist 7-Cl-kynurenic acid (Palazzo et al., 2009). Determining the signaling mechanism employed by GlyT2-PAG neurons with in the PAG will permit a more complete understanding of how GlyT2-PAG neurons fit into the PAG circuitry.

In conclusion, this study demonstrates that GlyT2-PAG neurons effectively and bidirectionally modulate nociceptive responses in mice and indicates they may also play a role in anxiety-like behaviors. Until recently, our understanding of vlPAG function has been primarily gleaned from global manipulations of all or most of the neurons in the area. To better understand PAG function and nociceptive control, there is a need to carefully investigate the function of subpopulations of neurons in the vlPAG and to identify which microcircuits within the PAG are active under a range of threatening situations (Yin et al., 2020; Yang et al., 2022). These types of studies will continue to improve the functional frameworks used to understand how this region coordinates dynamic nociceptive responses and give insights into how common comorbidities develop in chronic pain states.

## References

Ahmadi S, Muth-Selbach U, Lauterbach A, Lipfert P, Neuhuber WL, Zeilhofer HU (2003) Facilitation of spinal NMDA receptor currents by spillover of synaptically released glycine. Science 300:2094–2097.

Alexander GM, Rogan SC, Abbas AI, Armbruster BN, Pei Y, Allen JA, Nonneman RJ, Hartmann J, Moy SS, Nicolelis MA, McNamara JO, Roth BL (2009) Remote control of neuronal activity in transgenic mice expressing evolved G protein-coupled receptors. Neuron 63:27–39.

Anderson WB, Gould MJ, Torres RD, Mitchell VA, Vaughan CW (2014) Actions of the dual FAAH/MAGL inhibitor JZL195 in a murine inflammatory pain model. Neuropharmacology 81:224–230.

Aubrey KR, Rossi FM, Ruivo R, Alboni S, Bellenchi GC, Le Goff A, Gasnier B, Supplisson S (2007) The transporters GlyT2 and VIAAT cooperate to determine the vesicular glycinergic phenotype. J Neurosci 27:6273–6281.

Aubrey KR, Drew GM, Jeong HJ, Lau BK, Vaughan CW (2017) Endocannabinoids control vesicle release mode at midbrain periaqueductal grey inhibitory synapses. J Physiol 595:165–178.

Bærentzen S, Casado-Sainz A, Lange D, Shalgunov V, Tejada IM, Xiong M, L'Estrade ET, Edgar FG, Lee H, Herth MM, Palner M (2019) The chemogenetic receptor ligand clozapine N-oxide induces in vivo neuroreceptor occupancy and reduces striatal glutamate levels. Front Neurosci 13:187.

Bagley EE, Ingram SL (2020) Endogenous opioid peptides in the descending pain modulatory circuit. Neuropharmacology 173:108131.

Bailey KR, Crawley JN (2009) Anxiety-related behaviors in mice. In: Methods of behavior analysis in neuroscience, Chap 5, Ed 2. Boca Raton: CRC Press/Taylor & Francis.

Bandler R, Shipley MT (1994) Columnar organization in the midbrain periaqueductal gray: modules for emotional expression? Trends Neurosci 17:379–389.

Behbehani MM (1995) Functional characteristics of the midbrain periaqueductal gray. Prog Neurobiol 46:575–605.

Benarroch EE (2012) Periaqueductal gray: an interface for behavioral control. Neurology 78:210–217.

Botterill JJ, Khlaifia A, Walters BJ, Brimble MA, Scharfman HE, Arruda-Carvalho M (2021) Off-target expression of cre-dependent adeno-associated viruses in wild-type C57BL/6J mice. eNeuro 8: ENEURO.0363-21.2021.

Bourin M, Hascoët M (2003) The mouse light/dark box test. Eur J Pharmacol 463:55–65.

Brandão M, De Aguiar J, Graeff F (1982) GABA mediation of the anti-aversive action of minor tranquilizers. Pharmacol Biochem Behav 16:397–402.

Burger PM, Hell J, Mehl E, Krasel C, Lottspeich F, Jahn R (1991) GABA and glycine in synaptic vesicles: storage and transport characteristics. Neuron 7:287–293.

Cameron AA, Khan IA, Westlund KN, Willis WD (1995a) The efferent projections of the periaqueductal gray in the rat: a *Phaseolus vulgaris*-leucoagglutinin study. II. Descending projections. J Comp Neurol 351:585–601.

Cameron AA, Khan IA, Westlund KN, Cliffer KD, Willis WD (1995b) The efferent projections of the periaqueductal gray in the rat: a *Phaseolus vulgaris*-leucoagglutinin study. I. Ascending projections. J Comp Neurol 351:568–584.

Capelli P, Pivetta C, Soledad Esposito M, Arber S (2017) Locomotor speed control circuits in the caudal brainstem. Nature 551:373–377.

Carrive P (1993) The periaqueductal gray and defensive behavior: functional representation and neuronal organization. Behav Brain Res 58:27–47.

Chaudhry FA, Reimer RJ, Bellocchio EE, Danbolt NC, Osen KK, Edwards RH, Storm-Mathisen J (1998) The vesicular GABA transporter, VGAT, localizes to synaptic vesicles in sets of glycinergic as well as GABAergic neurons. J Neurosci 18:9733–9750.

Cheng ZF, Fields HL, Heinricher MM (1986) Morphine microinjected into the periaqueductal gray has differential effects on 3 classes of medullary neurons. Brain Res 375:57–65.

Chéry N, De Koninck Y (1999) Junctional versus extrajunctional glycine and GABA(A) receptor-mediated IPSCs in identified lamina I neurons of the adult rat spinal cord. J Neurosci 19:7342–7355.

Choi KH, Nakamura M, Jang IS (2013) Presynaptic glycine receptors increase GABAergic neurotransmission in rat periaqueductal gray neurons. Neural Plast 2013:954302.
De Luca-Vinhas MCZ, Macedo CE, Brandão ML (2006) Pharmacological assessment of the freezing, antinociception, and exploratory behavior organized in the ventrolateral periaqueductal gray. Pain 121:94–104.
de Mello Rosa GH, Ullah F, de Paiva YB, da Silva JA, Branco LGS, Corrado AP, Medeiros P, Coimbra NC, Franceschi Biagioni A (2022) Ventrolateral periaqueductal gray matter integrative system of defense and antinociception. Pflugers Plast 474:469–480.
Depaulis A, Morgan MM, Liebeskind JC (1987) GABAergic modulation of the analgesic effects of morphine microinjected in the ventral periaqueductal gray matter of the rat. Brain Res 436:223–228.
Doyle HH, Eidson LN, Sinkiewicz DM, Murphy AZ (2017) Sex differences in microglia activity within the periaqueductal gray of the rat: a potential mechanism driving the dimorphic effects of morphine. J Neurosci 37:3202–3214.
Dumoulin A, Rostaing P, Bedet C, Levi S, Isambert MF, Henry JP, Triller A, Gasnier B (1999) Presence of the vesicular inhibitory amino acid transporter in GABAergic and glycinergic synaptic terminal boutons. J Cell Sci 112:811–823.
Espejo EF, Stinus L, Cador M, Mir D (1994) Effects of morphine and naloxone on behaviour in the hot plate test: an ethopharmacological study in the rat. Psychopharmacology (Berl) 113:500–510.
Fanselow MS (1991) The midbrain periaqueductal gray as a coordinator of action in response to fear and anxiety. In: The midbrain periaqueductal gray matter: functional, anatomical, and neurochemical organization (Depaulis A, Bandler R, eds), pp 151–173. Boston: Springer US.
Foster E, Wildner H, Tudeau L, Haueter S, Ralvenius WT, Jegen M, Johannssen H, Hösli L, Haenraets K, Ghanem A, Conzelmann K-K, Bösl M, Zeilhofer HU (2015) Targeted ablation, silencing, and activation establish glycinergic dorsal horn neurons as key components of a spinal gate for pain and itch. Neuron 85:1289–1304.
François A, Low SA, Sypek EI, Christensen AJ, Sotoudeh C, Beier KT, Ramakrishnan C, Ritola KD, Sharif-Naeini R, Deisseroth K, Delp SL, Malenka RC, Luo L, Hantman AW, Scherrer G (2017) A brainstem-spinal cord inhibitory circuit for mechanical pain modulation by GABA and enkephalins. Neuron 93:822–839.e6.
Gomez JL, Bonaventura J, Lesniak W, Mathews WB, Sysa-Shah P, Rodriguez LA, Ellis RJ, Richie CT, Harvey BK, Dannals RF, Pomper MG, Bonci A, Michaelides M (2017) Chemogenetics revealed: DREADD occupancy and activation via converted clozapine. Science 357:503–507.
Goutaudier R, Coizet V, Carcenac C, Carnicella S (2019) DREADDs: the power of the lock, the weakness of the key. favoring the pursuit of specific conditions rather than specific ligands. eNeuro 6: ENEURO.0171-19.2019.
Hao S, Yang H, Wang X, He Y, Xu H, Wu X, Pan L, Liu Y, Lou H, Xu H, Ma H, Xi W, Zhou Y, Duan S, Wang H (2019) The lateral hypothalamic and BNST GABAergic projections to the anterior ventrolateral periaqueductal gray regulate feeding. Cell Rep 28:616–624.e5.
Hunskaar S, Berge O-G, Hole K (1986) A modified hot-plate test sensitive to mild analgesics. Behav Brain Res 21:101–108.
Jackman SL, Beneduce BM, Drew IR, Regehr WG (2014) Achieving high-frequency optical control of synaptic transmission. J Neurosci 34:7704–7714.
Keay K, Bandler R (2008) Emotional and behavioral significance of the pain signal and the role of the midbrain periaqueductal gray (PAG). In: The senses: A comprehensive reference (Masland RH, Albright TD, Albright TD, Masland RH, Dallos P, Oertel D, Firestein S, Beauchamp GK, Catherine Bushnell M, Basbaum AI, Kaas JH, Gardner EP, eds), pp 627–634. New York: Academic.
Keay KA, Bandler R (2001) Parallel circuits mediating distinct emotional coping reactions to different types of stress. Neurosci Biobehav Rev 25:669–678.
Keay KA, Bandler R (2015) Periaqueductal gray. In: The rat nervous system, Chap 10, Ed 4 (Paxinos G, ed), pp 207–221. San Diego: Academic Press.
Keay KA, Clement CI, Depaulis A, Bandler R (2001) Different representations of inescapable noxious stimuli in the periaqueductal gray and upper cervical spinal cord of freely moving rats. Neurosci Lett 313:17–20.
Korte SM, De Boer SF, Bohus B (1999) Fear-potentiation in the elevated plus-maze test depends on stressor controllability and fear conditioning. Stress 3:27–40.
Koutsikou S, Apps R, Lumb BM (2017) Top down control of spinal sensorimotor circuits essential for survival. J Physiol 595:4151–4158.
La-Vu MQ, Sethi E, Maesta-Pereira S, Schuette PJ, Tobias BC, Reis F, Wang W, Torossian A, Bishop A, Leonard SJ, Lin L, Cahill CM, Adhikari A (2022) Sparse genetically defined neurons refine the canonical role of periaqueductal gray columnar organization. Elife 11:e77115.
Lau BK, Vaughan CW (2014) Descending modulation of pain: the GABA disinhibition hypothesis of analgesia. Curr Opin Neurobiol 29:159–164.
Llorente-Berzal A, McGowan F, Gaspar JC, Rea K, Roche M, Finn DP (2022) Sexually dimorphic expression of fear-conditioned analgesia in rats and associated alterations in the endocannabinoid system in the periaqueductal grey. Neuroscience 480:117–130.
Loyd DR, Murphy AZ (2014) The neuroanatomy of sexual dimorphism in opioid analgesia. Exp Neurol 259:57–63.
Loyd DR, Morgan MM, Murphy AZ (2007) Morphine preferentially activates the periaqueductal gray–rostral ventromedial medullary pathway in the male rat: a potential mechanism for sex differences in antinociception. Neuroscience 147:456–468.
Lynch JW (2009) Native glycine receptor subtypes and their physiological roles. Neuropharmacology 56:303–309.
MacLaren DA, Browne RW, Shaw JK, Radhakrishnan SK, Khare P, España RA, Clark SD (2016) Clozapine N-oxide administration produces behavioral effects in Long–Evans rats: implications for designing DREADD experiments. eNeuro 3:ENEURO.0219-16.2016.
McIntire SL, Reimer RJ, Schuske K, Edwards RH, Jorgensen EM (1997) Identification and characterization of the vesicular GABA transporter. Nature 389:870–876.
Miranda CO, Hegedüs K, Wildner H, Zeilhofer HU, Antal M (2022) Morphological and neurochemical characterization of glycinergic neurons in laminae I–IV of the mouse spinal dorsal horn. J Comp Neurol 530:607–626.
Mitchell VA, Harley J, Casey SL, Vaughan AC, Winters BL, Vaughan CW (2021) Oral efficacy of Δ(9)-tetrahydrocannabinol and cannabidiol in a mouse neuropathic pain model. Neuropharmacology 189:108529.
Miyashita T, Shao YR, Chung J, Pourzia O, Feldman DE (2013) Long-term channelrhodopsin-2 (ChR2) expression can induce abnormal axonal morphology and targeting in cerebral cortex. Front Neural Circuits 7:8.
Mohrland JS, Gebhart GF (1980) Effects of focal electrical stimulation and morphine microinjection in the periaqueductal gray of the rat mesencephalon on neuronal activity in the medullary reticular formation. Brain Res 201:23–37.
Moreau JL, Fields HL (1986) Evidence for GABA involvement in midbrain control of medullary neurons that modulate nociceptive transmission. Brain Res 397:37–46.
Morgan M, Whitney P, Gold M (1998) Immobility and flight associated with antinociception produced by activation of the ventral and lateral/dorsal regions of the rat periaqueductal gray. Brain Res 804:159–166.
Morgan MM, Clayton CC (2005) Defensive behaviors evoked from the ventrolateral periaqueductal gray of the rat: comparison of opioid and GABA disinhibition. Behav Brain Res 164:61–66.
Nabekura J, Katsurabayashi S, Kakazu Y, Shibata S, Matsubara A, Jinno S, Mizoguchi Y, Sasaki A, Ishibashi H (2004) Developmental switch from GABA to glycine release in single central synaptic terminals. Nat Neurosci 7:17–23.
Natale CA, Christie MJ, Aubrey KR (2023) Spinal glycinergic currents are reduced in a rat model of neuropathic pain following partial

nerve ligation but not chronic constriction injury. J Neurophysiol 129:333–341.
Otsu Y, Aubrey KR (2022) Kappa opioids inhibit the GABA/glycine terminals of rostral ventromedial medulla projections in the superficial dorsal horn of the spinal cord. J Physiol 600:4187–4205.
Owen SF, Liu MH, Kreitzer AC (2019) Thermal constraints on in vivo optogenetic manipulations. Nat Neurosci 22:1061–1065.
Palazzo E, Guida F, Migliozzi A, Gatta L, Marabese I, Luongo L, Rossi C, de Novellis V, Fernández-Sánchez E, Soukupova M, Zafra F, Maione S (2009) Intraperiaqueductal gray glycine and d-serine exert dual effects on rostral ventromedial medulla on- and off-cell activity and thermoceptive threshold in the rat. J Neurophysiol 102:3169–3179.
Paxinos G, Franklin KBJ (2001) The mouse brain in stereotaxic coordinates, 2nd Edition. San Diego: Academic.
Perrin-Terrin A-S, Jeton F, Pichon A, Frugière A, Richalet J-P, Bodineau L, Voituron N (2016) The c-FOS protein immunohistological detection: a useful tool as a marker of central pathways involved in specific physiological responses in vivo and ex vivo. J Vis Exp (110):53613.
Rampon C, Luppi PH, Fort P, Peyron C, Jouvet M (1996) Distribution of glycine-immunoreactive cell bodies and fibers in the rat brain. Neuroscience 75:737–755.
Rosen S, Ham B, Mogil JS (2017) Sex differences in neuroimmunity and pain. J Neurosci Res 95:500–508.
Rousseau CV, Dugué GP, Dumoulin A, Mugnaini E, Dieudonné S, Diana MA (2012) Mixed inhibitory synaptic balance correlates with glutamatergic synaptic phenotype in cerebellar unipolar brush cells. J Neurosci 32:4632–4644.
Sagné C, El Mestikawy S, Isambert M-F, Hamon M, Henry JP, Giros B, Gasnier B (1997) Cloning of a functional vesicular GABA and glycine transporter by screening of genome databases. FEBS Lett 417:177–183.
Samineni VK, Grajales-Reyes JG, Copits BA, O'Brien DE, Trigg SL, Gomez AM, Bruchas MR, Gereau IR (2017) Divergent modulation of nociception by glutamatergic and GABAergic neuronal subpopulations in the periaqueductal gray. eNeuro 4:ENEURO.0129-16.2017.
Samineni VK, Grajales-Reyes JG, Sundaram SS, Yoo JJ, Gereau RW (2019) Cell type-specific modulation of sensory and affective components of itch in the periaqueductal gray. Nat Commun 10:4356.
Sandkühler J, Willmann E, Fu QG (1989) Blockade of GABAA receptors in the midbrain periaqueductal gray abolishes nociceptive spinal dorsal horn neuronal activity. Eur J Pharmacol 160:163–166.
Smith KS, Bucci DJ, Luikart BW, Mahler SV (2016) DREADDS: use and application in behavioral neuroscience. Behav Neurosci 130:137–155.
Tanaka I, Ezure K (2004) Overall distribution of GLYT2 mRNA-containing versus GAD67 mRNA-containing neurons and colocalization of both mRNAs in midbrain, pons, and cerebellum in rats. Neurosci Res 49:165–178.
Tonsfeldt KJ, Suchland KL, Beeson KA, Lowe JD, Li MH, Ingram SL (2016) Sex differences in GABAA signaling in the periaqueductal gray induced by persistent inflammation. J Neurosci 36:1669–1681.
Tovote P, Fadok JP, Lüthi A (2015) Neuronal circuits for fear and anxiety. Nat Rev Neurosci 16:317–331.
Tovote P, Esposito MS, Botta P, Chaudun F, Fadok JP, Markovic M, Wolff SB, Ramakrishnan C, Fenno L, Deisseroth K, Herry C, Arber S, Lüthi A (2016) Midbrain circuits for defensive behaviour. Nature 534:206–212.
Vaughan CW, Christie MJ (1997) Presynaptic inhibitory action of opioids on synaptic transmission in the rat periaqueductal grey in vitro. The J of Physiology 498:463–472.
Vaughn E, Eichhorn S, Jung W, Zhuang X, Dulac C (2022) Three-dimensional interrogation of cell types and instinctive behavior in the periaqueductal gray. bioRxiv 2022.06.27.497769.
Vermeirsch H, Meert TF (2004) Morphine-induced analgesia in the hot-plate test: comparison between NMRI(nu/nu) and NMRI mice. Basic Clin Pharmacol Toxicol 94:59–64.
Winters BL, Lau BK, Vaughan CW (2022) Cannabinoids and opioids differentially target extrinsic and intrinsic GABAergic inputs onto the periaqueductal grey descending pathway. J Neurosci 42:7744–7756.
Wojcik SM, Katsurabayashi S, Guillemin I, Friauf E, Rosenmund C, Brose N, Rhee J-S (2006) A shared vesicular carrier allows synaptic corelease of GABA and glycine. Neuron 50:575–587.
Yang L, Lu J, Guo J, Chen J, Xiong F, Wang X, Chen L, Yu C (2022) Ventrolateral periaqueductal gray astrocytes regulate nociceptive sensation and emotional motivation in diabetic neuropathic pain. J Neurosci 42:8184–8199.
Yin JB, et al. (2020) dmPFC-vlPAG projection neurons contribute to pain threshold maintenance and antianxiety behaviors. J Clin Invest 130:6555–6570.
Yoon C, Wook YY, Sik NH, Ho KS, Mo CJ (1994) Behavioral signs of ongoing pain and cold allodynia in a rat model of neuropathic pain. PAIN 59:369–376.
Yu W, Pati D, Pina MM, Schmidt KT, Boyt KM, Hunker AC, Zweifel LS, McElligott ZA, Kash TL (2021) Periaqueductal gray/dorsal raphe dopamine neurons contribute to sex differences in pain-related behaviors. Neuron 109:1365–1380.e5.
Zafra F, Aragón C, Olivares L, Danbolt NC, Giménez C, Storm-Mathisen J (1995) Glycine transporters are differentially expressed among CNS cells. J Neurosci 15:3952–3969.
Zeilhofer HU, Studler B, Arabadzisz D, Schweizer C, Ahmadi S, Layh B, Bösl MR, Fritschy JM (2005) Glycinergic neurons expressing enhanced green fluorescent protein in bacterial artificial chromosome transgenic mice. J Comp Neurol 482:123–141.
Zeilhofer HU, Acuña MA, Gingras J, Yévenes GE (2018) Glycine receptors and glycine transporters: targets for novel analgesics? Cell Mol Life Sci 75:447–465.
Zhang SP, Bandler R, Carrive P (1990) Flight and immobility evoked by excitatory amino acid microinjection within distinct parts of the subtentorial midbrain periaqueductal gray of the cat. Brain Res 520:73–82.

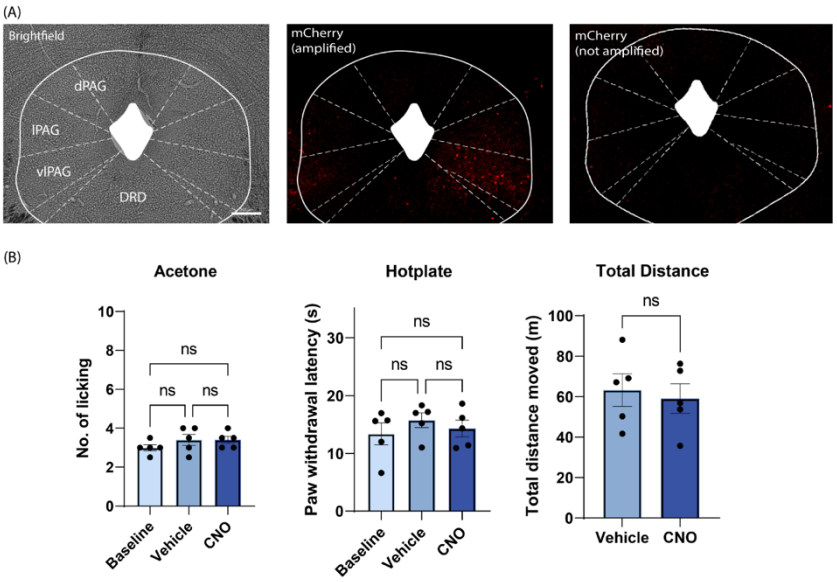


**Extended Data Figure 3-1**

Control experiments in GlyT2:Cre negative mice confirm that AAV-Cre-independent leak of vectors did not contribute to the CNO-stimulated behavioral changes. AAV5-hSyn-DIO-hM3D(Gq)-mCherry was stereotaxically injected into the vlPAG of cre-negative littermates of GlyT2::cre mice. *A*, Low-level cre-independent expression of mCherry was revealed following antibody amplification. Note: antibody amplification was not carried out in any of the injection site figures shown in the main text. *B*, Leak expression had no functional effect as CNO (3 mg/kg, i.p.) administration did not alter hind paw licking, PWL or locomotion of cre-negative animals injected with hM3Dq (blue bars) compared to vehicle controls. $n = 5$, values are presented as mean ± SEM

# Appendix 2: A pain modality-specific neuronal population within the mouse midbrain ventrolateral periaqueductal grey

**A pain modality-specific neuronal population within the mouse midbrain ventrolateral periaqueductal grey**

Kaley Nguyen[1,2,3], Caitlin Fenech[1,2,3], Myles Horton[1,2,3], Yo Otsu[1,2] and Karin Aubrey[1,2]

[1]Pain Management Research, Kolling Institute, Royal North Shore Hospital Northern Sydney Local Health District and Faculty of Medicine and Health, University of Sydney, Sydney, New South Wales 2065, Australia

[2]Sydney Pain Consortium, Faculty of Medicine and Health, University of Sydney, Sydney, New South Wales 2006, Australia

[3]School of Medical Sciences, Faculty of Medicine and Health, University of Sydney, Sydney, New South Wales 2006, Australia

Manuscript in preparation.

Contributions- CF and KA designed research; KN, YO, KA and CF, MH performed surgeries and carried out the experiments. KN, MH and CF analysed behavioural research; YO, KN and KA wrote the paper; all authors edited the paper.

**Abstract**

The ventrolateral periaqueductal grey (vlPAG) is a central node for the descending modulation of nociceptive signalling. In addition, it is involved in triggering both passive and active defence strategies associated with visceral and somatic pain respectively. However, it remains unclear whether distinct midbrain circuits within the vlPAG differentially process specific pain modalities. GlyT2-expressing neurons in the vlPAG represent a genetically defined inhibitory population previously shown to bidirectionally modulate thermal nociception. In this study, we employed a chemogenetic approach to selectively manipulate GlyT2 neurons in the vlPAG of male and female GlyT2::Cre mice, and assessed behavioural responses associated with acetic acid-induced visceral pain. Unlike thermal nociception, visceral nociceptive responses were unaffected by either activation or inhibition of GlyT2 neurons, although locomotor effects persisted. These findings provide first evidence for pain-modality-specific processing within the vlPAG and suggest that effective treatment of visceral pain requires targeted modulation of distinct neural circuits.